ENSEMBLE AND SINGLE-MOLECULE FLUORESCENCE STUDIES OF DNA MISMATCH REPAIR INITIATION BY MUTS

Lauryn E. Sass

A dissertation submitted to the faculty of the University of North Carolina at Chapel Hill in partial fulfillment of the requirements for the degree of Doctor of Philosophy in the Department of Chemistry**.**

Chapel Hill
2007

Approved by:

Advisor: Dr. Dorothy Erie

Reader: Dr. Nancy Thompson

Reader: Dr. Tom Kunkel

Dr. Linda Spremulli

Dr. Mark Schoenfish

ABSTRACT

LAURYN E. SASS

Ensemble and single-molecule fluorescence studies of
DNA mismatch repair initiation by MutS
(Under the direction of Dr. Dorothy A. Erie)

Single-molecule techniques have exploded in recent years and have become powerful in revealing the dynamic structure-function relationships of biological systems. In this dissertation, I have developed and applied ensemble and single-molecule fluorescence assays to observe the dynamics of mismatch repair initiation by repair enzyme MutS.

Models of DNA mismatch repair initiation by MutS have been established, and the foundations of these models typically make comparisons between conformational changes in the DNA and the protein and mismatch repair signaling by MutS. The DNA bending model suggests that conformation changes induced in mismatched DNA serve as the method in which MutS recognizes a mismatch and signals repair. However, there was no evidence of a dynamic equilibrium of DNA bending and unbending induced by MutS.

Single-molecule fluorescence assays were employed to follow this dynamic equilibrium between DNA bending and unbending induced by MutS. Results reveal that mismatched DNA-MutS complexes are, in fact, very dynamic, sampling a number of different DNA conformations with varied relative stabilities. These protein-DNA dynamics

may be essential for mismatch recognition and repair signaling by MutS. MutS is able to induce many different DNA conformations in mismatched DNA, and the conformational dynamics of the complexes vary depending on the mismatch. These observations suggest that conformational dynamics helps MutS to perform all of its functions, including recognizing a number of different base-base mismatches and base insertions/deletions, recruiting mismatch repair cofactors to signal repair, and signaling cell cycle arrest in response to DNA damage.

Increased DNA dynamics observed for MutS with a mutation in the conserved binding domain complement *in vivo* assays of mismatch repair and are consistent with observations that dynamic DNA conformational sampling serves as an important mechanism that MutS uses to signal repair. DNA conformational fluctuations were also induced by yeast MutSα, suggesting that eukaryotes employ similar protein-DNA dynamics in mismatch repair initiation by MutS.

These results develop a correlation between protein-DNA dynamics and biological function and begin to demystify how MutS is capable of performing so many different tasks in the cell.

To my husband, ‘Antoine’,
whose support, encouragement, and motivation keep me going,

&

To my parents, Norman and Cheryl,
for their continued love and support

ACKNOWLEDGEMENTS

I would like to first thank my amazing research advisor Dr. Dorothy Erie for allowing me to work in her lab and for being a wonderful mentor, teacher, and friend throughout my doctoral tenure. I would never have accomplished this work without her guidance, her thoughtful contributions, her time, and her patience. She has given me the valuable tools of problem solving and critical thinking, and the education that I received under her direction has been invaluable.

I would like to thank my wonderful collaborator Dr. Keith Weninger. Keith was brought to me through an impromptu google search, and he welcomed me into his lab and taught me extensive technical skills in the field of single-molecule fluorescence. His guidance has been essential in the success of my work, and his thoughtful discussions have been greatly valued.

I would like to thank all of my coworkers in the Erie lab, past and present. Every person from this lab has helped me or contributed to the success of this work in some way, and I have been fortunate to be a member of a group of incredibly talented scientists and great people. So, thanks to Liz, Erika, Vanessa, Ingrid, Cherie, Scott, Candi, Hong, Yong, Susan, Bob, Junghoon, and Na. I would also like to thank the amazing undergraduates that did research with me, Carmen and David.

I would like to thank my many collaborators who have contributed time, instrumentation, supplies, and expertise to my work: Dr. Keith Weninger and the Weninger lab; Dr. Peggy Hsieh and the Hsieh lab; Dr. Tom Kunkel and the Kunkel lab; Brian Eastwood (Dr. Russell Taylor lab, UNC); Dr. Ashutosh Tripathy and the UNC Macromolecular Interactions Facility; Dr. Haifa Johns; Dr. Nancy Thompson and the Thompson lab; the Pielak, Redinbo, Spremulli, Papanikolas, and Yousaf labs; and, the UNC Department of Chemistry.

I would like to thank my husband for putting up with my psychoneurosis during the past five years and still marrying me. This man is clearly the best husband on the planet.

Finally, I want to thank my family for their continued love and support and for teaching me than even the worst of floods can't bring us down.

TABLE OF CONTENTS

CHAPTER TWO
SINGLE-MOLECULE FRET STUDIES OF CONFORMATIONAL HETEROGENEITY IN PROTEIN-DNA COMPLEXES: Following dynamics of mismatched DNA-MutS complexes one molecule at a time

CHAPTER THREE
FLUORESCENCE STUDIES OF THE FUNCTION OF GLUTAMATE IN MISMATCH DNA BINDING AND BENDING BY TWO MUTS HOMOLOGS

CHAPTER FOUR
ENSEMBLE AND SINGLE-MOLECULE FRET REVEAL MISMATCHED DNA BENDING INDUCED BY YEAST MSH2-MSH6 (yMutSα)

CHAPTER FIVE
MATERIALS AND METHODS

LIST OF TABLES

LIST OF FIGURES

LIST OF ABBREVIATIONS

2D	Two-dimensional
6MI	6-methyl isoxanthopterin
Å	Angstrom
A	Alanine
α_c	Critical angle for TIRF
ADP	Adenosine diphosphate
AFM	Atomic force microscopy
Ala	alanine
A_{max}	Saturation anisotropy
ATP	Adenosine triphosphate
BME	Beta-mercaptoethanol
bp	Base-pair
BSA	Bovine serum albumin
C	Cysteine
CAT	Catalase
CCD	Charge-coupled device
CH_3	Methyl group
COT	cyclooctatetraene
d	Evanescent wave depth
DNA	Deoxyribonucleic acid
dNTP	Deoxyribonucleoside triphosphates
dsDNA	Double-stranded DNA
ΔT	Unpaired thymine base, thymine loop or bulge
D_{tot}	Total DNA concentration
DTT	dithiothreitol
E	Glutamate
E. coli	*Escherichia coli*
EDTA	Diaminoethanetetraacetic acid
EMSA	Electromobility gel shift assay

F	Phenylalanine
FRET	Fluorescence resonance energy transfer
G	Glycine
GC	Guanine-cytosine base-pair
Glu	Glutamate
GOX	Glucose oxidase
GT	Guanine-thymine mismatched base-pair
HNPCC	Hereditary non-polyposis colorectal cancer
HPLC	High performance liquid chromatography
I_A	Fluorescence intensity of FRET acceptor
I_D	Fluorescence intensity of FRET donor
I_d	Fluorescence intensity of donor in the absence of acceptor
I_{da}	Fluorescence intensity of donor in the presence of acceptor
IRC	Initial mismatch recognition complex
kcal	kilocalories
K_d	Dissociation constant
KDa	kilodaltons
KOH	Potassium hydroxide
L	Leucine
λ_o	Laser excitation light source for TIRF
mg	Milligram
$MgCl_2$	Magnesium chloride
mL	milliliter
μL	microliter
mM	Millimolar
MMR	Mismatch repair
MSH2	MutS homolog 2
MSH2-MSH3	Heterodimer of MutS homologs 2 and 3
MSH2-MSH6	Heterodimer of MutS homologs 2 and 6
MSH3	MutS homolog 3
MSH6	MutS homolog 6

MutS(α)	MutS and MutSα
n	Refractive index
N	nitrogen
NA	Numerical aperture
NaCl	Sodium chloride
NaOAc	Sodium acetate
NHS	N-hydroxysuccinimide ester
nm	nanometer
nM	Nanomolar
P	probability
PC	Personal computer
PEG	Polyethylene glycol
Phe	Phenylalanine
Pi	phosphate
pM	picomolar
P_{tot}	Total protein concentration
R	FRET donor-acceptor dye separation distance
R_o	Förster distance for FRET dye pair
S	Serine
SPR	Surface plasmon resonance
SSB	Single-strand binding protein
ssDNA	Single-stranded DNA
τ	lifetime
T	Tyrosine
TAMRA	carboxytetramethylrhodamine
Taq	*Thermus aquaticus*
T-bulge	Unpaired thymine base, thymine loop or bulge
TDP	Transition density plot
TIRF	Total internal reflection fluorescence
Tris-HCl	Trishydroxymethylaminomethane-hydrochloride
UDG	Uracil DNA glycosylase

URC	Ultimate mismatch recognition complex
UV	Ultraviolet
UVRD	E. coli helicase II
yMutSα	Heterodimer of MutS homologs 2 and 6 in yeast
yMutSβ	Heterodimer of MutS homologs 2 and 3 in yeast

CHAPTER ONE

INTRODUCTION
Advances in single-molecule techniques and application to studying the dynamics of DNA mismatch repair initiation by MutS

Introduction

The complex field of biological chemistry continues to require new experimental methods to better study the detailed nature of the biochemistry at hand. Standard biochemical assays, such as electromobility gel shift assays, have been employed for years providing knowledge of how a biological system functions. Crystallography has been extraordinary in elucidating the 3-dimensional structure of macromolecules. However, there exists a need for technology that provides information linking the structure of a biological system with its function. After all, most biological molecules inherently function due to changes in structure. In recent years, single-molecule biophysics premiered powerful technologies that allow measurements relating structure to biological function. Some of these methods include atomic force microscopy, optical tweezing, and fluorescence microscopy, among others. These methods have proven to offer the most '*bang for your buck'* in experimental biochemistry (Ha 2001; Cornish and Ha 2007; Deniz, Mukhopadhyay et al. 2007; Greenleaf, Woodside et al. 2007). With the ability to monitor dynamics, kinetics, equilibria, diffusion, and binding, in addition to corresponding structural changes (Ambrose,

Goodwin et al. 1999; Weiss 1999; Weiss 2000), it is no surprise that single-molecule technology is an enterprise worth exploring.

Standard biochemistry, and more recently crystallography and atomic force microscopy, have been the primary methods to study DNA mismatch repair and the function of the mismatch repair protein MutS (DNA mismatch repair reviewed in (Hsieh 2001; Kunkel and Erie 2005). Studies of *Thermus aquaticus* (*Taq*) MutS using a multitude of techniques are described in (Biswas and Hsieh 1996; Obmolova, Ban et al. 2000; Wang, Yang et al. 2003). In this dissertation, I have sought to develop and apply complementary ensemble and single-molecule fluorescence methods to study DNA binding, conformational dynamics, and kinetics of DNA mismatch repair initiation by MutS. The work described in the following chapters will reveal the potency of fluorescence technology in studying the structure-function relationships that facilitate the DNA mismatch repair pathway and its initiation by MutS.

Ensemble and single-molecule fluorescence: Biophysical approach to measuring macromolecular conformational dynamics and binding

Using fluorescence to measure the dynamics of single-molecules is powerful in that one can obtain a great deal of information about a given system in a short time (Gell, Brockwell et al. 2006). The dynamics and kinetics of a multitude of biological functions can be measured, and structural and conformational changes in macromolecules can also be observed in real time. By detecting single-molecules, ensemble averaging is eliminated, and multiple populations in a system may be isolated. Elimination of ensemble averaging becomes increasingly important when a system has two equally dominant populations, and

the ensemble average does not accurately represent either of the two. In addition, single-molecule measurements allow us to observe infrequent events that are typically lost in averaging. These technical benefits prompted us to employ single-molecule microscopy to measure conformational dynamics of protein-DNA complexes essential to DNA mismatch repair.

Fluorescence microscopy instrumentation: Total Internal Reflection Fluorescence (TIRF)

Total internal reflection fluorescence (TIRF) microscopy has recently gained significant popularity in the imaging of single-molecules. This technique offers the benefits of a low background signal and the ability to study molecules for extended periods of time (Moerner and Fromm 2003; Schneckenburger 2005; Wazawa and Ueda 2005). In this technique, a fluorescence excitation light source is directed on a surface through a prism, and the light is internally reflected off the surface back into the prism if the angle of incidence is greater than the critical angle (which is determined by the composition of the interface) (Figure 1.1 A) (Lieto, Cush et al. 2003; Moerner and Fromm 2003; Schneckenburger 2005; Wazawa and Ueda 2005). The critical angle (α_c) is defined by Snell's Law:

$$\alpha_C = \sin^{-1}\left(\frac{n_2}{n_1}\right)$$

where n_1 is the refractive index of the microscope slide, and n_2, the refractive index of the aqueous sample.

An evanescent wave of depth *d* results from this reflection at the surface, decaying in intensity from the surface following the relationship:

$$d = \frac{\lambda_o}{4\pi} \cdot \left(n_1^2 \sin^2 \alpha - n_2^2\right)^{-\frac{1}{2}}$$

where λ_o is the wavelength of incident light, and α is the incident angle. The evanescent wave typically penetrates to depths of ~ 150 to 200 nm from the surface. Therefore, only surface-bound molecules are excited, background fluorescence emission is reduced, and a greater sensitivity to detect single-molecules is achieved.

Fluorescence emission of the surface-bound molecules may be collected through a microscope objective lens and imaged on a high-resolution charge-coupled device or detected with a photodiode detector. A schematic of TIRF and a basic diagram of a TIRF microscope are shown in Figure 1.1 A and B. With this technique, many single molecules may be observed simultaneously, and a large number of statistics may be obtained in a short time.

FRET: Fluorescence resonance energy transfer to study conformational changes in biomolecules

TIRF alone may not be useful in studying changes in biological structure, but when combined with fluorescence resonance energy transfer (FRET), it becomes exceedingly powerful in allowing observations of conformational changes of single molecules. FRET has been commonly referred to as the 'molecular ruler' of biochemistry (Forster 1959; Stryer 1978; Wu and Brand 1994; Clegg 1995; Gell, Brockwell et al. 2006). FRET employs the spectroscopic properties of two fluorescent dyes of different colors. One dye serves as an energy donor, the other, as an energy acceptor. When the FRET donor is directly excited by light, it is capable of releasing this energy through multiple relaxation pathways including

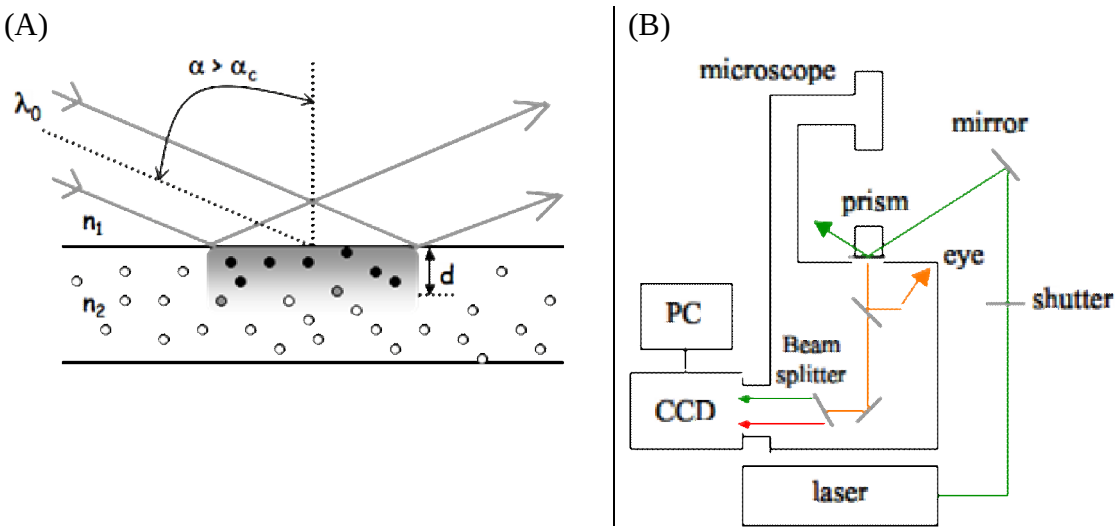

Figure 1.1 Total internal reflection fluorescence microscopy

(A) Schematic of total internal reflection (TIR) and how it works to excite surface-bound molecules (adopted from (Lieto, Cush et al. 2003)). Laser light of wavelength λ_0 is directed onto a surface comprised of two components with differing refractive indices (n_1 and n_2). The light is impinged at such an angle where it is completely reflected back into the medium of higher refractive index (in this case n_1). An evanescent wave of depth d results at the surface, and only molecules within that region are excited by the excitation light. (B) Basic schematic of a fluorescence microscope that incorporates TIR for sample excitation. Shown is through-prism TIR, where the excitation light is directed through a prism (n_1) to excite the sample (n_2). An alternative to through-prism TIR is through-objective TIR. In this case, the excitation light is coupled through the microscope objective to excite the sample.

internal conversion, intersystem crossing, collisional quenching, and, of course, fluorescence. However, if a suitable FRET acceptor dye is nearby, the donor dye can transfer some of that energy to the FRET acceptor.

Energy transfer from the FRET donor to the FRET acceptor is non-radiative and is an external conversion process resulting from the long-range dipole coupling of the two fluorescent dyes (Steinberg 1971; Stryer 1978; Wu and Brand 1994; Clegg 1995). There are three conditions that must be met for FRET to occur between a donor and an acceptor fluorophore: (1) The donor and the acceptor molecules must be in resonance such that there is an overlap between the emission band of the donor and the absorption band of the acceptor. (2) The quantum yield of the donor molecule and the extinction coefficient of the acceptor molecule must be sufficiently large. (3) The transition dipoles of the donor and acceptor molecules must be aligned or should have a high degree of rotational freedom (Stryer 1978; Wu and Brand 1994; Clegg 1995).

FRET results from dipole-dipole coupling of the donor and acceptor dyes, therefore energy transfer is a function of r^{-6} and follows the equation:

$$E_{FRET} = \frac{1}{1+\left(\frac{r}{R_o}\right)^6}$$

where E_{FRET} is the energy transfer efficiency, r is the distance of separation between the dyes, and R_o is the Förster distance for the dye pair, or the distance where energy transfer is 50%. The Förster distance for the FRET pair is dependent on the spectroscopic properties of the dyes as well as their relative rotational freedoms. Förster distances have been estimated for a variety of fluorescent dye pairs and may also be calculated directly from experimental

measurements. A graphical representation of the dependence of energy transfer on distance between the donor and acceptor dyes is shown in Figure 1.2.

FRET may be directly observed by monitoring the fluorescence intensity fluctuations of both the FRET donor dye and the FRET acceptor dye and is characterized by an anti-correlated change in the relative intensities of the two fluorophores. In single-molecule measurements, FRET efficiency may be directly calculated following the equation:

$$E_{FRET} = \frac{I_A}{I_A + I_D}$$

where I_A is the fluorescence intensity of the acceptor, and I_D, the fluorescence intensity of the donor.

By controlling the location of the FRET dye pair on the biomolecule, structural changes may be deduced from changes in the extent of FRET between the dye pair as a function of time. The distance dependence of FRET makes it a powerful technique in studying the conformational dynamics and kinetics of biological molecules and complexes. Appendix A outlines additional FRET theory and mathematical background.

Fluorescence anisotropy to observe macromolecular binding constants

Fluorescence anisotropy is a useful technique in measuring the binding of a protein to a fluorescently-labeled molecule of similar size or smaller (Lakowicz 1999). Fluorescence anisotropy is dependent on the rate of rotational diffusion of the fluorescent molecule (Lakowicz 1999). The sample is excited with polarized light, and molecules whose absorption dipoles are oriented parallel to the polarization of the incident light are excited. The intensity of the fluorescence emission of these molecules is measured both through a

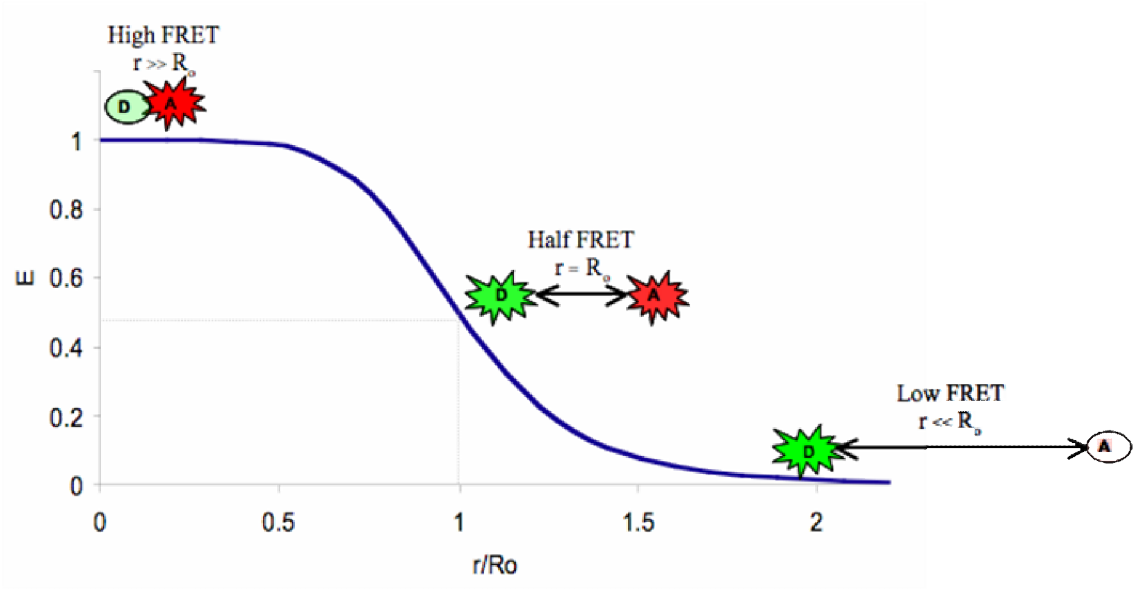

Figure 1.2 Distance dependence of FRET

The dependence of fluorescence resonance energy transfer (FRET) on distance between the FRET donor dye (green) and FRET acceptor dye (red). Energy transfer results from dipole-dipole coupling between the two dyes, therefore it is a function of r^{-6}. R_o represents the characteristic Förster distance for the dye pair, or the interdye distance where energy transfer is 50%. When the dyes are in close proximity, high FRET is observed (high emission from the FRET acceptor and low emission from the FRET donor). When the dyes are far apart, low FRET is observed (low emission from the FRET acceptor and high emission from the FRET donor). When the dyes are separated by a distance equal to the Förster distance for the pair (R_o), half FRET is observed (approximately equal emission from both the FRET donor and the FRET acceptor).

polarizer oriented parallel to the polarization of the excitation light ($I_{//}$) and through a polarizer oriented perpendicular to the polarization of the excitation light ($I_{\perp}$). Anisotropy (r) is a measure of the extent of polarization of the emitted light and is defined as

$$r = \frac{I_{//} + I_{\perp}}{I_{//} + 2I_{\perp}}$$

Anisotropy depends on both the lifetime of the fluorophore and the rotational diffusion of the fluorescent molecule in solution (Lakowicz 1999). When a small fluorescent molecule is bound by a larger molecule, the rate of rotational diffusion decreases, and anisotropy signal increases. As a result, fluorescence anisotropy allows us to directly observe protein association with other macromolecules.

DNA mismatch repair: background

The cell is a workhorse carrying out millions of processes simultaneously to maintain proper function. DNA replication is a primary cellular process setting the foundation for the central dogma of biology. The DNA replication machinery synthesizes ~ 500 DNA base-pairs every second in bacteria (~ 50 per second in eukaryotes), and the cell has evolved a complex network of repair pathways to pick-up the mistakes that escape DNA polymerase proofreading (Campbell, Reece et al. 1999; Lewin 2000). DNA mismatch repair (MMR) is just one of many of these repair pathways in the cell. The DNA mismatch repair machinery locates and corrects mismatches in base-pairing and repairs small base insertions or deletions that may result from polymerase misincorporation and strand slippage, respectively (Kolodner and Marsischky 1999; Hsieh 2001; Kunkel and Erie 2005). DNA mismatch repair is a highly conserved repair pathway essential to the maintenance of genomic stability, and

the proteins that initiate MMR are conserved throughout both prokaryotes and eukaryotes (Au, Welsh et al. 1992; Drummond, Li et al. 1995; Buermeyer, Deschenes et al. 1999; Jiricny and Marra 2003). Recent genetic studies in humans have shown a proclivity toward tumor development in patients with mutations in the family of genes essential to MMR. Such mutations have been subsequently linked to more than 85% of hereditary non-polyposis colorectal cancer (HNPCC) as well as other sporadic cancers (Modrich 1989; Modrich 1995; Loeb, Loeb et al. 2003).

The malignant consequences of malfunctioning DNA MMR have spawned great interest in the understanding of the details of this repair process. From the sequence-specific binding of the repair proteins to mismatched DNA to the structural consequences they induce, many researchers are interested in elucidating the mechanism of MMR in both prokaryotes and eukaryotes.

In prokaryotes, the proteins MutS, MutL, and MutH are responsible for MMR initiation and have been researched extensively. MutS and MutL are ATPases and function as homodimers in prokaryotes. The more complex eukaryotic mismatch repair systems have several MutS homologs (Msh genes) and MutL homologs (Mlh genes) that are also ATPases and function as heterodimers. In eukaryotes, different MutS homologs function in the repair of specific base mismatches or base insertion/deletion loops. Msh2-Msh3 (MutSβ) has been shown to function primarily in the repair of base insertion/deletion loops greater than 2 bases, while Msh2-Msh6 (MutSα) most efficiently repairs base-base mismatches and small insertion/deletion loops of 1-2 bases (Drummond, Li et al. 1995; Acharya, Wilson et al. 1996; Kunkel and Erie 2005). The conserved MutS and MutL homologs are outlined in Table 1.1.

To date, *Escherichia coli* provides the best understood MMR pathway and serves as a prototypical model on which models of repair in more complex organisms may be based (Lahue and Modrich 1988; Modrich 1989; Modrich and Lahue 1996; Harfe and Jinks-Robertson 2000). A model of methyl-directed mismatch repair in *E. coli* is shown in Figure 1.3. The first step in the mismatch repair pathway is the location of a mismatched base pair by MutS (Au, Welsh et al. 1992). After locating a mismatch, MutS recruits MutL in an ATP-dependent manner generating a MutS-MutL multimeric complex at the DNA mismatch (Modrich and Lahue 1996; Kunkel and Erie 2005). This complex activates the latent endonuclease activity of MutH, which nicks the newly synthesized daughter strand at a downstream hemi-methylated GATC site. Helicase enters the game and begins to unwind the DNA toward the mismatch, and (depending on the position of the nick relative to the mismatch), exonucleases degrade the daughter strand to within about 100 bases past the location of the mismatch. DNA Polymerase III resynthesizes the excised portion of the DNA, and the final nick is sealed by DNA ligase.

Mismatch repair in eukaryotes is slightly more mysterious. The mismatch is first located by a heterodimeric MutS homolog (typically MutSα or MutSβ), and a heterodimeric MutL homolog (most typically MutLα) is subsequently recruited. However, there is no strand-discriminating MutH homolog or hemi-methylated dGATC sites, making the eukaryotic MMR process poorly understood and the subject of extensive research in the mismatch repair field (Drummond, Li et al. 1995; Palombo, Gallinari et al. 1995; Acharya, Wilson et al. 1996; Alani 1996; Buermeyer, Deschenes et al. 1999; Clark, Cook et al. 1999).

E. coli, Taq	*S. Cerevisiae*	*Human*	Function
MutS	yMutSα (yMsh2-Msh6)	hMutSα (hMsh2-Msh6)	Single base mismatch and small insertion/ deletion (1-2 bases) loop repair
-	yMutSβ (yMsh2-Msh3)	hMutSβ (hMsh2-Msh3)	Large insertion/deletion (≥ 2 bases) loop repair
MutL	yMutLα (yMlh1-Pms1)	hMutLα (hMlh1-Pms2)	Matchmaker protein in mismatch repair
-	yMutLβ (yMlh1-Mlh2)	hMutLβ (hMlh1-Pms1)	Suppresses some insertion/deletion mutagenesis in yeast, unknown function in humans
-	yMutLγ yMlh1-Mlh3	hMutLγ hMlh1-Mlh3	Suppresses some insertion/deletion mutagenesis, participates in meiosis
MutH	None	None	Nicks nascent strand at hemimethylated dGATC sites in prokaryotes

Table 1.1 Proteins involved in mismatch repair initiation

MutS, MutL, and MutH in prokaryotes and known homologs in eukaryotes (adopted from (Kunkel and Erie 2005) and (Schofield and Hsieh 2003)).

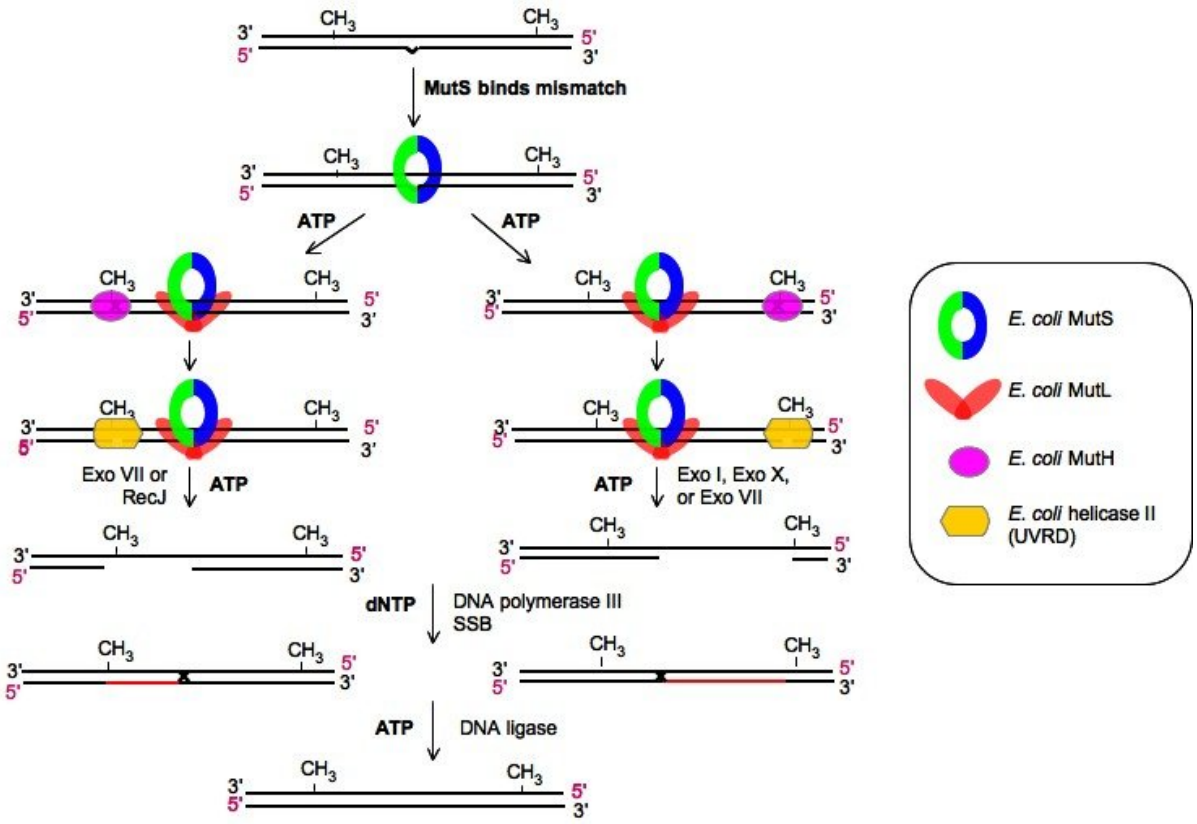

Figure 1.3 Model for methyl-directed DNA mismatch repair in E. coli

MutS: A closer look at a hard-working enzyme

An interesting question surrounding DNA mismatch repair is how the repair process is initiated. MutS and MutS homologs have the particularly difficult task of locating a single base mismatch or base insertion/deletion mismatch over the millions of regular DNA base pairs in the cell. Moreover, mismatches do not significantly distort the DNA, and often the difference between a normal Watson-Crick base-pairing (for example, a GC base-pair) and a mismatch (for example, a GT mismatch) is small (Isaacs, Rayens et al. 2002; Natrajan, Lamers et al. 2003).

Crystal structures of MutS and MutSα bound to a number of different mismatched DNA bases and base insertion/deletions have been solved (Lamers, Perrakis et al. 2000; Obmolova, Ban et al. 2000; Natrajan, Lamers et al. 2003; Warren, Pohlhaus et al. 2007). The structure of MutS from *Thermus aquaticus* (*Taq*) is shown in Figure 1.4. The crystal structures reveal that only two specific amino acid contacts from one subunit of the MutS dimer are made between MutS or MutSα (collectively referred to as MutS(α)) and the mismatched base: stacking of a phenylalanine with the mismatched base and hydrogen bonding of a glutamate with the N3 of the mismatched thymine or N7 of the mismatched purine (Lamers, Perrakis et al. 2000; Obmolova, Ban et al. 2000; Natrajan, Lamers et al. 2003; Warren, Pohlhaus et al. 2007). All other interactions between MutS and the DNA are non-specific backbone contacts.

The primary observation in these structures is that the DNA is distinctly kinked at the mismatch site, stabilized both by the specific amino acid interactions with the mismatch as well as the non-specific contacts along the backbone. This bending at the mismatch site has been proposed to function in mismatch recognition (Jiricny and Marra 2003; Kunkel and Erie

2005). However, each crystal structure reveals the same contacts and approximately the same degree of DNA bending at every type of mismatch even though different mismatches are repaired with different efficiencies *in vivo* (Kramer, Kramer et al. 1984). In addition, there seems to be an inverse correlation between the facility for a mismatch to bend and its repair efficiency (Wang, Yang et al. 2003). In fact, the DNA mismatches most efficiently repaired in the cell induce the least distortion in the DNA (Kunkel and Erie 2005).

While the crystal structures have served a valuable purpose in revealing what the MutS-DNA complex looks like, there remain questions surrounding the mechanism in which MutS and MutSα recognize different mismatches and signal repair.

Structure-function models describing mismatch repair initiation by MutS and MutS homologs

A catalog of research has been devoted to understanding how MutS initiates and signals mismatch repair. Several models have been proposed to describe this repair process (Figure 1.5), all of which place emphasis on a correlation between changes in structure and function.

(1) The translocation model, supported by electron microscopy images, suggests that MutS binds to a mismatch and ATP hydrolysis by MutS mediates the formation of an α-loop (Figure 1.5 A) (Allen, Makhov et al. 1997; Blackwell, Martik et al. 1998). This looped conformation has been suggested to be important in recruiting subsequent mismatch repair cofactors. In this model, the looped conformation brings the MutS/MutL complex in closer proximity to the hemi-methylated GATC sites, signaling the recruitment of MutH and activating its latent endonuclease activity to begin excision and repair (Allen, Makhov et al. 1997; Blackwell, Martik et al. 1998).

(A)

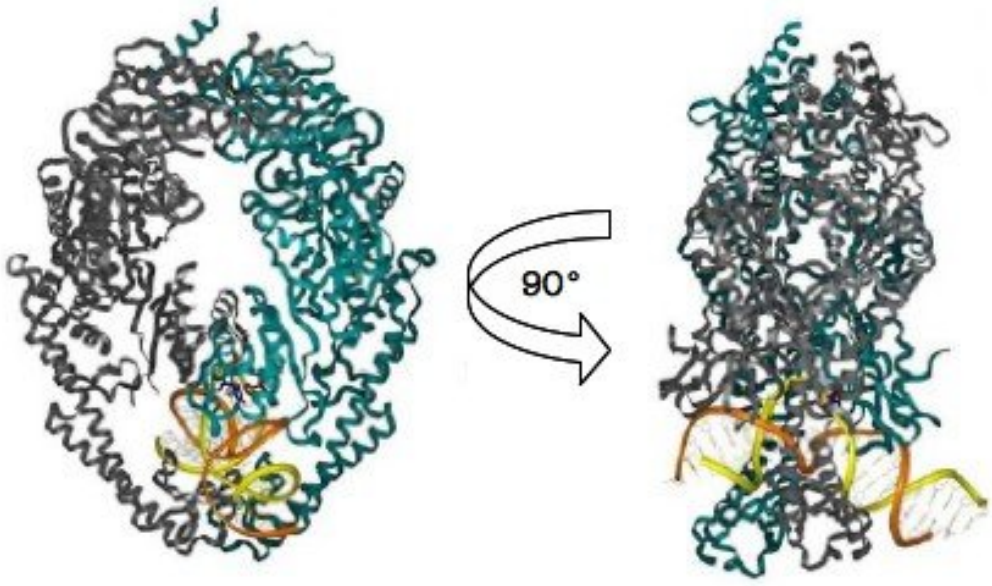
90°

(B)

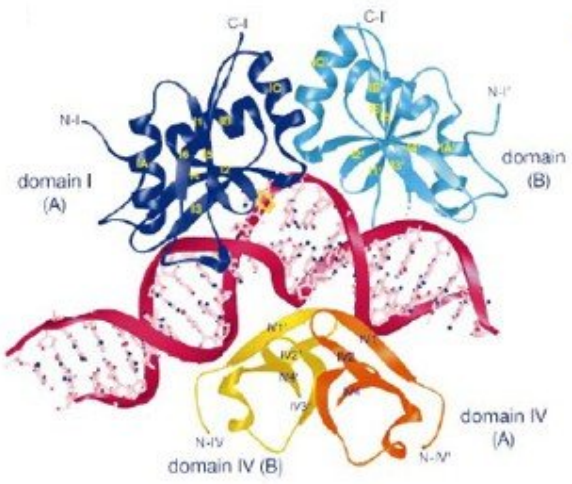
C-I
C-I'
N-I
N-I'
domain I
(A)
domain
(B)
N-IV
domain IV (B)
domain IV
(A)
N-IV'

(C)

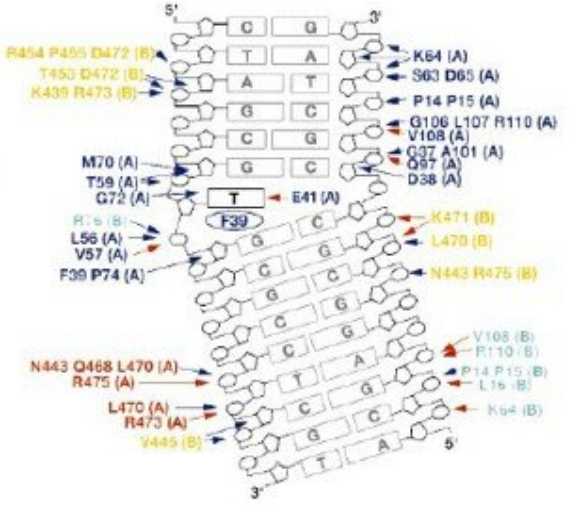
5'
3'
R454 P455 D472 (B)
T450 D472 (B)
K439 R473 (B)
K64 (A)
S63 D65 (A)
P14 P15 (A)
G106 L107 R110 (A)
V108 (A)
G37 A101 (A)
Q97 (A)
D38 (A)
M70 (A)
T59 (A)
G72 (A)
E41 (A)
F39
L56 (A)
V57 (A)
F39 P74 (A)
K471 (B)
L470 (B)
N443 R475 (B)
N443 Q468 L470 (A)
R475 (A)
L470 (A)
R473 (A)
V445 (B)
5'
3'

Figure 1.4 Crystal structure of *Taq* MutS bound to an unpaired thymine

(A) Structure of *Taq* MutS bound to an unpaired thymine (ΔT) (Obmolova, Ban et al. 2000). MutS binds a mismatch as a homodimer, and the subunits are shown in blue and gray. Each subunit takes the shape of a comma, and the dimerization interface creates two channels, one enclosing the DNA (shown in orange and yellow), and the other large enough to accommodate duplex DNA but whose function remains unknown (Obmolova, Ban et al. 2000). The ATP-binding site is located at the top of the enzyme approximately 70 Å from the DNA binding site. (B) Close-up view of the MutS-DNA interface. The DNA is shown in magenta, and the unpaired thymine bulge (shown in yellow) is rotated out of the DNA into the minor groove by ~ 3 Å. Each monomer of MutS is separated into five domains, two of which are shown interacting with the DNA: domains I and IV from both subunits of the homodimer (denoted subunits A and B). Subunit A contributes the specific Glu and Phe contacts with the mismatch, and a host of other non-specific contacts along the DNA backbone further stabilize the distinct ~ 60° kink in the DNA (bend angle is defined in Figure 1.6). The amino acid contacts with the DNA are shown in (C). Red arrows denote hydrogen bonding interactions while blue arrows represent Van der Waals contacts.

(2) The molecular switch model represents mismatch repair initiation by MutS in a slightly different manner. This model suggests that ADP-bound MutS first binds to mismatched DNA. Once bound, ADP is exchanged for ATP, inducing a conformational change in MutS to create a sliding clamp MutS-ATP complex (Figure 1.5 B) (reviewed in (Acharya, Foster et al. 2003)). Additional MutS-ADP molecules are then capable of binding the naked mismatch site, and the multi-MutS-DNA complex functions in signaling repair.

(3) The DNA bending model (Figure 1.5 C) has been proposed based on crystal structures and atomic force microscopy (AFM) images of MutS-DNA complexes. In this model, MutS scans the DNA, bending the DNA as it moves in search of a mismatch. Upon location of a mismatched base pair, the specific amino acid contacts (Glu and Phe) are made with the mismatch, and specific kinking is induced (Drotschmann, Yang et al. 2001; Schofield, Brownewell et al. 2001). This conformation is the primary conformation observed in all MutS-DNA crystal structures (Figure 1.4) and is suggested in this model to serve as the initial mismatch recognition complex (IRC) (Wang, Yang et al. 2003; Kunkel and Erie 2005). The DNA then undergoes a conformational change to an unkinked MutS-DNA conformation (observed by AFM, Figure 1.6), where unbending acts as a mismatch recognition checkpoint and the precursor to ATP-hydrolysis and downstream repair events (Wang, Yang et al. 2003; Kunkel and Erie 2005). This model proposes that the mismatched DNA-MutS complexes in the unbent conformation are the ‘ultimate mismatch recognition complexes’ (URC) that signal repair.

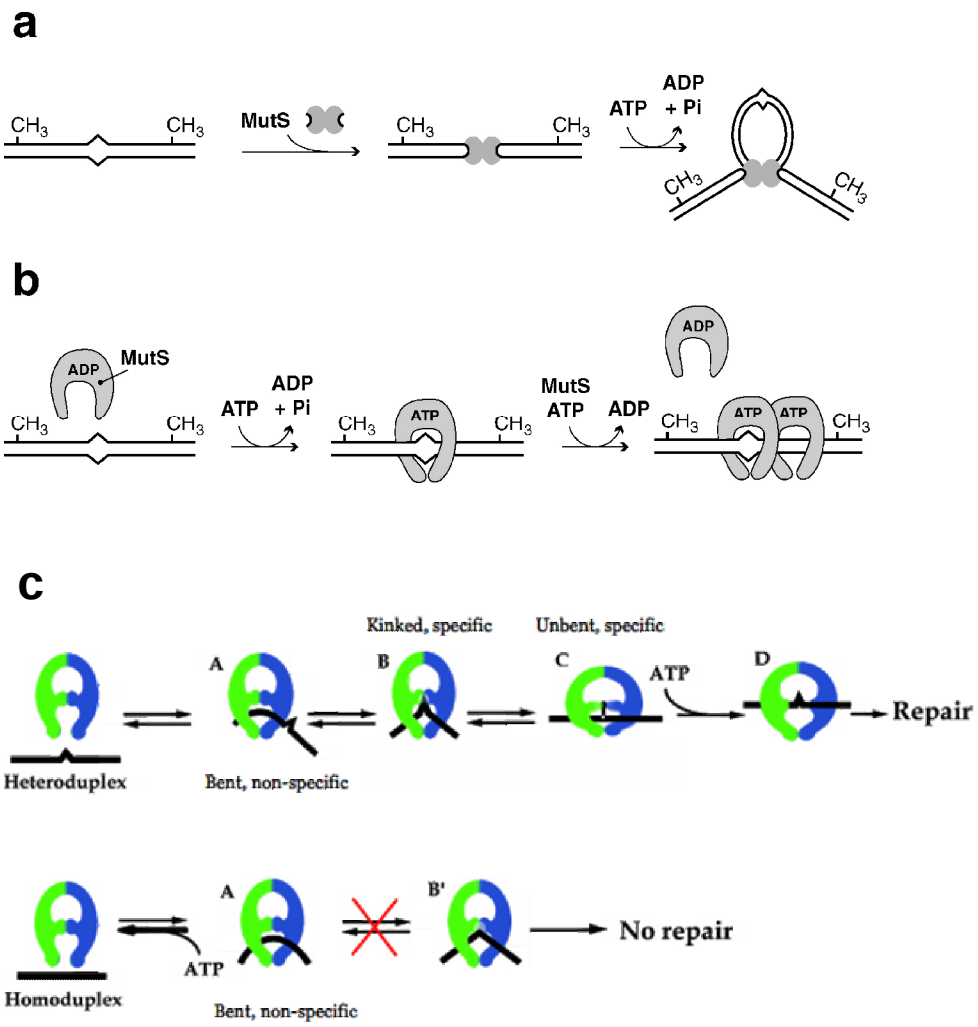

Figure 1.5 Models for mismatch repair initiation by MutS

DNA mismatch repair initiation models for mismatch recognition and repair signaling (Kunkel and Erie 2005). (A) The translocation model; (B) The molecular switch model; (C) The DNA bending model. MutS is shown shaded in gray in (A) and (B) and represented as a dimer in green and blue in (C).

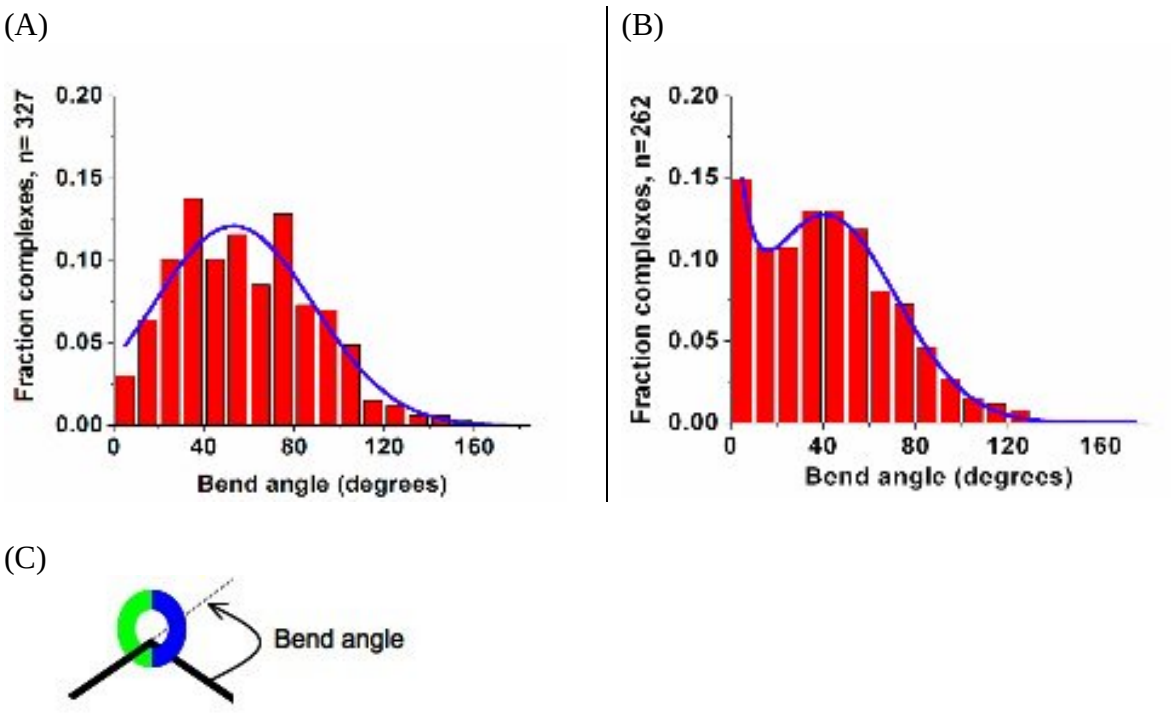

Figure 1.6 DNA bend angle distributions for MutS-DNA complexes determined by AFM

Distribution of DNA bend angles for *Taq* MutS bound to (A) homoduplex DNA sites, and (B) T-bulge mismatched DNA sites (Tessmer and Yang, et. al, submitted). Bend angle is defined as the distortion of the DNA from its linear form (C). Results revealed that while MutS induces bending in homoduplex DNA(~ 55°), it induces two unique conformations in mismatched DNA: bent (~ 42°) and unbent (~ 0°). The unbent conformation appears to be specific to the mismatch, suggesting that this conformation may play a role in mismatch verification and repair signaling, serving as the foundation of the DNA bending model of mismatch repair initiation.

Research scope and objectives

Structure-function-dynamics: A third dimension to studying MMR initiation by MutS

The foundation of the three models for MMR initiation is structure-function relationships between MutS and the DNA. The DNA bending model for mismatch repair initiation by MutS has suggested that MutS induces multiple conformations when bound to mismatched DNA. However, it is difficult to deduce the dynamic nature of DNA bending and unbending from crystal structures and AFM images alone. This model in particular offers motivation to develop additional techniques that would allow us to study the conformational dynamics of MutS-DNA complexes and use dynamics as a third dimension to understanding mismatch recognition and discrimination, as well as repair initiation and signaling. The goal of this dissertation was to develop fluorescence techniques that may be applied to learn more about the dynamic nature of MMR initiation by MutS and MutS homologs.

Dissertation objectives

The primary objectives of this work were to design fluorescently-labeled mismatched DNA substrates and develop fluorescence experimental protocols to measure: (1) mismatched DNA binding by MutS and MutS homologs and mutants; (2) mismatched DNA bending induced by MutS and MutS homologs and mutants using ensemble FRET; and, (3) dynamics and kinetics of mismatched DNA bending induced by MutS and MutS homologs and mutants using single-molecule fluorescence microscopy. Fluorescence anisotropy assays were designed to allow us to quickly and accurately measure the DNA binding properties of

MutS and observe how conserved mutations in MutS affect mismatched DNA binding. Ensemble and single-molecule FRET assays were further developed to reveal the dynamic nature of DNA bending induced by MutS and to offer insight into the nature of protein-DNA dynamics. The development of these tools with applications to DNA mismatch repair have opened the door to a host of experiments to explore DNA binding and dynamic bending of different mismatched and damaged DNA substrates, to analyze the role of point mutations in MutS in mismatched DNA binding and bending, and to relate the dynamics of protein-DNA interactions with biological function.

Achievements and Dissertation Overview

This research began with the goal of developing fluorescence techniques, both ensemble and high-resolution single-molecule methods, to measure the dynamics of mismatched DNA-MutS complexes, and this goal has been realized. During my research tenure, I have designed fluorescence assays, assembled a single-molecule fluorescence microscope, and performed a host of fluorescence experiments to monitor DNA binding and bending by mismatch repair protein MutS and MutS homologs and mutants.

The bulk of this work has been devoted to method and analysis development measuring mismatched DNA binding and bending induced by *Thermus aquaticus (Taq)* MutS (Chapter 2). In this work, I optimized experimental techniques to measure the conformational dynamics of single protein-DNA complexes and developed analysis methods to extract the number of unique conformational species, conformational transitions, kinetics, and DNA binding properties for MutS bound to multiple mismatches. I further applied these methods to study the DNA binding and bending properties of MutS with a mutation in one of

the conserved residues involved in mismatch recognition (Chapter 3) and to study the mismatch DNA binding and bending properties of eukaryotic MutS homolog yeast Msh2-Msh6 (Chapter 4). Experimental techniques and methods are also described in detail (Chapter 5).

The application of these experimental techniques and analysis methods will be employed to study the structure-function dynamics of protein-DNA complexes for years to come. This work has been established to study mismatch binding and conformational dynamics induced by MutS, however this research has been fruitful and robust with a host of potential applications for future work in DNA mismatch repair and DNA damage repair, among others.

References

Acharya, S., P. L. Foster, et al. (2003). "The coordinated functions of the E. coli MutS and MutL proteins in mismatch repair." Mol Cell **12**(1): 233-46.

Acharya, S., T. Wilson, et al. (1996). "hMSH2 forms specific mispair-binding complexes with hMSH3 and hMSH6." Proc Natl Acad Sci U S A **93**(24): 13629-34.

Alani, E. (1996). "The Saccharomyces cerevisiae Msh2 and Msh6 proteins form a complex that specifically binds to duplex oligonucleotides containing mismatched DNA base pairs." Mol Cell Biol **16**(10): 5604-15.

Allen, D. J., A. Makhov, et al. (1997). "MutS mediates heteroduplex loop formation by a translocation mechanism." Embo J **16**(14): 4467-76.

Ambrose, W. P., P. M. Goodwin, et al. (1999). "Single Molecule Fluorescence Spectroscopy at Ambient Temperatures." Chem. Rev. **99**: 2929-2956.

Au, K. G., K. Welsh, et al. (1992). "Initiation of methyl-directed mismatch repair." J Biol Chem **267**(17): 12142-8.

Biswas, I. and P. Hsieh (1996). "Identification and characterization of a thermostable MutS homolog from Thermus aquaticus." J Biol Chem **271**(9): 5040-8.

Blackwell, L. J., D. Martik, et al. (1998). "Nucleotide-promoted release of hMutSalpha from heteroduplex DNA is consistent with an ATP-dependent translocation mechanism." J Biol Chem **273**(48): 32055-62.

Buermeyer, A. B., S. M. Deschenes, et al. (1999). "Mammalian DNA mismatch repair." Annu Rev Genet **33**: 533-64.

Campbell, N., J. Reece, et al. (1999). Biology. Menlo Park, Addison Wesley Longman, Inc.

Clark, A. B., M. E. Cook, et al. (1999). "Functional analysis of human MutSalpha and MutSbeta complexes in yeast." Nucleic Acids Res **27**(3): 736-42.

Clegg, R. M. (1995). "Fluorescence resonance energy transfer." Curr Opin Biotechnol **6**(1): 103-10.

Cornish, P. V. and T. Ha (2007). "A survey of single-molecule techniques in chemical biology." ACS Chem Biol **2**(1): 53-61.

Deniz, A. A., S. Mukhopadhyay, et al. (2007). "Single-molecule biophysics: at the interface of biology, physics and chemistry." J R Soc Interface.

Drotschmann, K., W. Yang, et al. (2001). "Asymmetric recognition of DNA local distortion. Structure-based functional studies of eukaryotic Msh2-Msh6." J Biol Chem **276**(49): 46225-9.

Drummond, J. T., G. M. Li, et al. (1995). "Isolation of an hMSH2-p160 heterodimer that restores DNA mismatch repair to tumor cells." Science **268**(5219): 1909-12.

Forster, T. (1959). "Transfer Mechanisms of electronic excitation." Discussions of the Faraday Society **27**: 7-17.

Gell, C., D. Brockwell, et al. (2006). Handbook of Single Molecule Fluorescence Spectroscopy. New York, Oxford University Press.

Greenleaf, W. J., M. T. Woodside, et al. (2007). "High-Resolution, Single-Molecule Measurements of Biomolecular Motion." Annu Rev Biophys Biomol Struct **36**: 171-190.

Ha, T. (2001). "Single-molecule fluorescence methods for the study of nucleic acids." Curr Opin Struct Biol **11**(3): 287-92.

Harfe, B. D. and S. Jinks-Robertson (2000). "DNA mismatch repair and genetic instability." Annu Rev Genet **34**: 359-399.

Hsieh, P. (2001). "Molecular mechanisms of DNA mismatch repair." Mutat Res **486**(2): 71-87.

Isaacs, R. J., W. S. Rayens, et al. (2002). "Structural differences in the NOE-derived structure of G-T mismatched DNA relative to normal DNA are correlated with differences in (13)C relaxation-based internal dynamics." J Mol Biol **319**(1): 191-207.

Jiricny, J. and G. Marra (2003). "DNA repair defects in colon cancer." Curr Opin Genet Dev **13**(1): 61-9.

Kolodner, R. D. and G. T. Marsischky (1999). "Eukaryotic DNA mismatch repair." Curr Opin Genet Dev **9**(1): 89-96.

Kramer, B., W. Kramer, et al. (1984). "Different base/base mismatches are corrected with different efficiencies by the methyl-directed DNA mismatch-repair system of E. coli." Cell **38**(3): 879-87.

Kunkel, T. A. and D. A. Erie (2005). "DNA mismatch repair." Annu Rev Biochem **74**: 681-710.

Lahue, R. S. and P. Modrich (1988). "Methyl-directed DNA mismatch repair in Escherichia coli." Mutat Res **198**(1): 37-43.

Lakowicz, J. R. (1999). Topics in Fluorescence Spectroscopy. New York, Kluwe Academic/Plenum Publishers.

Lamers, M. H., A. Perrakis, et al. (2000). "The crystal structure of DNA mismatch repair protein MutS binding to a G x T mismatch." Nature **407**(6805): 711-7.

Lewin, B. (2000). Genes VII. Oxford, Oxford University and Cell Press.

Lieto, A. M., R. C. Cush, et al. (2003). "Ligand-receptor kinetics measured by total internal reflection with fluorescence correlation spectroscopy." Biophys J **85**(5): 3294-302.

Loeb, L. A., K. R. Loeb, et al. (2003). "Multiple mutations and cancer." Proc Natl Acad Sci U S A **100**(3): 776-81.

Modrich, P. (1989). "Methyl-directed DNA mismatch correction." J Biol Chem **264**(12): 6597-600.

Modrich, P. (1995). "Mismatch repair, genetic stability and tumour avoidance." Philos Trans R Soc Lond B Biol Sci **347**(1319): 89-95.

Modrich, P. and R. Lahue (1996). "Mismatch repair in replication fidelity, genetic recombination, and cancer biology." Annu Rev Biochem **65**: 101-33.

Moerner, W. E. and D. P. Fromm (2003). "Methods of single-molecule fluorescence spectroscopy and microscopy." Rev. Sci. Instrum. **74**(8): 3597-3619.

Natrajan, G., M. H. Lamers, et al. (2003). "Structures of Escherichia coli DNA mismatch repair enzyme MutS in complex with different mismatches: a common recognition mode for diverse substrates." Nucleic Acids Res **31**(16): 4814-21.

Obmolova, G., C. Ban, et al. (2000). "Crystal structures of mismatch repair protein MutS and its complex with a substrate DNA." Nature **407**(6805): 703-10.

Palombo, F., P. Gallinari, et al. (1995). "GTBP, a 160-kilodalton protein essential for mismatch-binding activity in human cells." Science **268**(5219): 1912-4.

Schneckenburger, H. (2005). "Total internal reflection fluorescence microscopy: technical innovations and novel applications." Curr Opin Biotechnol **16**(1): 13-8.

Schofield, M. J., F. E. Brownewell, et al. (2001). "The Phe-X-Glu DNA binding motif of MutS. The role of hydrogen bonding in mismatch recognition." J Biol Chem **276**(49): 45505-8.

Schofield, M. J. and P. Hsieh (2003). "DNA mismatch repair: molecular mechanisms and biological function." Annu Rev Microbiol **57**: 579-608.

Steinberg, I. (1971). "Long-range non-radiative transfer of electronic excitation energy in proteins and polypeptides." Annual Reviews of Biochemistry **40**: 83-114.

Stryer, L. (1978). "Fluorescence energy transfer as a spectroscopic ruler." Annu Rev Biochem **47**: 819-46.

Wang, H., Y. Yang, et al. (2003). "DNA bending and unbending by MutS govern mismatch recognition and specificity." Proc Natl Acad Sci U S A **100**(25): 14822-7.

Warren, J. J., T. J. Pohlhaus, et al. (2007). "Structure of the Human MutSalpha DNA Lesion Recognition Complex." Mol Cell **26**(4): 579-92.

Wazawa, T. and M. Ueda (2005). "Total internal reflection fluorescence microscopy in single molecule nanobioscience." Adv Biochem Eng Biotechnol **95**: 77-106.

Weiss, S. (1999). "Fluorescence spectroscopy of single biomolecules." Science **283**(5408): 1676-83.

Weiss, S. (2000). "Measuring conformational dynamics of biomolecules by single molecule fluorescence spectroscopy." Nat Struct Biol **7**(9): 724-9.

Wu, P. and L. Brand (1994). "Resonance energy transfer: methods and applications." Anal Biochem **218**(1): 1-13.

CHAPTER TWO

SINGLE-MOLECULE FRET STUDIES OF CONFORMATIONAL HETEROGENEITY IN PROTEIN-DNA COMPLEXES

Following dynamics of mismatched DNA-MutS complexes one molecule at a time

Introduction

A host of cellular functions are governed by protein-DNA conformational changes and, specifically, protein-induced DNA distortion. Proteins such as integration host factor (IHF), TATA binding protein, Cro protein, p53, and lactose repressor protein (Lac1) induce dramatic bending in host DNA to regulate gene expression (Lyubchenko, Shlyakhtenko et al. 1991; Erie, Yang et al. 1994; Morgan, Okamoto et al. 2005; Kuznetsov, Sugimura et al. 2006; Sugimura and Crothers 2006; Pan and Nussinov 2007). Some DNA repair enzymes such as DNA glycosylases and XPC-HR23B also bend their cognate DNA prior to excising or repairing the damaged bases (Janicijevic, Sugasawa et al. 2003; Walker, McCullough et al. 2006). In addition, protein-induced DNA bending has been linked to damage recognition and repair initiation by MutS, the enzyme that locates mismatches in base pairing and functions in signaling initiation of mismatch repair.

The crystal structures of MutS and MutSα bound to multiple different DNA mismatched bases and base insertion/deletions have all revealed that MutS and MutSα induce bending in the DNA at the mismatch site (Lamers, Perrakis et al. 2000; Obmolova,

Ban et al. 2000; Natrajan, Lamers et al. 2003; Warren, Pohlhaus et al. 2007). However, all of these structures are empirically similar even though different mismatches are repaired with different efficiencies *in vivo* (Kramer, Kramer et al. 1984). In an effort to gain additional insight into the correlation between DNA structure and MutS function, AFM studies were conducted to observe potential structural heterogeneity in mismatched DNA-MutS complexes. Results revealed that two unique DNA conformations were induced by MutS at the mismatched base: bent and unbent (Wang, Yang et al. 2003). From these results, the DNA bending model for mismatch repair initiation was proposed (Figure 1.5 B). This model suggests that MutS first locates a mismatch and induces bending at the mismatched site (Wang, Yang et al. 2003; Kunkel and Erie 2005). MutS then undergoes a conformational change to generate an unbent DNA-MutS conformation. This model proposes that the unbent DNA conformation serves as the precursor to ATP hydrolysis and functions in signaling repair (Wang, Yang et al. 2003).

Although the model proposed by AFM data predicts that the DNA conformations observed are in equilibrium, there is no evidence supporting a dynamic equilibrium between DNA bending and unbending induced by MutS. Furthermore, the model suggests that the DNA conformational pathway to repair is *first* DNA bending *followed by* DNA unbending, and formation of the unbent conformation is totally necessary for repair to proceed (Wang, Yang et al. 2003). These results posed a need to develop additional techniques that would allow the measurement of dynamic DNA conformational changes induced by MutS, and we established a single-molecule FRET assay to measure these dynamics.

Single-molecule FRET is a powerful technique that has gained popularity to study the dynamics and conformational fluctuations of individual biomolecules. Most recent work

using single-molecule FRET has focused on studying motor proteins, conformational changes or folding in single proteins or nucleic acids, or binding interactions between biomolecules (Deniz, Laurence et al. 2000; Kim, Nienhaus et al. 2002; Lipman, Schuler et al. 2003; Margittai, Widengren et al. 2003; Rhoades, Gussakovsky et al. 2003; Weninger, Bowen et al. 2003; Ha 2004; Rhoades, Cohen et al. 2004; Bowen, Weninger et al. 2005; Myong, Rasnik et al. 2005; Li, Augustine et al. 2007). We use single-molecule FRET to measure the conformational dynamics of single protein-DNA complexes. From this work, we have gained a better understanding of the dynamics of mismatched DNA-MutS complexes and have further established a relationship between these dynamics and mismatch recognition and repair signaling by MutS.

Results

Mismatch-specific DNA bending induced by MutS

We used single-molecule FRET to examine MutS-induced DNA conformational fluctuations. We measured the dynamics of three DNA substrates in the absence and presence of MutS: perfectly paired DNA (homoduplex) and two mismatched DNA substrates, either a GT base-base mismatch or a single base insertion (an unpaired thymine, T-bulge or ΔT). DNA substrates were modified with a FRET donor (TAMRA) and a FRET acceptor (Cy5) located 19 base pairs apart with the mismatch located approximately halfway between the two fluorophores (Figure 2.1 A-B). The DNA was biotinylated at one end for adsorption to the surface of a quartz slide for TIRF excitation (see Materials and Methods for details). DNA conformational changes may be measured for these substrates because upon

bending, changes in the relative proximity of the two dyes results in changes in the FRET efficiency between them (Figure 2.1 A).

For DNA in the absence of MutS, single-molecule FRET trajectories show that all molecules maintain a single conformation for the duration of the time trace (Figure 2.2). The distributions of FRET efficiencies for all three DNA substrates show a single peak centered at FRET ~ 0.24 with breadths of 0.15 to 0.16 (Figure 2.3 A-C, black cityscape). The breadths of the FRET efficiency distributions for these DNA substrates dictate the error in the measurement and the accuracy with which a single FRET conformation can be determined (Gell, Brockwell et al. 2006). These results indicate that the presence of a mismatched base pair or bulge does not significantly change the intrinsic bending properties of the DNA, consistent with other studies (Isaacs, Rayens et al. 2002; Natrajan, Lamers et al. 2003).

From the FRET efficiency distribution of free DNA, we are able to estimate the dynamic range of our experimental measurements. We estimated the FRET pair dye separation on our DNA substrates to be ~ 72 Å based on a helical model of DNA previously described (Clegg, Murchie et al. 1993; Jares-Erijman and Jovin 1996; Deniz, Dahan et al. 1999). We calculated an approximate Förster distance (R_o) of 59 Å for our FRET pair in this experimental design following the equation $FRET = 1 / (1 + (r / R_o)^6)$ (Lakowicz 1999). Our calculated Förster distance is consistent with previous studies that determined the Förster distance for this FRET pair to be 65 Å (± 5 Å) (Deniz, Dahan et al. 1999). By this estimation, we expect that our FRET assay is sensitive to changes in DNA bending ranging from 0° to ~ 120°.

(A)

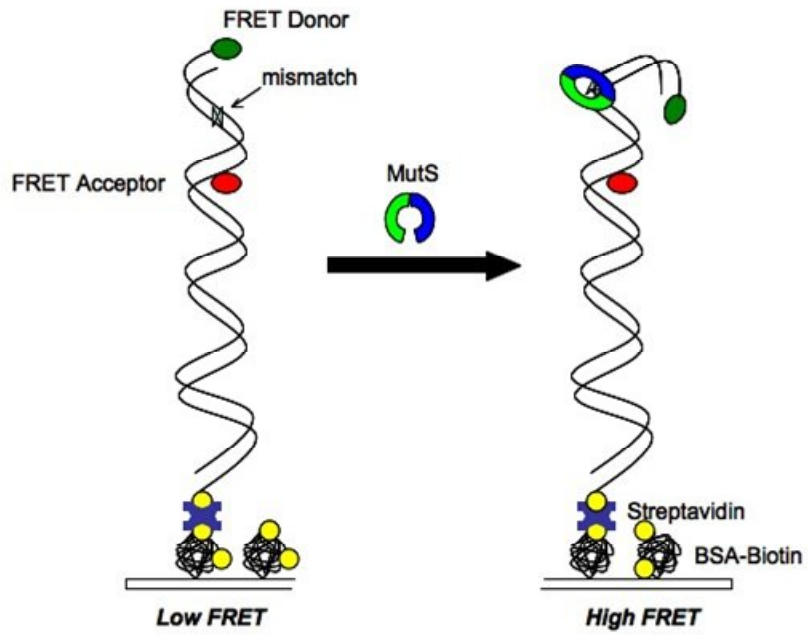

(B)

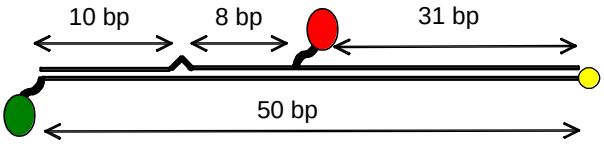

Figure 2.1 DNA substrates and experimental design for single-molecule FRET

Experimental design (A) and DNA substrate (B) to measure DNA bending induced by MutS. The FRET donor and acceptor dyes are shown in green and red, respectively, and the biotin is shown in yellow. Upon MutS-induced bending, the dyes become close in proximity and increased FRET is observed.

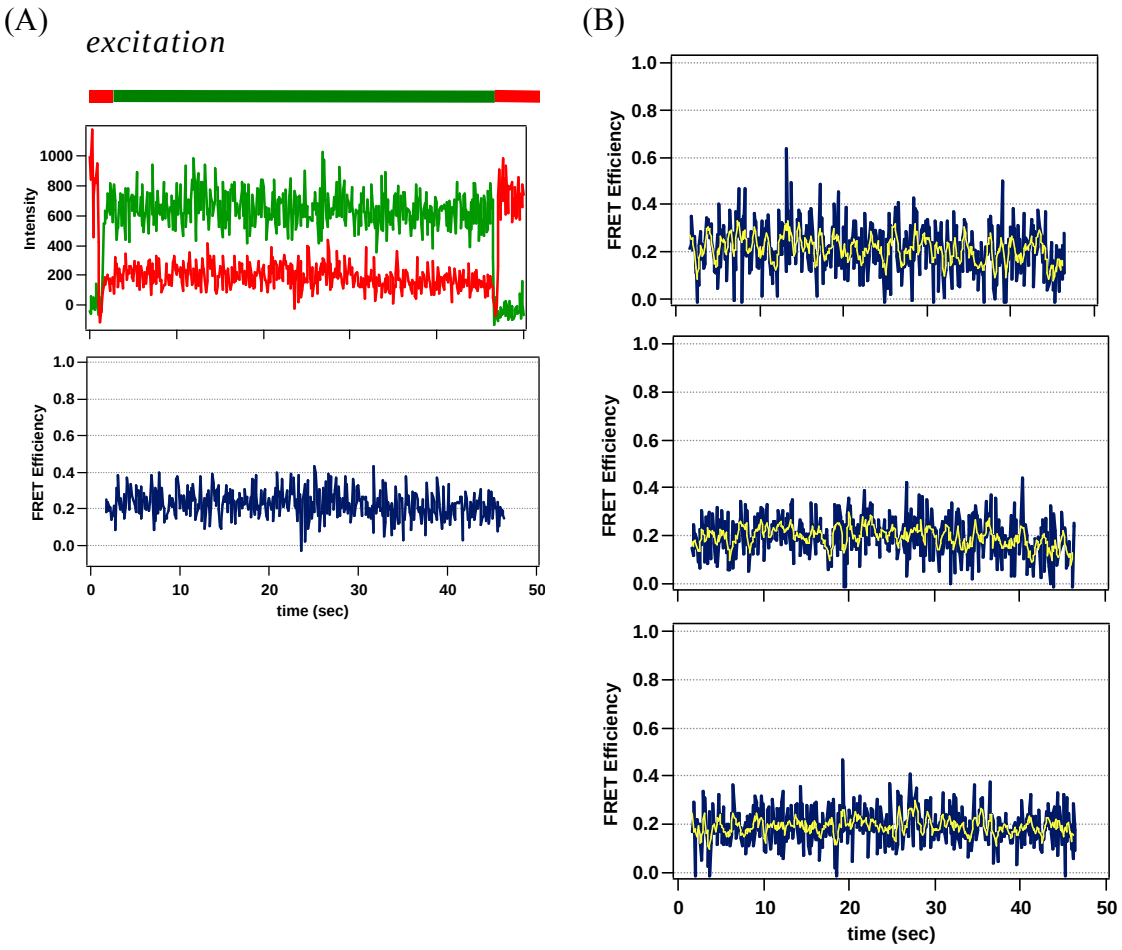

Figure 2.2 Sample single-molecule traces of mismatched DNA in the absence of MutS

(A) FRET donor and acceptor emission traces are shown in green and red, respectively. An alternating red and green laser excitation scheme is employed to select for single molecules and determine accurate backgrounds. Calculated FRET efficiencies as a function of time are shown in blue and are only calculated when the molecules are subjected to excitation by the green laser. (B) Additional FRET traces for single-molecules with added smoothing (5-point box average, yellow overlay).

In the presence of *Taq* MutS, dynamic DNA conformational fluctuations are observed for both ΔT and GT mismatched DNA substrates (Figure 2.4). Single-molecule FRET traces revealed that ΔT-MutS complexes displayed slow and infrequent conformational transitions, and the most stable DNA conformations were positioned at medium FRET values (less DNA bending, unbent or 'straight' DNA conformations) (Figure 2.4 A). In contrast, single molecule FRET traces of GT-MutS complexes displayed fast and frequent conformational changes among conformations at high FRET (more bent) and low FRET (less bent or unbent) (Figure 2.4 B). The distribution of FRET conformations sampled for these mismatched DNA-MutS complexes are shown in Figure 2.3 A-C (colored bars). These distributions show that ΔT-MutS complexes are shifted to lower FRET (less DNA bending) than GT-MutS complexes, consistent with AFM observations (Tessmer and Yang, submitted). Interestingly, single-molecule FRET trajectories reveal substantially different dynamics for MutS bound to each of these mismatched DNA substrates (Figure 2.4).

For homoduplex DNA, addition of 200 nM MutS did not result in any conformational transitions in the FRET time traces, and the FRET efficiency distribution of states is almost identical to that in the absence of MutS (Figure 2.3 C). Ensemble fluorescence measurements using the same substrate showed no effect on donor or acceptor emission with increasing MutS concentration, and no binding to this substrate was detected by fluorescence anisotropy (data not shown). These results imply that non-specific binding of MutS to the DNA is insignificant and has a minimal effect on the fluorescent properties of the dyes and the calculated FRET efficiencies. In contrast, MutS-induced DNA conformational changes at a mismatch are clearly distinguishable from the FRET signal of free DNA by shifts to

higher FRET efficiencies and by measurable conformational dynamics in the DNA molecules during the FRET time traces (Figures 2.3 and 2.4).

Multiple stable DNA conformations for ΔT-MutS complexes

Different DNA conformational changes are observed for MutS bound to two different mismatches. ΔT-MutS complexes are not very dynamic, with single FRET efficiencies (or DNA conformations) typically dominating each single-molecule FRET trace. Conformational changes were observed in a subset of molecules (~ 20% of the molecules measured), but transitions appeared to be slow and infrequent (Figure 2.4 A). The FRET efficiency distribution for all FRET states observed in 759 molecules is shown in Figure 2.3 A. The breadth of this distribution is larger than the breadth of the distribution of free DNA, suggesting that 2 or more DNA conformations comprise the distribution of FRET states sampled in ΔT-MutS complexes. In addition, we observe conformational transitions between multiple different FRET efficiencies further revealing that MutS induces a number of different conformations in ΔT DNA.

To characterize the different DNA conformations sampled and to record transition trajectories between these conformations from single-molecule FRET traces, we employed a custom analysis script to measure FRET transition edges based on a Gaussian derivative kernal (described in Appendix B, Figure B.1). This analysis provided us with each FRET efficiency (or DNA conformation) sampled in each single-molecule FRET trace as well the dwell time of each conformation and the sequence of transitions between different FRET states.

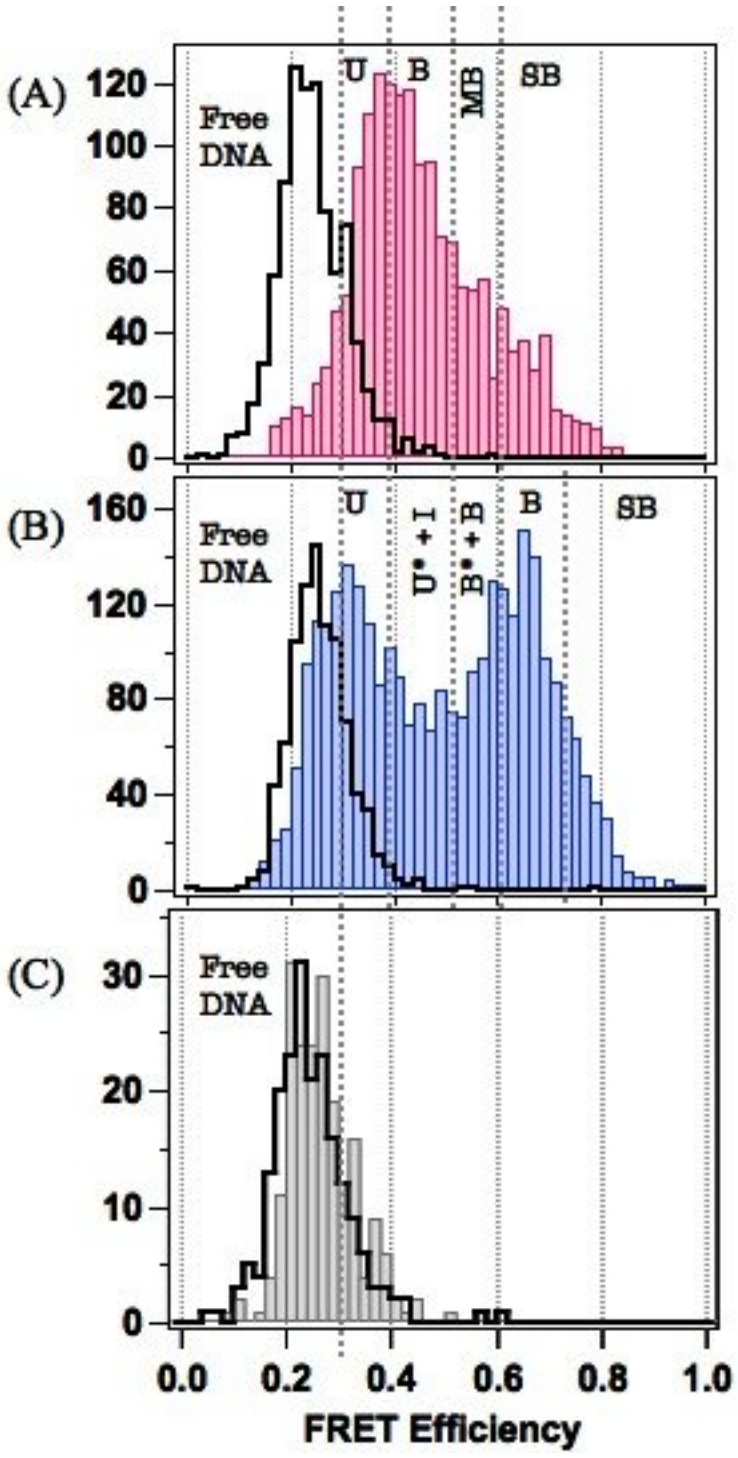
(A)
Free DNA
U
B
MB
SB
120
100
80
60
40
20
0
(B)
Free DNA
U
U* + I
B* + B
B
SB
160
120
80
40
0
(C)
Free DNA
30
20
10
0
0.0
0.2
0.4
0.6
0.8
1.0
FRET Efficiency

Figure 2.3 FRET efficiency distributions for mismatched DNA in the absence and presence of MutS

FRET efficiency distributions of conformations sampled for three DNA substrates in the absence of MutS (black cityscape) and presence of MutS (solid bars). (A) FRET distribution for all FRET values sampled in ΔT-MutS complexes (red bars, 1663 conformations sampled in 759 molecules). Of these molecules, 449 molecules were selected (of over 2500 total molecules observed) which displayed constant FRET conformations for 30 seconds or longer, and 310 molecules were selected which had 2 conformations or more observed in a single trace. Black cityscape represents the FRET distribution for free ΔT DNA (2169 molecules). (B) FRET efficiency distribution for all conformations sampled in 1095 GT-MutS molecules (blue bars, 2992 conformations). Recorded FRET efficiencies are averaged for at least 2 seconds of data collection or for the lifetime of the state (for molecules that undergo a conformational change, see Appendix B). Black cityscape represents the FRET distribution of free GT DNA (895 molecules). (C) FRET Efficiency distributions for homoduplex DNA in the absence (black cityscape, 200 molecules) and presence (gray bars, 200 molecules) of MutS. Recorded FRET efficiencies are averaged for at least 2 seconds (20 frames) of data collection. FRET efficiencies associated with unique DNA conformational species (***free DNA, U, B***, etc.), as determined by analysis of conformational transitions and lifetimes, are shown on the distributions.

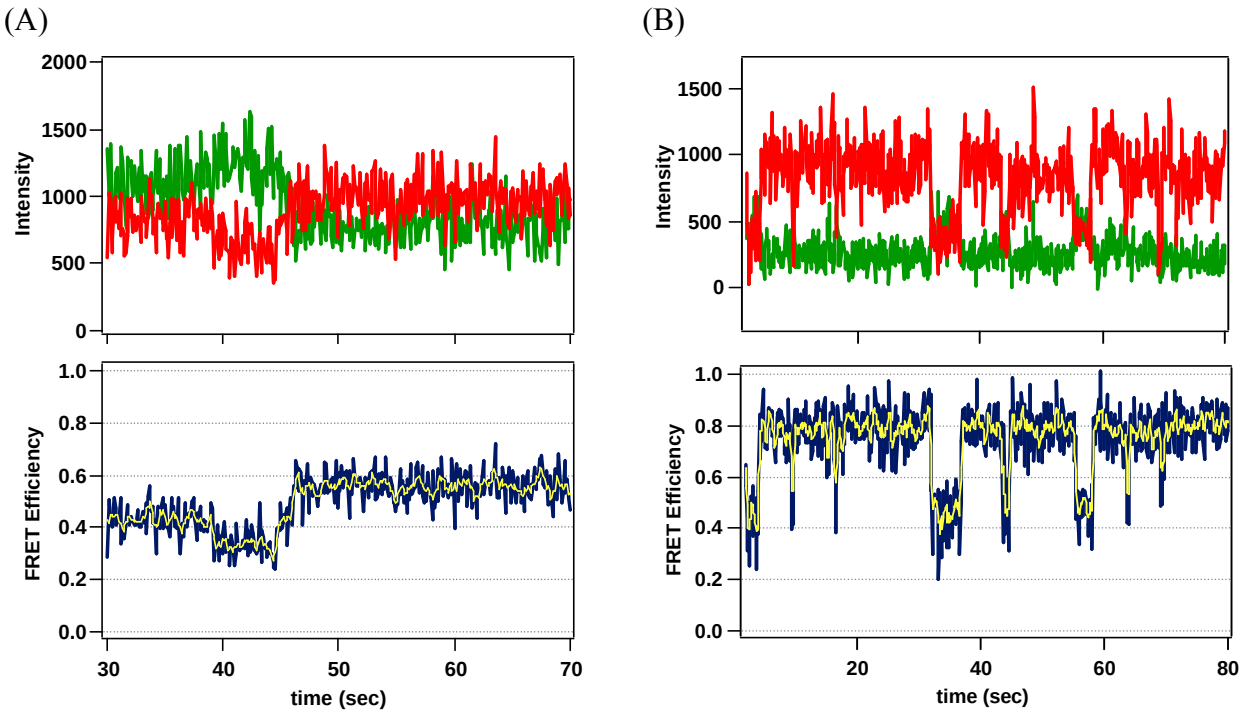

Figure 2.4 Single-molecule FRET trajectories for mismatched DNA in the presence of MutS

Sample individual molecule FRET trajectories for ΔT mismatched DNA (A) and GT mismatched DNA (B) in the presence of MutS with calculated corresponding FRET efficiencies. Traces show slow transitions between medium FRET states (less bent) in ΔT-MutS complexes (A), however considerable conformational changes between high FRET (more bent) and low FRET (less bent) states are observed for GT-MutS complexes (B).

From the transition sequences, we constructed a 3-dimensional histogram recording all conformational transitions from the starting FRET value ('FRET before transition', y-axis) to the next successive FRET value in the FRET trace ('FRET after transition', x-axis), with the number of times the event occurred plotted on the z-axis (Figure 2.5). In this transition density plot (TDP), density above the diagonal line represents DNA conformational transitions from higher to lower FRET (more bent to less bent), and density below the diagonal line represents DNA conformational transitions from lower to higher FRET (less bent to more bent). Density near the diagonal line represents small changes in FRET (or small changes in DNA bending), with the change in the bend angle increasing with distance away from the diagonal line.

The transition density distribution for all conformational transitions observed in ΔT-MutS complexes is shown in Figure 2.5 B. To extract individual transition peaks from this complex distribution, the TDP was deconvoluted into isolated areas of density that appeared to represent individual transition peaks (details on this analysis provided in Appendix B, Figure B.2). These isolated areas were each fit to two-dimensional Gaussian distributions as described (McKinney, Joo et al. 2006). 2D Gaussian fits for individual transitions were then summed to generate a transition density plot of the combined fits (Figure 2.5 C). The sum of the fitted distributions reproduced a 'smoother' version the raw transition density distribution, signifying that the 2D Gaussian fitting analysis was accurately representing the transition peaks.

The transition density distribution reveals transitions with FRET efficiencies that are the same as the FRET efficiencies observed for free DNA (at FRET ~ 0.24), suggesting that a contribution of transitions appear to be due to the binding and unbinding of MutS to the ΔT

DNA. To investigate the binding events directly, we employed a flow experiment to directly observe the conformations that are induced in the DNA immediately upon MutS binding. These transitions are shown as a transition density plot in Figure 2.5 D. The binding transition density reveals two peaks representing two unique conformations in which MutS binds ΔT DNA, located at FRET ~ 0.36 and FRET ~ 0.46 (denoted conformations ***U*** and ***B***). The relative difference in the densities of the two peaks shows that there is a higher probability of MutS binding ΔT into conformation ***U*** than conformation ***B***.

From the transition density plots in Figure 2.5, we isolated 7 conformational transitions in ΔT-MutS complexes as well as 1 binding transition. From the binding transition, we could infer at least 1 unbinding transition. A summary of these transitions is shown in Figure 2.5 E and Table 2.1. We did not isolate any binding transitions into conformation ***B*** in the TDP in Figure 2.5 B, further revealing that ***U*** is the preferred ΔT binding conformation. After binding, a host of transitions into more bent conformations (conformations denoted bent (***B)***, moderately bent (***MB)***, and super-bent (***SB***)) appear as the complexes approach dynamic equilibrium. The transition density plot also reveals that MutS typically unbinds ΔT from the unbent conformation ***U***. A schematic of these observations is shown in Figure 2.6.

A diverse population of conformations for MutS bound to a GT mismatch

GT mismatched DNA in the presence of MutS, in stark contrast to observations for ΔT-MutS, display large and sharp DNA conformational changes (Figure 2.3 B). Fluorescence time traces for these DNA complexes reveal a host of dynamics with the complexes switching between multiple conformations over a range of different FRET

(A)

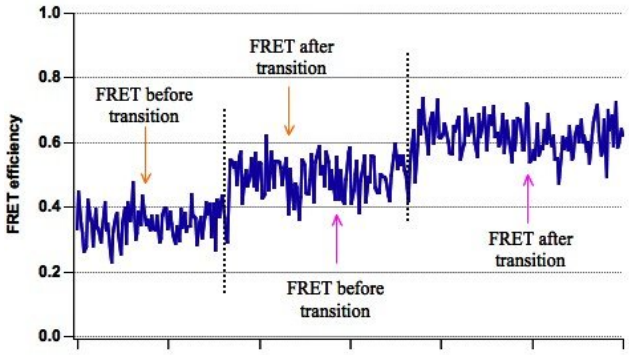
FRET efficiency
FRET after transition
FRET before transition
FRET after transition
FRET before transition

(B)

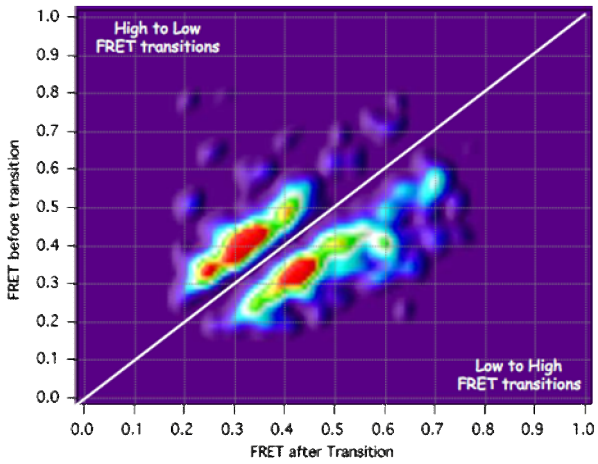
High to Low FRET transitions
Low to High FRET transitions
FRET before transition
FRET after Transition

(C)

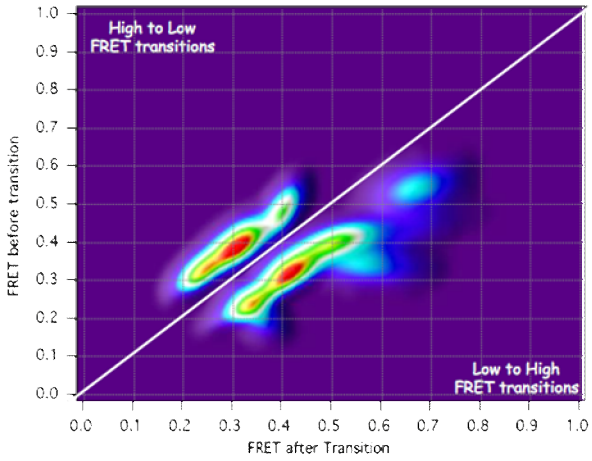
High to Low FRET transitions
Low to High FRET transitions
FRET before transition
FRET after Transition

(D)

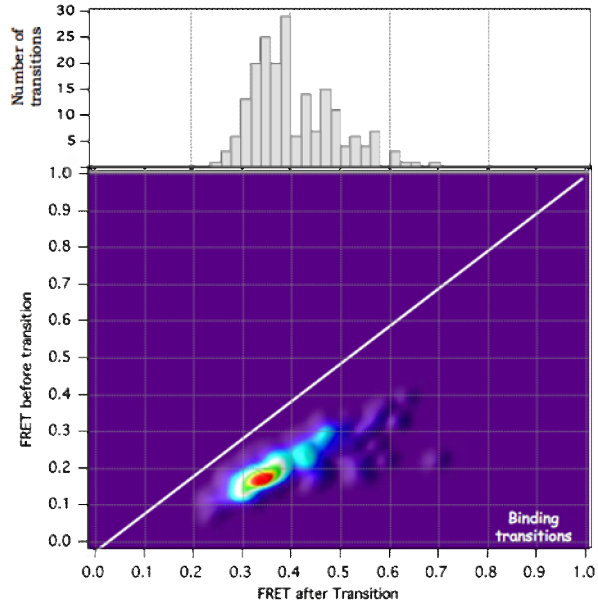
Number of transitions
Binding transitions
FRET before transition
FRET after Transition

(E)

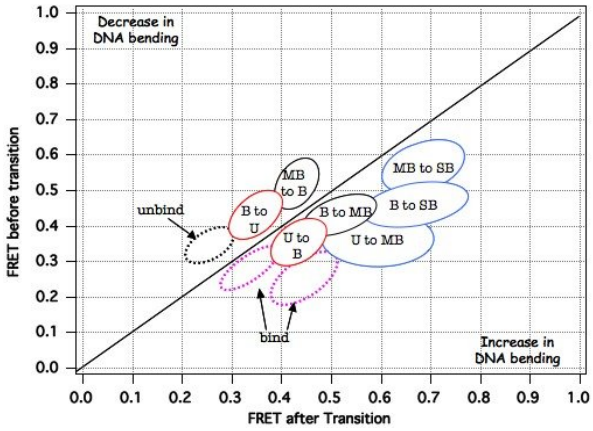
Decrease in DNA bending
unbind
B to U
MB to B
B to MB
MB to SB
B to SB
U to B
U to MB
bind
Increase in DNA bending
FRET before transition
FRET after Transition

Figure 2.5 Transition density plots representing conformational changes in ΔT-MutS complexes

(A) Sample FRET trace showing how FRET transitions were determined. Dotted lines in the trace represent transition edges determined by a Gaussian derivative kernal analyis (described in Appendix B). (B) TDP representing raw transition data obtained from single-molecule FRET trajectories (585 transitions observed in 310 molecules). 3D transition density plots were generated using ImageJ software with an interactive 3D surface plot plug-in (Image J 1.37v, NIH). This plug-in generates surface plots with dark to light color contrast and allows for some noise in the surface to be smoothed. (C) TDP representing the sum of the 2D gaussian fits of peaks observed in (B). (D) Binding transitions for MutS to a ΔT. The distribution of FRET efficiencies revealing the first conformation induced immediately upon MutS binding the ΔT DNA is shown as a 2D histogram above the TDP. (E) Schematic showing the unique conformational transitions observed for ΔT-MutS complexes. Red circles represent the most frequently observed transitions, while blue circles represent transitions in which the reverse transition was not observed. Blacked dashed circles represent unbinding events and magenta dashed circles represent binding events (Table 2.1). A schematic of these transitions is shown in Figure 2.6.

ΔT-MutS complexes		FRET before transition	FRET after transition	Transition probability
Conformational transitions	*U to B*	0.36	0.44	0.40
	U to MB	0.37	0.58	0.31
	B to U	0.42	0.34	0.47
	B to MB	0.43	0.52	0.26
	B to SB	0.45	0.62	0.26
	MB to B	0.51	0.43	0.48
	MB to SB	0.56	0.68	0.52
Binding transitions	*free to U*	0.26	0.37	~ 0.70
	*free to B**	0.29	0.46	~ 0.30
Unbinding transition	*U to free*	0.35	0.27	0.29

Table 2.1 FRET transitions observed in ΔT-MutS complexes

FRET values associated with conformational transitions, binding transitions, and unbinding transitions determined from 2-dimensional Gaussian fits of the deconvoluted transition density plots shown in Figures 2.5. Transition probabilities were calculated from the number of transitions comprising each 2D Gaussian peak.

* denotes binding transitions observed in the flow binding experiment but not observed in the conformational transitions of these complexes measured after MutS had been incubated with the ΔT DNA for many minutes (ranging from 5 to 60 minutes).

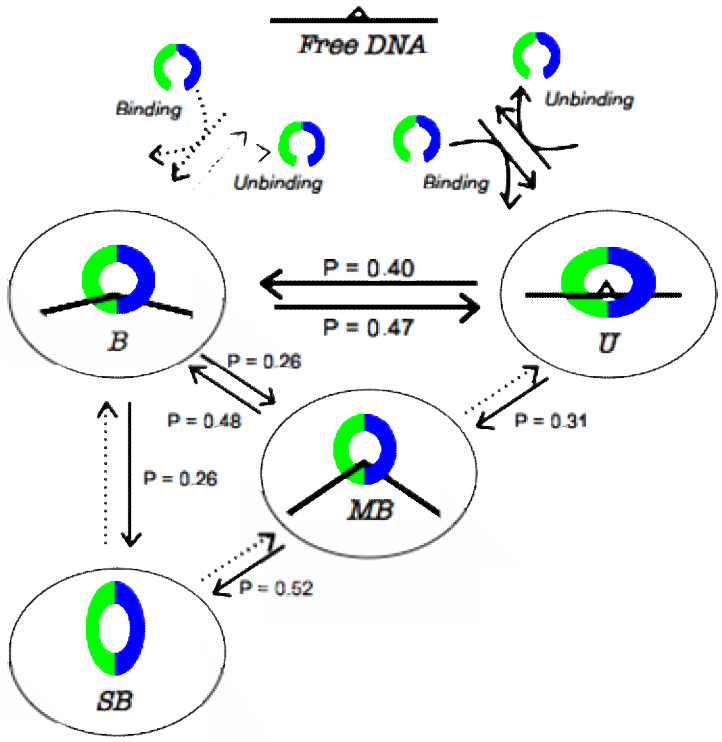

Figure 2.6 Model of ΔT-MutS conformational transitions

Model representing binding, unbinding, and conformational transitions determined from single-molecule ΔT-MutS FRET trajectories. MutS is represented as a dimer with subunits shown in blue and green. Transitions probabilities are shown. Dashed arrows represent transitions that were not observed in our experiment.

efficiencies. We extracted all FRET efficiencies, the dwell times at each FRET efficiency, and transition trajectories for these complexes from the Gaussian derivative kernal analysis mentioned previously (and described in Appendix B). A distribution of the FRET efficiencies sampled in 1095 individual GT mismatch DNA molecules in the presence of MutS is shown in Figure 2.3 B. At first glance, it appears that there are two dominant conformations, one centered at FRET ~ 0.31 (less DNA bending) and a second centered at FRET ~ 0.62 (more DNA bending).

The distribution of FRET efficiencies indicates that the conformations characterized by high FRET efficiencies (more bent) and low FRET efficiencies (less bent) occur with equal frequencies; however, analysis of the dwell times of each FRET efficiency reveals that they have substantially different stabilities. The relative stability of each FRET state is calculated as the product of the frequency of the state and the average time it resides in that state (or, its 'dwell time'). Comparison of the relative stabilities of all FRET efficiencies measured for GT-MutS complexes suggests that high FRET states (more bent) are more stable than lower FRET states (less bent) by approximately 5-fold (Figure 2.7 A). The observation of two dominant conformations, and the relative stabilities associated with them, are consistent with AFM results that revealed two distinct conformational states for GT-MutS complexes: bent and unbent (Wang, Yang et al. 2003).

In the GT-MutS FRET efficiency distribution, there is substantial overlap between the peak at low FRET efficiencies and the FRET efficiencies associated with free DNA (clearly represented by an overlap in the distributions shown in Figure 2.3 B). To determine if these FRET efficiencies represent free, unbound DNA or a 'straight' GT-MutS conformation, we measured the conformational dynamics of these complexes at a 10-fold reduced MutS

concentration. Under these conditions, we expected the average dwell time in the unbound state to increase by approximately 10-fold while the average dwell times associated with unique GT-MutS conformations to remain approximately the same.

The FRET efficiencies observed for GT mismatch DNA with a reduced concentration of MutS reveal a distinct increase in the relative stability of FRET efficiencies below FRET ~ 0.30, while all other stabilities appeared consistent with the distribution at 10-fold higher MutS concentration (Figure 2.7) (with the exception of an increase in stability observed for the high FRET peak at ~ 0.80, which will be discussed later). These results clearly demonstrate that FRET efficiencies below ~ 0.30 represent free, unbound GT mismatched DNA (consistent with observations for the ΔT DNA) while FRET efficiencies between 0.30 and 1.0 represent a number of GT-MutS complexes with varying degrees of DNA bending induced by MutS.

Conformational transitions of dynamic GT-MutS complexes

GT-MutS complexes display a heterogeneous distribution of FRET efficiencies (Figure 2.3 B), and a variety of transitions between multiple FRET efficiencies were observed (exemplified in Figure 2.4 B and 2.8 A). To better analyze these conformational transitions, we generated a 3D transition density plot for GT-MutS transitions (Figure 2.8 B). In contrast to ΔT-MutS transitions shown in Figure 2.5, clear transition peaks in the TDP for GT-MutS transitions were difficult to discern.

To deconvolute transition peaks in this TDP, we first performed a flow experiment to isolate transitions that were due to MutS binding the DNA. The transition density plot for GT binding transitions is shown in Figure 2.8 D. Unlike the ΔT substrate, MutS is capable of

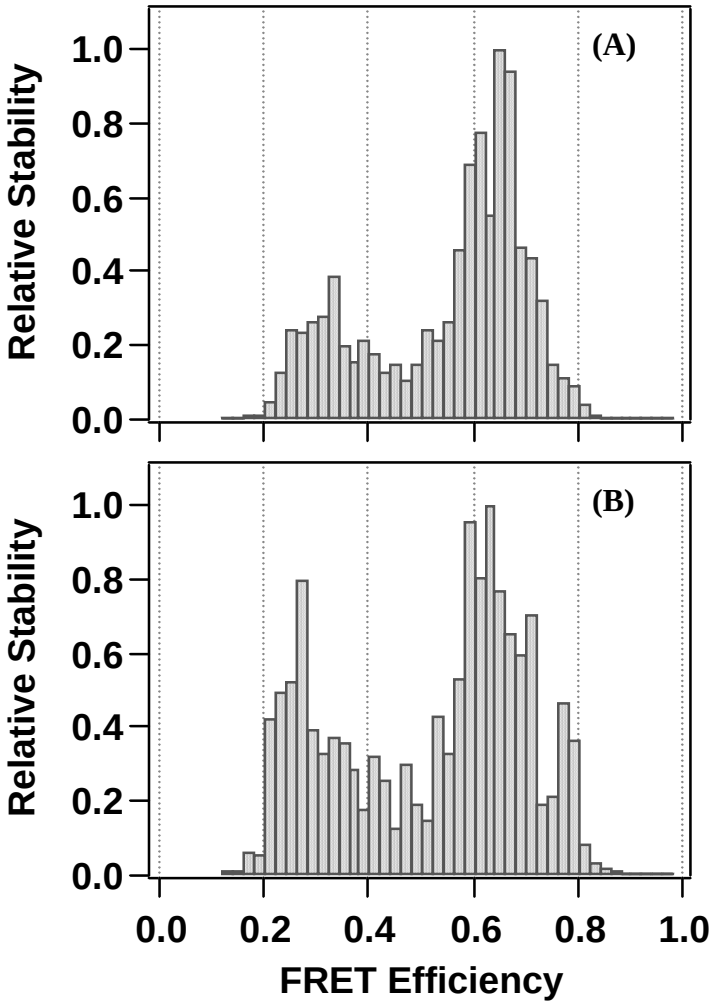

Figure 2.7 Relative stabilities of GT-MutS complexes

Relative stabilities determined for FRET states for GT-MutS complexes at (A) 200 nM MutS (2597 conformations), and (B) 20 nM MutS (1345 conformations). Stability was calculated from the product of the frequency of occurrence of the state and its average dwell time. FRET efficiency is separated by 0.02 bin widths in both distributions. Relative stability decreases to 0 before FRET 0.20 and after FRET 0.80 as expected due to reduced population densities at these FRET efficiencies.

binding the GT mismatch in multiple DNA conformations, with the bent state at FRET ~ 0.60 (conformation ***B***) serving as the preferred binding conformation.

With the binding transitions isolated from the transition density, we focused on separating additional conformational transitions comprising the TDP for GT-MutS complexes. To tease apart unique transitions, we fragmented the FRET efficiency distribution in Figure 2.3 B and characterized unique FRET states or DNA conformations by lifetime. This analysis is described in Appendix B (Figure B.3), and results are summarized in Table 2.2. Lifetime analysis reveals that 5 unique GT-MutS conformational species comprise the FRET efficiency distribution of states in addition to the FRET state associated with free, unbound DNA (Table 2.2).

From the results of the lifetime analysis, we returned to the transition density plot and sectored it by unique FRET states (or DNA conformations) distinguished by lifetime (analysis shown in Appendix B, Figure B.4). Transition density peaks within each FRET state were then fit to 2D Gaussian distributions similar to the analysis of ΔT-MutS transitions described. From this analysis, we isolated 12 conformational transitions among FRET states as well as 3 binding transitions and 4 unbinding transitions (Figure 2.8 E, Table 2.3). These Gaussian fits were summed together and regenerated the raw transition density plot, revealing that our peak fitting analysis provided an accurate estimate of the individual transition peaks (Figure 2.8 C). A schematic of all conformational transitions, binding, and unbinding events for GT-MutS are shown in Figure 2.9 and outlined in detail in Table 2.3.

Conformation	FRET state	Description	Lifetime at 200 nM MutS (τ, sec)	Lifetime at 20 nM MutS (τ, sec)
Free DNA	0 to 0.29	Free DNA	2.3	42
U	0.30 to 0.40	Low FRET, unbent GT-MutS complex	1.5	3
U*	0.41 to 0.50	Unbent, stable intermediate conformation	0.75	0.3
I	0.41 to 0.50	Stable intermediate conformation	6.6	11
B*	0.51 to 0.60	Bent, stable intermediate conformation	1.5	1
B	0.51 to ~0.75	High FRET, bent GT-MutS complex	15	10.5
SB	~0.75 to 1.0	Very high FRET, 'super'-bent GT-MutS complex	~15	~10.5

Table 2.2 GT-MutS conformations and corresponding FRET efficiencies and lifetimes

Unique GT-MutS conformations and corresponding FRET efficiencies (or FRET state) and lifetimes associated with those conformations at two different MutS concentrations.

(A)

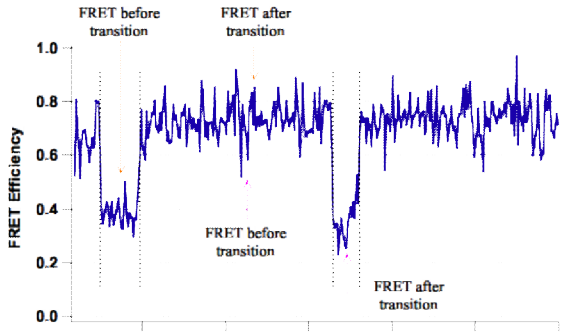
FRET before transition
FRET after transition
FRET Efficiency
1.0
0.8
0.6
0.4
0.2
0.0
FRET before transition
FRET after transition

(B)

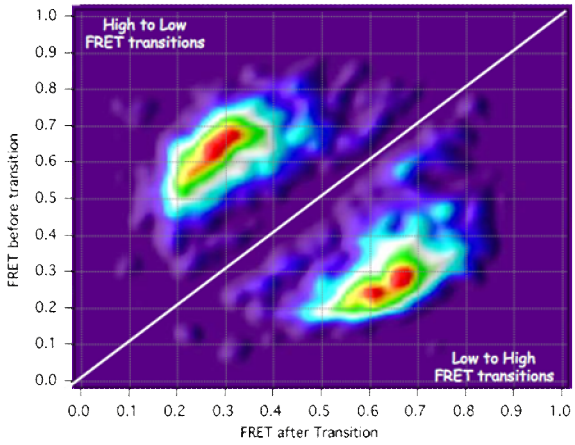
High to Low FRET transitions
Low to High FRET transitions
FRET before transition
FRET after Transition
0.0 0.1 0.2 0.3 0.4 0.5 0.6 0.7 0.8 0.9 1.0

(C)

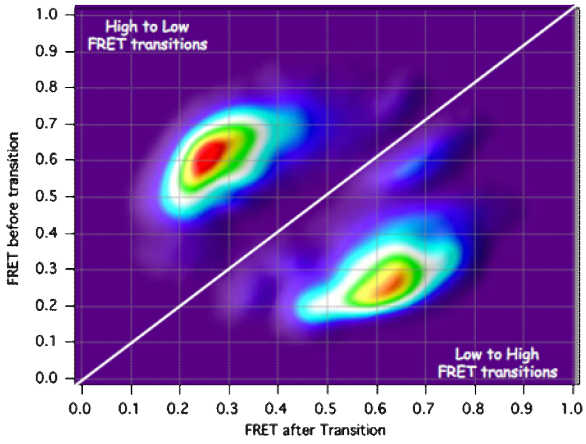
High to Low FRET transitions
Low to High FRET transitions
FRET before transition
FRET after Transition
0.0 0.1 0.2 0.3 0.4 0.5 0.6 0.7 0.8 0.9 1.0

(D)

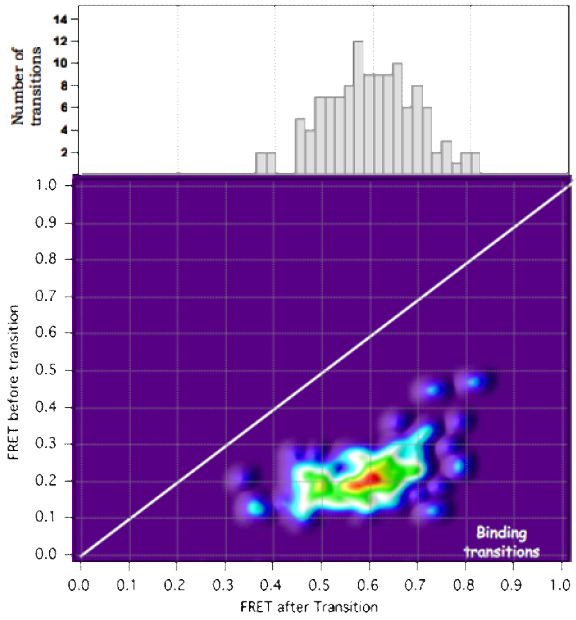
Number of transitions
14
12
10
8
6
4
2
Binding transitions
FRET before transition
FRET after Transition
0.0 0.1 0.2 0.3 0.4 0.5 0.6 0.7 0.8 0.9 1.0

(E)

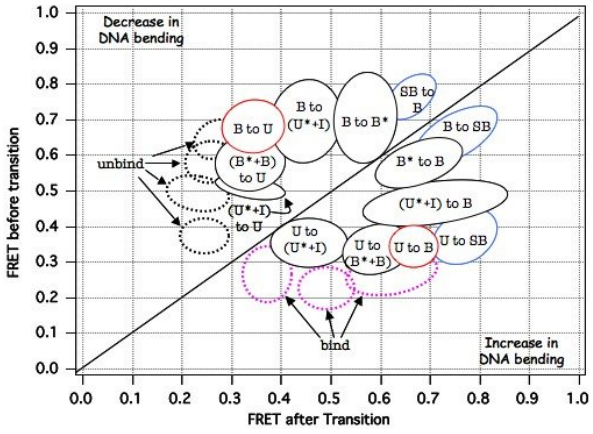
Decrease in DNA bending
Increase in DNA bending
B to U
B to (U*+I)
B to B*
SB to B
B to SB
unbind
(B*+B) to U
B* to B
(U*+I) to U
(U*+I) to B
U to (U*+I)
U to (B*+B)
U to B
U to SB
bind
FRET before transition
FRET after Transition
0.0 0.1 0.2 0.3 0.4 0.5 0.6 0.7 0.8 0.9 1.0

Figure 2.8 Transition density plots representing conformational changes in GT-MutS complexes

(A) Sample FRET trace showing how FRET transitions were determined. Dotted lines in the trace represent transition edges determined by a Gaussian derivative kernal analyis (described in Appendix B). (B) TDP representing raw transition data obtained from single-molecule FRET trajectories (3254 transitions in 701 molecules). (C) TDP representing the sum of the 2D Gaussian fits of peaks observed in (B). (D) Binding transitions for MutS to a GT. A distribution of the FRET efficiencies that are induced immediately upon MutS binding the GT is shown as a histogram above the TDP. (E) Schematic showing the unique conformational transitions observed for GT-MutS complexes. Red circles represent the most frequently observed transitions (apart from binding and unbinding transitions), while blue circles represent transitions in which the forward and reverse transitions are not observed with equal frequency. Blacked dashed circles represent unbinding events and magenta dashed circles represent binding events (Table 2.3). A schematic of these transitions is shown in Figure 2.9.

GT-MutS complexes		FRET before transition	FRET after transition
Conformational transitions	*U to (U*+I)*	0.34	0.46
	U to (B+B)*	0.33	0.58
	U to B	0.34	0.66
	U to SB	0.36	0.75
	(U+I) to U*	0.50	0.33
	(U+I) to B*	0.45	0.69
	(B+B) to U*	0.58	0.34
	(B+B) to B*	0.57	0.67
	B to U	0.67	0.34
	B to (U+I)*	0.69	0.45
	B to (B+B)*	0.69	0.56
	B to SB	0.64	0.72
	SB to B	0.75	0.65
Binding transitions	*free to U*	0.27	0.37
	free to (U+I)*	0.23	0.49
	free to (B+B+SB)*	0.27	0.61
Unbinding transitions	*U to free*	0.37	0.24
	(U+I) to free*	0.49	0.24
	(B+B) to free*	0.57	0.26
	B to free	0.64	0.28

Table 2.3 FRET transitions observed in GT-MutS complexes

FRET values associated with conformational transitions, binding transitions, and unbinding transitions determined from 2-dimensional Gaussian fits of the deconvoluted transition density plots shown in Figures 2.8. Further analysis on GT-MutS transitions were pursued to isolate unique conformations represented in the mixed FRET states. Those results are described in Appendix B and shown in Table 2.4.

(A)

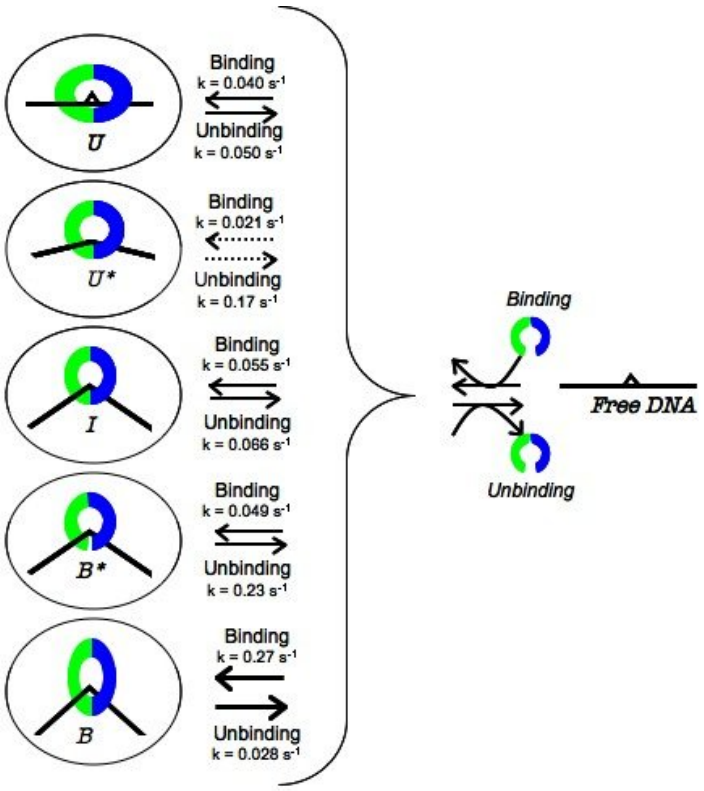
Binding
k = 0.040 s-1
Unbinding
k = 0.050 s-1
U
Binding
k = 0.021 s-1
Unbinding
k = 0.17 s-1
U*
Binding
k = 0.055 s-1
Unbinding
k = 0.066 s-1
I
Binding
k = 0.049 s-1
Unbinding
k = 0.23 s-1
B*
Binding
k = 0.27 s-1
Unbinding
k = 0.028 s-1
B
Binding
Free DNA
Unbinding

(B)

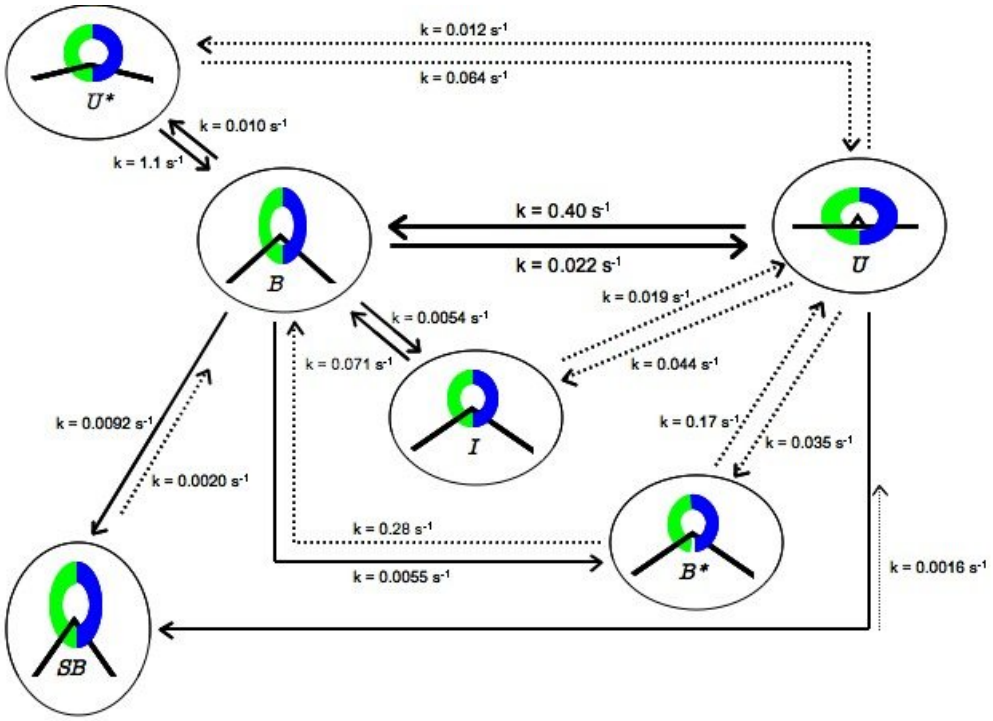
k = 0.012 s-1
k = 0.064 s-1
U*
k = 0.010 s-1
k = 1.1 s-1
B
k = 0.40 s-1
k = 0.022 s-1
U
k = 0.019 s-1
k = 0.0054 s-1
k = 0.071 s-1
k = 0.044 s-1
I
k = 0.0092 s-1
k = 0.0020 s-1
k = 0.17 s-1
k = 0.035 s-1
k = 0.28 s-1
k = 0.0055 s-1
B*
k = 0.0016 s-1
SB

Figure 2.9 Model of GT-MutS conformational transitions

Model representing binding and unbinding transitions (A) and conformational transitions (B) determined from single-molecule GT-MutS FRET trajectories. MutS is represented as a dimer with subunits shown in blue and green. The rate of each transition is shown. Dashed arrows represent transitions that were observed infrequently. A summary of these transitions is outlined in Tables 2.3 and 2.4.

Lifetimes of GT-MutS conformations dictate kinetic rates and free energy barriers of conformational transitions

We isolated 5 unique conformational species from lifetime analysis of all GT-MutS conformations sampled (Table 2.2, analysis described in Appendix B). The fit parameter $1/\tau$ from the lifetime decay curves represents the kinetic rate constant of that conformation, denoted k_{app}. This rate constant represents the sum of the rates of all transitions observed from this unique conformation. The kinetic rates of each conformational transition may therefore be determined by the following set of equations:

$$k_{U,app} = (k_{U\to U^*}) + (k_{U\to I}) + (k_{U\to B^*}) + (k_{U\to B}) + (k_{U\to SB}) + (k_{U\to free})$$
$$k_{U^*,app} = (k_{U^*\to U}) + (k_{U^*\to B}) + (k_{U^*\to free})$$
$$k_{I,app} = (k_{I\to U}) + (k_{I\to B}) + (k_{I\to free})$$
$$k_{B^*,app} = (k_{B^*\to U}) + (k_{B^*\to B}) + (k_{B^*\to free})$$
$$k_{B,app} = (k_{B\to U}) + (k_{B\to U^*}) + (k_{B\to I}) + (k_{B\to B^*}) + (k_{B\to SB}) + (k_{SB\to B}) + (k_{B\to free})$$

where k_{app} is the kinetic rate determined from the decay constant of the fit to frequency vs. dwell time (Figure B.3). The rates of individual transitions may be further determined by the probability of occurrence of that transition following the generic equation:

$$k_{x\to y} = k_{x,app} \times \left(\frac{P_{x\to y}}{P_{x\to all}} \right)$$

where *x* and *y* represent the 'start' and 'stop' conformations comprising the transition, respectively, and *P* represents the probability of that transition (determined from the number of times each transition was observed). These kinetic rates and the corresponding transition probabilities are outlined in Table 2.4.

We calculated the relative free energy barrier of each conformational transition by the relationship $\Delta G‡ = -RTlnk$, where R is the gas constant, T is the temperature of the experiment (298 K), and k is the kinetic rate constant of the transition. In addition, we used the kinetic rate constants to determine the equilibrium constants of individual transitions where $K_{eq} = k_f / k_r$ (Table 2.4). From these equilibrium constants, we calculated the relative free energies of each conformation ($\Delta\Delta G = -RTlnK_{eq}$).

From this analysis, we generated a free energy diagram of the conformational transitions of GT-MutS complexes (Figure 2.10 A-B) and a free energy diagram of the binding and unbinding transitions of GT-MutS complexes (Figure 2.10 C). In these diagrams, the location of the conformation in the y-dimension is determined by relative free energies of each conformation, with conformation ***B*** serving as the conformation from which the others are referenced. This conformation was selected as the reference state because it was the most stable and frequently observed of all conformations. For simplicity, the calculated relative free energies do not account for the concentration of MutS, however addition of this concentration factor would change the absolute free energies of the conformations but would not impose a difference in the *relative* free energies of the conformations. Curved lines represent the observed transitions among the various conformational states, and dotted lines represent the free energy transition barriers.

The free energy diagrams of the GT-MutS conformational transitions (Figure 2.10 A-B) have several interesting features. First, the relative free energy of transitions between bending and unbending (conformations ***U*** and ***B***) is lower than free energies of transitions among all other MutS-GT conformations. The probability of transitions between ***U*** and ***B*** is larger than the probability of any other conformational transition (Table 2.4), so it is not

surprising that this transition has a low transition barrier. A second interesting feature of the free energy diagram is the transition energy barrier between conformations ***B*** and ***U****. Results reveal an energy barrier of ~ 2.7 kcal/mol for conformational transitions from ***B*** to ***U****, however there is no transition barrier to overcome in the transition from ***U**** to ***B***. This result and the calculated kinetic rate constants confirm that conformation ***U**** probably represents an intermediate transition state between conformations ***U*** and ***B*** (Figure 2.10 A) as originally predicted from the low relative stability of this conformation (Figure 2.7). The free energy diagram also reveals that conformation ***SB*** is the most thermodynamically stable of all the conformations, but a high energy barrier must be overcome for complexes to transition into and out of this conformation (Figure 2.10 A and C, dashed lines).

The diagram in Figure 2.10 C documents the free energies determined from conformational changes induced at the GT mismatch upon MutS binding and unbinding. This diagram shows that binding and release from conformation ***B*** have the lowest transition barriers, and binding and release from conformation ***SB*** (which were not measured in our experiments) are expected to have the highest binding and unbinding transition barriers.

Comparative look at DNA dynamics induced by MutS in both mismatches

It is clear from the FRET efficiency distributions in Figure 2.3 that similar FRET conformations are sampled for both ΔT-MutS and GT-MutS complexes; however, the frequency of occurrence of these states (as well as their stabilities as dictated by average dwell times and frequency of occurrence) differ considerably between the two mismatches. The relative FRET distributions of states are consistent with the relative DNA bend angles observed by AFM for both of these mismatches (Tessmer and Yang, manuscript in preparation), however the FRET results clearly reveal substantial differences in

GT-MutS complexes		Transition rate (s^{-1})	Transition probability	$\Delta G‡$ (kcal/mol)		K_{eq}
Conformational transitions	*U to U**	0.012	0.018	2.6	U↔U*	0.19
	U to U*	0.064	0.048	1.6		
	U to I	0.044	0.066	1.8	U↔I	2.3
	I to U	0.019	0.12	2.3		
	*U to B**	0.035	0.053	2.0	U↔B*	0.21
	B to U*	0.17	0.25	1.0		
	U to B	0.40	0.59	0.54	U↔B	18
	B to U	0.022	0.28	2.3		
	U to B*	1.1	0.82	~ 0	U*↔B	110
	*B to U**	0.010	0.13	2.7		
	I to B	0.071	0.45	1.6	I↔B	13
	B to I	0.0054	0.067	3.1		
	B to B*	0.28	0.41	0.75	B*↔B	51
	*B to B**	0.0055	0.069	3.1		
	B to SB	0.0092	0.12	2.8	B↔SB	4.6
	SB to B	0.0020	~ 1	3.7		
	U to SB	0.13	0.20	1.2	U↔SB	*84†*
	SB to U	*0.0016†*	*~ 0†*	*3.8†*		
Binding/ Unbinding transitions	*free to U*	0.040	0.093	1.9	free↔U	4.0×10^6
	U to free	0.050	0.075	1.8		
	*free to U**	0.021	0.049	2.3	free↔U*	6.2×10^5
	U to free*	0.17	0.13	1.0		
	free to I	0.055	0.13	1.7	free↔I	4.2×10^6
	I to free	0.066	0.42	1.6		
	*free to B**	0.049	0.11	1.8	free↔B*	1.0×10^5
	B to free*	0.23	0.34	0.87		
	free to B	0.27	0.62	0.78	free↔B	4.7×10^7
	B to free	0.028	0.34	2.1		

Table 2.4 Kinetic rates and transition free energies of GT-MutS binding, unbinding, and conformational transitions

GT-MutS conformational transitions and binding/unbinding transitions and corresponding kinetic rates and transition free energies determined from 2-dimensional Gaussian fits of the deconvoluted transition density plots shown in Figures 2.8, B.5, and B.6. Transition probabilities were directly calculated from the number of transitions comprising each 2D transition peak. Transition free energies were calculated from the rate of transition (k) by the relationship: $\Delta G‡ = -RTlnk$, where R is the gas constant (1.987 cal/K·mol), and T is the temperature of the experiment (298 K). Equilibrium constants for DNA conformational transitions induced by MutS were determined by the ratio of the forward rate of the transition to the reverse rate of the transition. Equilibrium constants for binding and unbinding transitions represent the association constants and were determined by the ratio of the binding and unbinding kinetic rates, accounting for the total concentration of MutS in the sample (2×10^{-7} moles/L) where

$$K_{assoc} = \frac{k_{bind}}{k_{unbind} \cdot [MutS]}$$

However, for simplicity, the concentration of MutS was not included in the calculation of relative free energies represented in Figure 2.10.

†Transitions from ***SB*** to ***U*** were not directly observed, but the kinetic rate, transition free energy barrier, and equilibrium constant were calculated indirectly from other transition rates in the kinetic scheme.

(A)

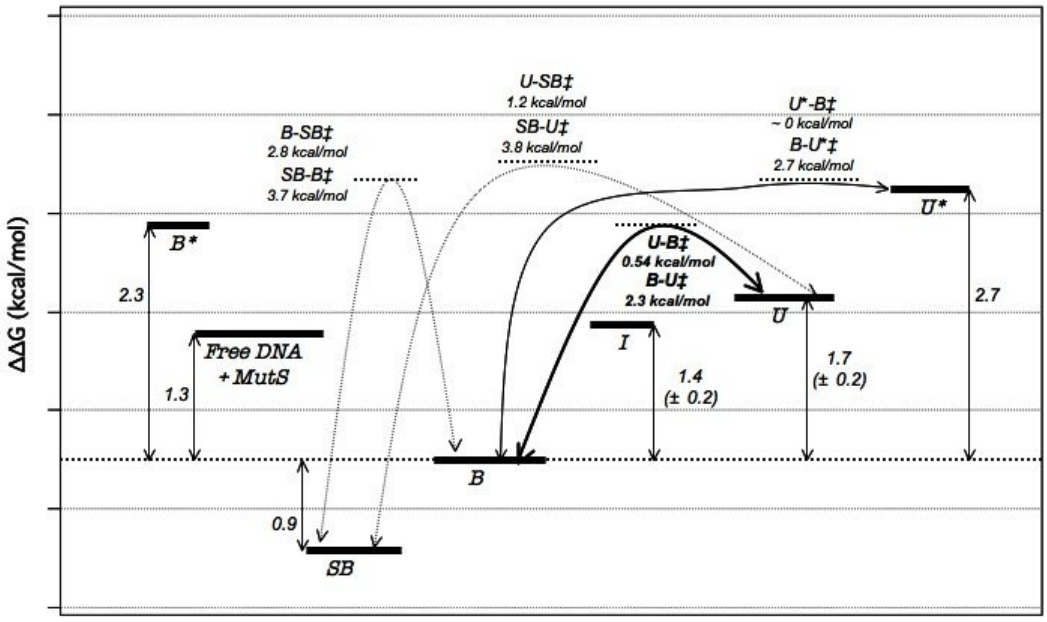
ΔΔG (kcal/mol)
U-SB‡
1.2 kcal/mol
SB-U‡
3.8 kcal/mol
B-SB‡
2.8 kcal/mol
SB-B‡
3.7 kcal/mol
U*-B‡
~ 0 kcal/mol
B-U*‡
2.7 kcal/mol
U*
B*
2.3
U-B‡
0.54 kcal/mol
B-U‡
2.3 kcal/mol
2.7
U
I
Free DNA
+ MutS
1.3
1.4
(± 0.2)
1.7
(± 0.2)
B
0.9
SB

(B)

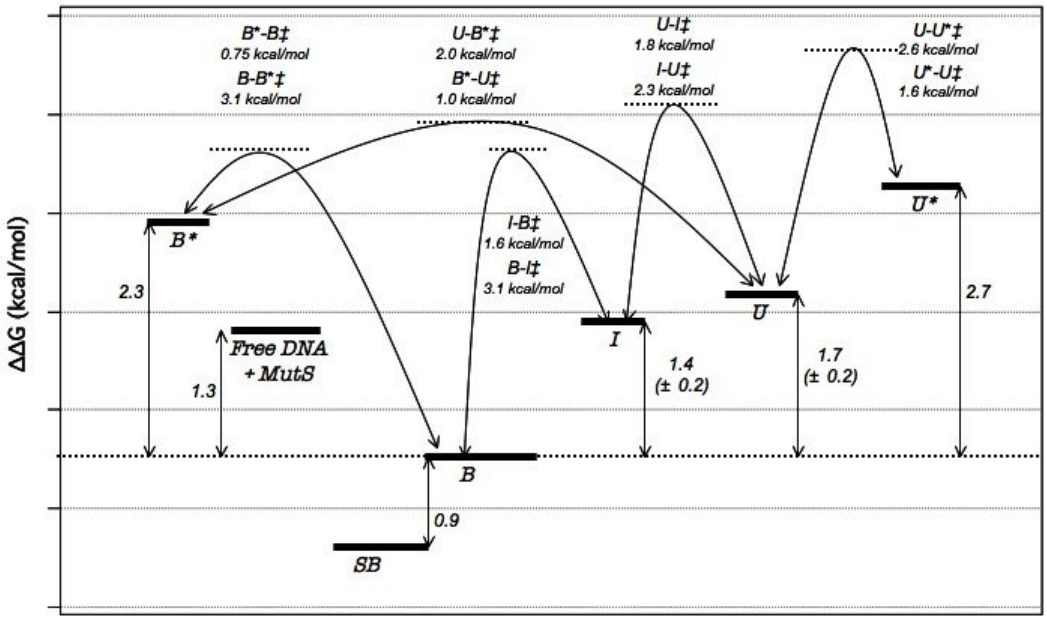
ΔΔG (kcal/mol)
B*-B‡
0.75 kcal/mol
B-B*‡
3.1 kcal/mol
U-B*‡
2.0 kcal/mol
B*-U‡
1.0 kcal/mol
U-I‡
1.8 kcal/mol
I-U‡
2.3 kcal/mol
U-U*‡
2.6 kcal/mol
U*-U‡
1.6 kcal/mol
U*
B*
I-B‡
1.6 kcal/mol
B-I‡
3.1 kcal/mol
2.3
2.7
U
I
Free DNA
+ MutS
1.3
1.4
(± 0.2)
1.7
(± 0.2)
B
0.9
SB

(C)

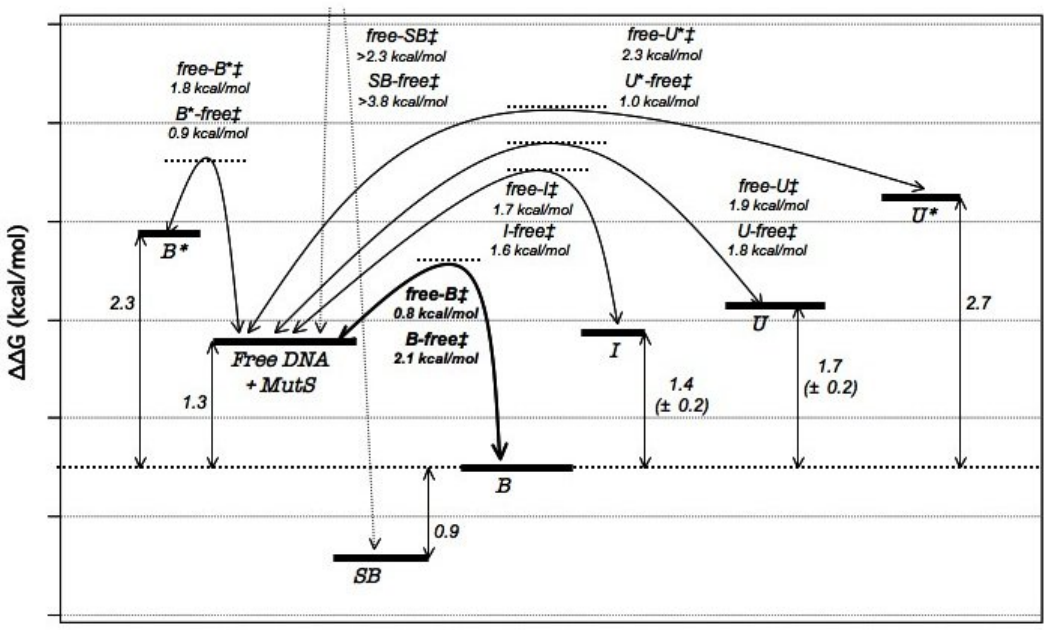

Figure 2.10 Free energy diagrams of GT-MutS conformational and binding transitions

Free energy diagrams representing the conformational transitions of GT-MutS complexes (A-B) and the binding transitions of MutS to GT mismatched DNA (C). The relative free energies of the states are shown in reference to the most frequently observed conformation ***B***. Deviations in the relative free energies of conformations ***U*** and ***I*** were determined by calculated differences in the relative free energies of these states with respect to every other state. All other relative free energies between each of these states were consistent with the relative free energies with respect to conformation ***B*** (to within ~ 0.1 kcal). The relative free energy of free DNA does not account for MutS concentration, therefore it is denoted as '*Free DNA + MutS*' on this free energy diagram.

conformational stability and dynamics between these two mismatched DNA substrates when bound by MutS.

The most apparent difference between the conformational transitions of ΔT-MutS and GT-MutS complexes are represented in FRET traces from individual molecules (Figure 2.4) and documented in the transition density plots for the two substrates (Figures 2.5 and 2.8). Most transitions for ΔT-MutS lie close to the diagonal line in the TDP (Figure 2.5). These results show that the DNA conformational changes in ΔT-MutS complexes are smaller, with less overall bending induced in the DNA (judged by the FRET efficiency distribution shifted to intermediate FRET values) and smaller changes in DNA bend angles induced upon conformational transitions. In contrast, the GT-MutS transitions lie distant from the diagonal line in the TDP revealing that these complexes undergo large conformational transitions between bent and unbent DNA conformations (Figure 2.8). In these complexes, more drastic changes in DNA bending are observed.

An additional difference between these two mismatches is the conformations that MutS induces immediately upon binding. MutS preferentially binds a GT mismatch in conformation ***B*** (stable bent conformation), consistent with AFM observations and models that predict DNA bending is the first conformation induced at a mismatch by MutS (Wang, Yang et al. 2003; Kunkel and Erie 2005). However, MutS prefers to bind ΔT in a relatively unbent conformation (conformation ***U***), contradictory to the suggested models for mismatch recognition. Unbinding transitions follow a similar pathway, where MutS appears to unbind ΔT from conformation ***U*** but will unbind GT from any conformation (***U, U*, I, B*,*** and ***B***). These discrepancies may be the result of differences in the transition barriers between conformations for the two mismatches.

Discussion

Crystal structures of MutS(α)-mismatched DNA complexes and *in vitro* and *in vivo* assays of mismatch binding and repair by MutS are incongruent in that all the structures are relatively the same while the relative binding affinities and repair efficiencies of these mismatches are quite different (Kramer, Kramer et al. 1984; Su, Lahue et al. 1988; Lamers, Perrakis et al. 2000; Obmolova, Ban et al. 2000; Natrajan, Lamers et al. 2003; Warren, Pohlhaus et al. 2007). DNA kinking in the crystal structures was suggested to function in mismatch recognition, but differences in mismatch binding affinities and repair efficiencies reveal that there is a dimension to mismatch repair not revealed by crystal structures alone. Studies using atomic force microscopy uncovered a second, unbent DNA conformational state induced by MutS at a mismatch, suggesting that there may be an equilibrium between bending and unbending that is essential for mismatch repair to proceed (Wang, Yang et al. 2003). These results provided a static image of MutS-DNA complexes and left unanswered questions regarding the equilibrium between these DNA conformational species and the dynamic conformational path to mismatch repair.

To observe these dynamics and explore questions correlating DNA structural changes to mismatch repair function, we employed single-molecule FRET to measure conformational dynamics of mismatched DNA in the presence of MutS. Results revealed distinct differences in DNA dynamics for MutS bound to two different mismatches suggesting that DNA dynamics might have a part in governing mismatch repair.

An energy landscape perspective on protein-DNA conformational transitions

The DNA conformational dynamics for MutS bound to two mismatches revealed that protein-DNA complexes form a number of unique conformations of different relative stabilities that can dynamically interconvert. We used the kinetic rates determined for binding, unbinding, and conformational transitions in the dynamic GT-MutS complexes to investigate the free energy landscape of these protein-DNA complexes. We calculated the relative free energies of all GT-MutS conformations and determined the free energy barriers of the transitions. The resulting free energy diagram revealed a significantly 'bumpy' free energy landscape dominated by a number of local free energy minima, varied transition barriers among conformations, and a thermodynamically stable conformation that is long-lived and from which transitions are not frequently observed (Figure 2.10). The free energy diagram showed that conformational transitions favored a pathway between conformations ***B*** and ***U*** (DNA bending and unbending, respectively), although a host of other conformational transitions, with relatively higher transition energy barriers, were apparent (Figure 2.10 B).

A number of features of the free energy diagram are similar to protein-folding free energy landscapes (Frauenfelder, Sligar et al. 1991; Onuchic, Luthey-Schulten et al. 1997; Onuchic and Wolynes 2004). For example, transition intermediates on path between bending and unbending were observed (conformations ***U**** and ***B****), and a stable conformational intermediate state was isolated (conformation ***I***). In addition, a thermodynamically stable conformation (***SB***), similar to 'frustration' or 'mini-traps' in protein folding that may slow-down the folding process (Stein 1985; Onuchic and Wolynes 2004), was isolated in the free energy analysis of conformational transitions of GT-MutS complexes. These similarities

may suggest that the rules that govern protein folding free energy landscapes (or folding funnels) may also govern the energy landscapes of protein-DNA conformational dynamics.

We were unable to perform the complementary free energy analysis on ΔT-MutS complexes because all conformations were very stable and long-lived, and conformational transitions between states were not frequently observed. However, we are able to make inferences about the free energy of these complexes in comparison to the GT-MutS complexes. First, MutS has an ~ 8-fold tighter binding constant to a ΔT than a GT mismatch (5 nM vs. 40 nM) (Yang, Sass et al. 2005), suggesting that the relative free energies of the ΔT-MutS complexes are ~ 2 kcal/mol more thermodynamically stable than GT-MutS complexes.

Second, ΔT-MutS complexes sample the unbent DNA conformation with longer lifetimes than observed for GT-MutS complexes. This observation might suggest that the transition free energy barrier between bending and unbending is lower for these complexes in comparison to the GT-MutS complexes. Reduced transition barriers may also explain why we observe MutS binding ΔT in the unbent conformation while preferentially binding GT in a bent conformation (Figures 2.5 D and 2.8 D). Prior studies have suggested that bending is the initial mismatch recognition conformation for both insertion-deletion and base-base mismatches (Wang, Yang et al. 2003) (Tessmer and Yang, submitted). Our observation of MutS binding GT in a bent conformation is consistent with this suggestion, and we observe some binding to ΔT in a bent conformation. However, the majority of binding events of MutS to ΔT appear to directly induce the unbent conformation. This result suggests that the initial recognition of these mismatches (formation of the bent conformation) may be the

same, but the transition barrier from the bent conformation to the unbent conformation may be lower for a ΔT-MutS complex relative to a GT-MutS complex.

This suggestion is consistent with studies of base-flipping enzymes that induce DNA bending prior to DNA unbending/base-flipping (Krosky, Song et al. 2005; Youngblood and Reich 2006). Studies of the DNA binding properties of uracil DNA glycosylase (UDG) showed that bases lacking base pair hydrogen bonding interactions (such as the ΔT) are more flexible and have lower bending free energies, and the transition barrier through the bent conformation and into an unbent, base-flipped conformation was reduced by ~ 3 kcal/mol (Krosky, Song et al. 2005). In addition, conformational transitions observed in DNA methyltransferase EcoRI showed that the enzyme-DNA complex transitions from a bent DNA conformation to an unbent, base-flipped DNA conformation within the first 25 ms after binding the DNA (Youngblood and Reich 2006). Therefore, it is extremely possible that MutS binds the ΔT in the bent state but immediately undergoes a conformational change into the unbent state, a transition occurring faster than the time resolution of our experiment. This analysis suggests that MutS induces bending in both of these mismatches upon recognition, but the transition barrier to unbending is different between the two mismatches.

Free energies of transitions and asymmetry in transition density plots reveal that protein-DNA complexes may form kinetic traps

The free energy diagram for GT-MutS conformational transitions reveals that DNA conformation ***SB*** is thermodynamically stable, with a high energy barrier to transition from this conformation (~ 3.7 to 3.8 kcal/mol, Figure 2.10). A similar conformation was also observed in ΔT-MutS complexes, represented by conformation ***SB*** in the pathway (Figure

2.5 E and Figure 2.6). These super-bent conformations are significantly long-lived for both mismatches and rarely transition back into one of the other conformations, implying that these super-bent protein-DNA complexes may be thermodynamically stable kinetic traps.

This phenomenon is similar to what has been observed in synthesizing enzymes such as RNA polymerase (Erie 2002) and in RNA or protein folding pathways (Treiber and Williamson 1999; Chen and Clark 2004), where formation of a non-productive conformation halts the function/folding of the biomolecule. This super-bent, trapped conformation in mismatched DNA-MutS complexes may simulate a cell cycle checkpoint, either recognized as a non-productive conformation that awaits the release of MutS from the DNA to begin the mismatch recognition cycle all over again or serving as a conformation that MutS induces to signal a specific action in the cell. The latter hypothesis will be addressed later.

This super-bent kinetic trap prevents mismatched DNA-MutS complexes from ever reaching conformational equilibrium. The rate of transitions from this conformation is much slower than the dissociation rate of MutS; therefore, MutS would unbind the DNA before a conformational equilibrium would be reached. The difference in the relative stability of this conformation at two different MutS concentrations (Figure 2.7) confirms this observation. If every MutS-DNA conformation reached equilibrium, the relative stabilities of each of these conformations would be the same at both concentrations.

Protein-DNA dynamics predict a mechanism for mismatch recognition and signaling by MutS

MutS is a protein with an incredibly difficult job. Not only must this enzyme locate 12 different DNA base pair mismatches as well as DNA base insertion/deletions, but it must

also signal repair of these mismatches *and* serve as a cell cycle checkpoint in signaling apoptosis in response to DNA damage (Salsbury, Clodfelter et al. 2006). The DNA bending model, combining mismatched DNA-MutS crystal structures with AFM data, was the first to suggest that different DNA conformations were induced by MutS at a mismatch and each served a different purpose. In this model, DNA bending functions in mismatch recognition while DNA unbending functions in signaling repair (Wang, Yang et al. 2003).

Our observations here reveal that these protein-DNA complexes are even more diverse than the DNA bending model predicts. Not only do we observe DNA bending and unbending, but we have isolated a number of intermediate conformations as well as a very stable super-bent conformation. So, why does MutS induce so many different DNA conformations? It is possible that the heterogeneous population of DNA conformations induced by MutS contributes to mismatch recognition and helps MutS to distinguish between every type of DNA mismatch. Different degrees of DNA bending and different dynamics between conformational states may, in a way, serve as a mismatch 'fingerprint'.

In addition, the sampling of a number of different DNA conformations, ranging from unbent (***U***) to super-bent (***SB***), may serve as a signaling mechanism employed by MutS either to induce initiation of mismatch repair (signaled by ***U***?) or to induce cell-cycle arrest (signaled by ***SB***?).

The DNA bending model predicts that the unbent DNA conformation is necessary for repair to be signaled by MutS. The protein-DNA dynamics shown here for MutS bound to two different mismatches imply that both the frequency *and* the lifetime in which the unbent DNA conformation is sampled may govern repair signaling and may affect how *efficiently* the mismatch is repaired. Our results reveal that, when considering the timescale of cellular

mismatch repair response, both of these mismatched DNA-MutS complexes sample the unbent conformation sufficiently. This high frequency of DNA unbending would explain why both of these mismatches are repaired well *in vivo*. However, we have observed an increase in the conformational dynamics of mismatched DNA bound by a mutant MutS protein that is deficient in mismatch repair *in vivo* (results described in Chaper 3). These results begin to clarify the DNA bending model by suggesting that both the frequency and lifetime of the unbent DNA conformation could play a role in mismatch repair signaling by MutS.

The DNA bending model for mismatch repair initiation by MutS further proposed that the unbent conformation is one in which the mismatched base is flipped-out of the DNA helix (Wang, Yang et al. 2003). Although no direct evidence of base-flipping induced by MutS has been shown, our observations of bending and unbending kinetics and the corresponding free energies of the two different mismatched DNA-MutS complexes, one with the mismatched base participating in hydrogen bonding base pair interactions (GT) and one with the mismatch base lacking such interactions (ΔT), are consistent with base-flipping schemes observed for UDG and EcoRI (Krosky, Song et al. 2005; Youngblood and Reich 2006). While these results do not directly prove that the mismatch base has been flipped, they offer support to the hypothesis that MutS is capable of base-flipping (Krosky, Song et al. 2005; Youngblood and Reich 2006).

The detailed protein-DNA dynamics shown here offer an additional dimension to studying mismatch repair initiation by MutS. These results support the DNA bending model of mismatch repair initiation by MutS and suggest that the kinetics of conformational sampling offers an important contribution to mismatch recognition and repair by MutS.

Conclusions

For the first time, we have observed the conformational dynamics of mismatched DNA-MutS complexes. Our results reveal that while crystal structures predict similar conformations of MutS bound to different types of DNA mismatches, the dynamics of these complexes vary depending on the nature of the mismatch. A number of different DNA conformations ranging from super-bent (***SB***) to unbent (***B***) were observed in addition to a host of intermediate conformations. These results reveal that protein-DNA complexes are incredibly heterogeneous and dynamic, and the unique conformations sampled and the fluctuations between these conformations may serve an important biological role. The dynamics observed in mismatched DNA-MutS complexes may serve as a mechanism to help MutS discriminate between different mismatches, and conformational sampling may be important in governing mismatch repair and/or apoptotic signaling by MutS.

Acknowledgements

I would like to thank Dr. Keith Weninger for an invaluable collaboration that helped to bring all the experiments described in this chapter to life. I would like to thank Brian Eastwood for writing the analysis script used to extract transition sequences and lifetimes from individual FRET traces. I want to thank my coworker Cherie Lanyi for writing the script used to generate 3D transition density distributions and for very thoughtful discussions about the kinetic analysis of these data. Finally, I want to thank my boss Dorothy for having faith that I could accomplish these single-molecule fluorescence experiments and for many many many thoughtful and valuable discussions of this work.

Materials and Methods

DNA substrates

Fluorescently-labeled single-stranded oligonucleotides and complementary strands were purchased HPLC-purified from Integrated DNA Technologies. DNA substrates contained TAMRA oligonucleotide (5'-Biotin-TGTCGGGGCTGGCTTAAGGTGTGAA ATACCTCATCTCGAG CGTGCCGATA-TAMRA-3') anealed to one of the following: ΔT (5'-TATCGGCACGTCTCGAGATG-Cy5-3'); GT (5'-TATCGGCACGTTCGAGATG-Cy5-3'); or GC (5'-TATCGGCACGCTCGAGATG-Cy5-3'), to create dsDNA fragments containing a +1 T-bulge (ΔT), a GT base mismatch, and GC homoduplex dsDNA, respectively. Oligonucleotides were annealed in buffer containing 20 mM Tris-HCl pH 7.8, 100 mM NaOAc, and 5 mM $MgCl_2$ in a 1:1 ratio at 65°C for 20 minutes followed by slow cooling. When the temperature reached 55°C, an additional complementary strand was added and annealed to complete the duplex DNA substrate (5-AGGTATTTCACAC CTTAAGCCAGCCCCGACA-3'). The substrate was allowed to slowly cool to room temperature.

Slide and sample preparation

Quartz microscope slides and flow channels were prepared as previously described (Weninger, Bowen et al. 2003). Slides were thoroughly cleaned by 15 minute incubations in a bath sonicator in the following series of solvents: alconox, acetone, ethanol, 1 M KOH, ethanol, 1 M KOH. Slides were rinsed and stored in water and flamed under a propane torch to dry immediately before use. Flow channels were created in the slides by adhering a no. 1.5 coverslip to the slide using Scotch double-sided tape as a spacer. Edges were sealed with

epoxy. DNA samples were inserted into the channels through small holes drilled in the quartz slide prior to cleaning.

The quartz surface was treated first with biotinylated-BSA (1 mg/mL, 5 minute incubation) followed by streptavidin (0.1 mg/mL, 5 minute incubation), similar to methods previously described (McKinney, Freeman et al. 2005). Annealed biotinylated, fluorescently-labeled, mismatched DNA was added to the treated surfaces at 10 to 30 pM for 5 minutes, and the unbound DNA was rinsed away with chilled buffer. Samples were imaged at room temperature in the above buffer with the addition of enzymatic oxygen scavenging components (2% glucose, 1% β-mercaptoethanol, 0.1 mg/mL glucose oxidase, 0.025 mg/mL catalase) to enhance fluorophore lifetime and with the addition of triplet state quencher cyclooctatetraene (~50 μM) to reduce dye blinking.

MutS was allowed to bind the DNA for at least 5 minutes prior to image collection. Images were collected both in the presence and absence of MutS.

TIR Fluorescence Microscopy

Data were collected using a prism-type total internal reflection fluorescence (TIRF) laser microscope as described (Weninger, Bowen et al. 2003; Bowen, Weninger et al. 2005). Two lasers were directed onto the prism, one at 532 nm to directly excite the donor dye (TAMRA) and one at 635 nm to directly excite the acceptor dye (Cy5) at the quartz-solution interface. Fluorescence emission was collected through a 60x 1.2 NA water immersion objective and split by a 645 nm dichroic mirror into short and long wavelength paths. These paths were filtered for TAMRA and Cy5 emissions using HQ 585/70 and HQ 700/75 bandpass filters, respectively. The respective spectrally-resolved emissions were relayed as

dual images on an intensified charge-coupled device camera. Images were exposed at 10 frames per second and collected using software written in-house.

Data Analysis

Observed intensities of single-molecules were integrated with software written in-house to obtain individual fluorescence emission time traces as described (Bowen, Weninger et al. 2005). Emission traces were background corrected, and FRET efficiencies were calculated from the respective donor and acceptor emissions as $E = (I_A)/(I_D + I_A)$, where I_D and I_A are the intensities of the donor fluorophore and acceptor fluorophore, respectively.

Dynamic FRET efficiency traces were analyzed using an edge detection algorithm to separate step transitions and calculate the average FRET efficiency and lifetime of each step as well as the sequence of FRET transitions. Step edges were convolved with a derivative Gaussian kernel as originally described by Canny (Canny 1986), and scale spaces were modified with varying thresholds to eliminate false edges due to noise in the data. Average FRET efficiencies were calculated for each step, with the first and last 1-4 frames at the transition edges being excluded from the average. Lifetimes at each FRET efficiency and transition sequences were also extracted. Additional details on experimental materials and methods are outlined in Appendix B and Chapter 5.

References

Bowen, M. E., K. Weninger, et al. (2005). "Single-molecule studies of synaptotagmin and complexin binding to the SNARE complex." Biophys J **89**(1): 690-702.

Canny, J. (1986). "A computational approach to edge detection." IEEE Trans. Pattern Anal. Mach. Intell. **8**(6): 679-698.

Chen, Y. R. and A. C. Clark (2004). "Kinetic traps in the folding/unfolding of procaspase-1 CARD domain." Protein Sci **13**(8): 2196-206.

Clegg, R. M., A. I. Murchie, et al. (1993). "Observing the helical geometry of double-stranded DNA in solution by fluorescence resonance energy transfer." Proc Natl Acad Sci U S A **90**(7): 2994-8.

Deniz, A. A., M. Dahan, et al. (1999). "Single-pair fluorescence resonance energy transfer on freely diffusing molecules: observation of Forster distance dependence and subpopulations." Proc Natl Acad Sci U S A **96**(7): 3670-5.

Deniz, A. A., T. A. Laurence, et al. (2000). "Single-molecule protein folding: diffusion fluorescence resonance energy transfer studies of the denaturation of chymotrypsin inhibitor 2." Proc Natl Acad Sci U S A **97**(10): 5179-84.

Erie, D. A. (2002). "The many conformational states of RNA polymerase elongation complexes and their roles in the regulation of transcription." Biochim Biophys Acta **1577**(2): 224-39.

Erie, D. A., G. Yang, et al. (1994). "DNA bending by Cro protein in specific and nonspecific complexes: implications for protein site recognition and specificity." Science **266**(5190): 1562-6.

Frauenfelder, H., S. G. Sligar, et al. (1991). "The energy landscapes and motions of proteins." Science **254**(5038): 1598-603.

Gell, C., D. Brockwell, et al. (2006). Handbook of Single Molecule Fluorescence Spectroscopy. New York, Oxford University Press.

Ha, T. (2004). "Structural dynamics and processing of nucleic acids revealed by single-molecule spectroscopy." Biochemistry **43**(14): 4055-63.

Isaacs, R. J., W. S. Rayens, et al. (2002). "Structural differences in the NOE-derived structure of G-T mismatched DNA relative to normal DNA are correlated with differences in (13)C relaxation-based internal dynamics." J Mol Biol **319**(1): 191-207.

Janicijevic, A., K. Sugasawa, et al. (2003). "DNA bending by the human damage recognition complex XPC-HR23B." DNA Repair (Amst) **2**(3): 325-36.

Jares-Erijman, E. A. and T. M. Jovin (1996). "Determination of DNA helical handedness by fluorescence resonance energy transfer." J Mol Biol **257**(3): 597-617.

Kim, H. D., G. U. Nienhaus, et al. (2002). "Mg2+-dependent conformational change of RNA studied by fluorescence correlation and FRET on immobilized single molecules." Proc Natl Acad Sci U S A **99**(7): 4284-9.

Kramer, B., W. Kramer, et al. (1984). "Different base/base mismatches are corrected with different efficiencies by the methyl-directed DNA mismatch-repair system of E. coli." Cell **38**(3): 879-87.

Krosky, D. J., F. Song, et al. (2005). "The origins of high-affinity enzyme binding to an extrahelical DNA base." Biochemistry **44**(16): 5949-59.

Kunkel, T. A. and D. A. Erie (2005). "DNA mismatch repair." Annu Rev Biochem **74**: 681-710.

Kuznetsov, S. V., S. Sugimura, et al. (2006). "Direct observation of DNA bending/unbending kinetics in complex with DNA-bending protein IHF." Proc Natl Acad Sci U S A **103**(49): 18515-20.

Lakowicz, J. R. (1999). Topics in Fluorescence Spectroscopy. New York, Kluwe Academic/Plenum Publishers.

Lamers, M. H., A. Perrakis, et al. (2000). "The crystal structure of DNA mismatch repair protein MutS binding to a G x T mismatch." Nature **407**(6805): 711-7.

Li, Y., G. Augustine, et al. (2007). "Kinetics of complexin binding to the SNARE complex: correcting single molecule FRET measurements for hidden events." Biophys J.

Lipman, E. A., B. Schuler, et al. (2003). "Single-molecule measurement of protein folding kinetics." Science **301**(5637): 1233-5.

Lyubchenko, Y., L. Shlyakhtenko, et al. (1991). "DNA bending induced by Cro protein binding as demonstrated by gel electrophoresis." Proc Natl Acad Sci U S A **88**(12): 5331-4.

Margittai, M., J. Widengren, et al. (2003). "Single-molecule fluorescence resonance energy transfer reveals a dynamic equilibrium between closed and open conformations of syntaxin 1." Proc Natl Acad Sci U S A **100**(26): 15516-21.

McKinney, S. A., A. D. Freeman, et al. (2005). "Observing spontaneous branch migration of Holliday junctions one step at a time." Proc Natl Acad Sci U S A **102**(16): 5715-20.

McKinney, S. A., C. Joo, et al. (2006). "Analysis of single-molecule FRET trajectories using hidden Markov modeling." Biophys J **91**(5): 1941-51.

Morgan, M. A., K. Okamoto, et al. (2005). "Single-molecule spectroscopic determination of lac repressor-DNA loop conformation." Biophys J **89**(4): 2588-96.

Myong, S., I. Rasnik, et al. (2005). "Repetitive shuttling of a motor protein on DNA." Nature **437**(7063): 1321-5.

Natrajan, G., M. H. Lamers, et al. (2003). "Structures of Escherichia coli DNA mismatch repair enzyme MutS in complex with different mismatches: a common recognition mode for diverse substrates." Nucleic Acids Res **31**(16): 4814-21.

Obmolova, G., C. Ban, et al. (2000). "Crystal structures of mismatch repair protein MutS and its complex with a substrate DNA." Nature **407**(6805): 703-10.

Onuchic, J. N., Z. Luthey-Schulten, et al. (1997). "Theory of protein folding: the energy landscape perspective." Annu Rev Phys Chem **48**: 545-600.

Onuchic, J. N. and P. G. Wolynes (2004). "Theory of protein folding." Curr Opin Struct Biol **14**(1): 70-5.

Pan, Y. and R. Nussinov (2007). "Structural Basis for p53 Binding-induced DNA Bending." J Biol Chem **282**(1): 691-699.

Rhoades, E., M. Cohen, et al. (2004). "Two-state folding observed in individual protein molecules." J Am Chem Soc **126**(45): 14686-7.

Rhoades, E., E. Gussakovsky, et al. (2003). "Watching proteins fold one molecule at a time." Proc Natl Acad Sci U S A **100**(6): 3197-202.

Salsbury, F. R., Jr., J. E. Clodfelter, et al. (2006). "The molecular mechanism of DNA damage recognition by MutS homologs and its consequences for cell death response." Nucleic Acids Res **34**(8): 2173-85.

Stein, D. L. (1985). "A model of protein conformational substates." Proc Natl Acad Sci U S A **82**(11): 3670-3672.

Su, S. S., R. S. Lahue, et al. (1988). "Mispair specificity of methyl-directed DNA mismatch correction in vitro." J Biol Chem **263**(14): 6829-35.

Sugimura, S. and D. M. Crothers (2006). "Stepwise binding and bending of DNA by Escherichia coli integration host factor." Proc Natl Acad Sci U S A **103**(49): 18510-4.

Treiber, D. K. and J. R. Williamson (1999). "Exposing the kinetic traps in RNA folding." Curr Opin Struct Biol **9**(3): 339-45.

Walker, R. K., A. K. McCullough, et al. (2006). "Uncoupling of nucleotide flipping and DNA bending by the t4 pyrimidine dimer DNA glycosylase." Biochemistry **45**(47): 14192-200.

Wang, H., Y. Yang, et al. (2003). "DNA bending and unbending by MutS govern mismatch recognition and specificity." Proc Natl Acad Sci U S A **100**(25): 14822-7.

Warren, J. J., T. J. Pohlhaus, et al. (2007). "Structure of the human MutSalpha DNA lesion recognition complex." Mol Cell **26**(4): 579-92.

Weninger, K., M. E. Bowen, et al. (2003). "Single-molecule studies of SNARE complex assembly reveal parallel and antiparallel configurations." Proc Natl Acad Sci U S A **100**(25): 14800-5.

Yang, Y., L. E. Sass, et al. (2005). "Determination of protein-DNA binding constants and specificities from statistical analyses of single molecules: MutS-DNA interactions." Nucleic Acids Res **33**(13): 4322-34.

Youngblood, B. and N. O. Reich (2006). "Conformational transitions as determinants of specificity for the DNA methyltransferase EcoRI." J Biol Chem **281**(37): 26821-31.

CHAPTER THREE

FLUORESCENCE STUDIES OF THE FUNCTION OF GLUTAMATE IN MISMATCH DNA BINDING AND BENDING BY TWO MUTS HOMOLOGS

Introduction

The work described in Chapter 2 shows measurements of DNA conformational dynamics induced by wild-type *Taq* MutS at two different mismatches. Those results support hypotheses proposed in the DNA bending model of mismatch repair initiation by MutS (Figure 3.1) and reveal the dynamic equilibria that exists between a variety of DNA conformations when MutS is bound at the mismatch. We suggest from results in Chapter 2 that dynamic sampling of an unbent DNA-MutS conformation plays a role in mismatch repair signaling by MutS, while the many other DNA-MutS conformations may function in mismatch recognition and perhaps in signaling damage response.

Tessmer and Yang (2007 manuscript in preparation) have used AFM to analyze how mutations in the DNA binding motif of MutS affect the formation of bent and unbent DNA conformations. Their work led to suggestions that MutS 'scans' the DNA in search of a mismatch, forming a series of non-specific contacts along the DNA backbone while the electrostatic repulsion of the glutamate residue in the DNA binding domain facilitates smooth bending in the DNA (Wang, Yang et al. 2003; Kunkel and Erie 2005) (Tessmer and Yang,

manuscript in preparation). Upon locating a mismatch base pair, smooth bending in the DNA is converted to a sharp kink due to the local flexibility in the DNA at the mismatch (Lamers, Perrakis et al. 2000; Obmolova, Ban et al. 2000; Junop, Obmolova et al. 2001; Schofield, Nayak et al. 2001; Selmane, Schofield et al. 2003; Wang, Yang et al. 2003; Kunkel and Erie 2005) (Tessmer and Yang, manuscript in preparation).

At this juncture, the two specific contacts between MutS(α) (collective term for MutS and MutSα) and the mismatched base are achieved: phenylalanine (F39 in *Taq* MutS and F337 in yeast Msh6) stacks with the mismatched base and glutamate (E41 in *Taq* MutS and E339 in yeast Msh6) hydrogen bonds with the N3 of the mismatched thymine or N7 of the mismatched purine (Lamers, Perrakis et al. 2000; Obmolova, Ban et al. 2000; Natrajan, Lamers et al. 2003). The conserved Phe has been shown to have a major part in mismatch recognition, where mutation of this residue to alanine reduces specific mismatch binding by 3 orders of magnitude (Malkov, Biswas et al. 1997; Yamamoto, Schofield et al. 2000; Drotschmann, Yang et al. 2001) (Tessmer and Yang, manuscript in preparation). The Glu contact has been proposed to function both in stabilizing the formation of MutS-DNA complexes and presumably stabilizing the kinked DNA conformation observed in crystal structures (Drotschmann, Yang et al. 2001; Schofield, Brownewell et al. 2001). It was additionally suggested that Glu facilitates unbending of the DNA at the mismatch site (Figure 3.1) (Wang, Yang et al. 2003) (Tessmer and Yang, manuscript in preparation).

In vivo studies of conserved Glu mutations in *E. coli* MutS revealed that changing Glu38 to alanine resulted in some loss of repair of mismatches, both base-base mismatches and insertion/deletion loop mismatches (Holmes, Scarpinato et al. 2007). In contrast, the same work performed in yeast revealed that changing Glu339 in Msh6 to

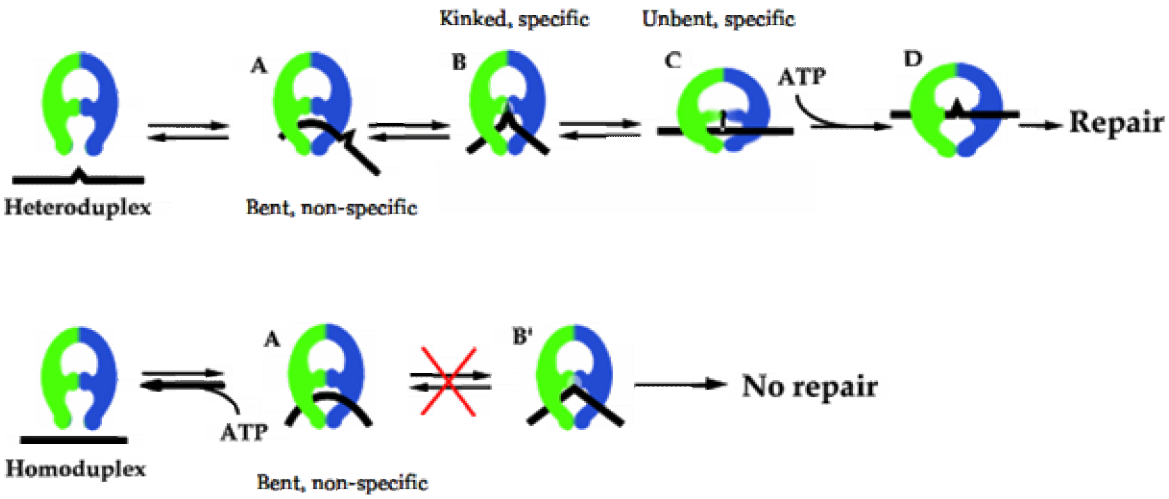

Figure 3.1 DNA bending model for mismatch repair initiation by MutS

DNA bending model for mismatch repair initiation by MutS proposed by Wang and Yang et. al. In this model, DNA bending at the mismatch (noted as 'kinked, specific') is the initial mismatch recognition complex. The DNA undergoes a conformational change to the 'unbent, specific' complex, which is suggested in this model to serve as the precursor to ATP hydrolysis and to function in signaling repair.

alanine conferred a mutator phenotype for base-base mismatches, but the residue appeared to be expendable for repair of single base insertion/deletion mismatches (Holmes, Scarpinato et al. 2007). Structural observations of *Taq* MutS (E41A)-mismatched DNA complexes with AFM support this mutator phenotype observed *in vivo*. *Taq* MutS (E41A) displayed wild-type mismatch binding and induced identical DNA bending at an insertion/deletion mismatch (ΔT). However, DNA bending observed at a base-base mismatch (GT) induced by the Glu mutant protein was characteristically different from observations of bending at a GT mismatch induced by the wild-type protein (Tessmer and Yang, manuscript in preparation).

The primary objective of the work described here is to further explore the effects of the Glu-to-Ala mutation in the mismatch binding motif of *Taq* MutS and yeast MutSα on mismatch binding, mismatch recognition, and DNA conformational flexibility and dynamics. Fluorescence anisotropy binding data of *Taq* MutS and yMutSα (wild-type and DNA binding motif mutants *Taq* MutS (E41A) and yMutSα (E339A)) to various mismatches were collected to explore the role of the glutamate in mismatch binding affinity and mismatch discrimination. Further studies using single-molecule fluorescence resonance energy transfer (FRET) to measure dynamic DNA bending induced by *Taq* MutS (E41A) offer insight into the role of Glu in DNA recognition, bending, and conformational stability. The combined DNA binding and bending results support the role of this amino acid in the DNA binding motif of MutS(α) in both recognizing various mismatches and stabilizing MutS-DNA complexes.

The results described here are (1) consistent with *in vivo* observations of mismatch repair in yeast Msh6 (E339A) (Holmes, Scarpinato et al. 2007), (2) complementary to the observed DNA conformations measured for *Taq* MutS (E41A) *in vitro* using AFM (Tessmer

and Yang, manuscript in preparation), (3) unique in revealing how DNA conformational dynamics are affected by removing a conserved residue from the DNA binding motif of MutS(α), and (4) support observations that dynamic conformational sampling may govern mismatch repair initiation by MutS (discussed in Chapter 2).

Results

Wild-type Taq MutS and yMutSα DNA binding by fluorescence anisotropy

A host of techniques can be used to determine the binding affinity of an enzyme to a substrate including electromobility gel shift assays (EMSA), surface plasmon resonance (SPR), and filter binding assays, among others (Carey 1991; Lohman and Bujalowski 1991; Myszka 2000). We sought to employ fluorescence anisotropy as an assay to measure mismatch binding of wild-type *Taq* MutS and yMutSα as well as the mismatch binding properties of these MutS homologs with a mutation in the conserved DNA binding motif. The binding of wild-type *Taq* MutS using fluorescence anisotropy was performed and compared to results previously determined by other techniques to explore the accuracy of binding measurements using anisotropy (Table 3.1) (Schofield, Nayak et al. 2001; Yang, Sass et al. 2005). Binding of *Taq* MutS to short, fluorescently-labeled mismatch DNA substrates (Figure 5.1 A) revealed binding constants of 5 ± 4.9 nM and 40 ± 25 nM for a ΔT and a GT mismatch, respectively (Figure 3.2, solid curves). Binding constants were determined by the average of at least 4 independent binding curves for the two mismatches (see Materials and Methods).

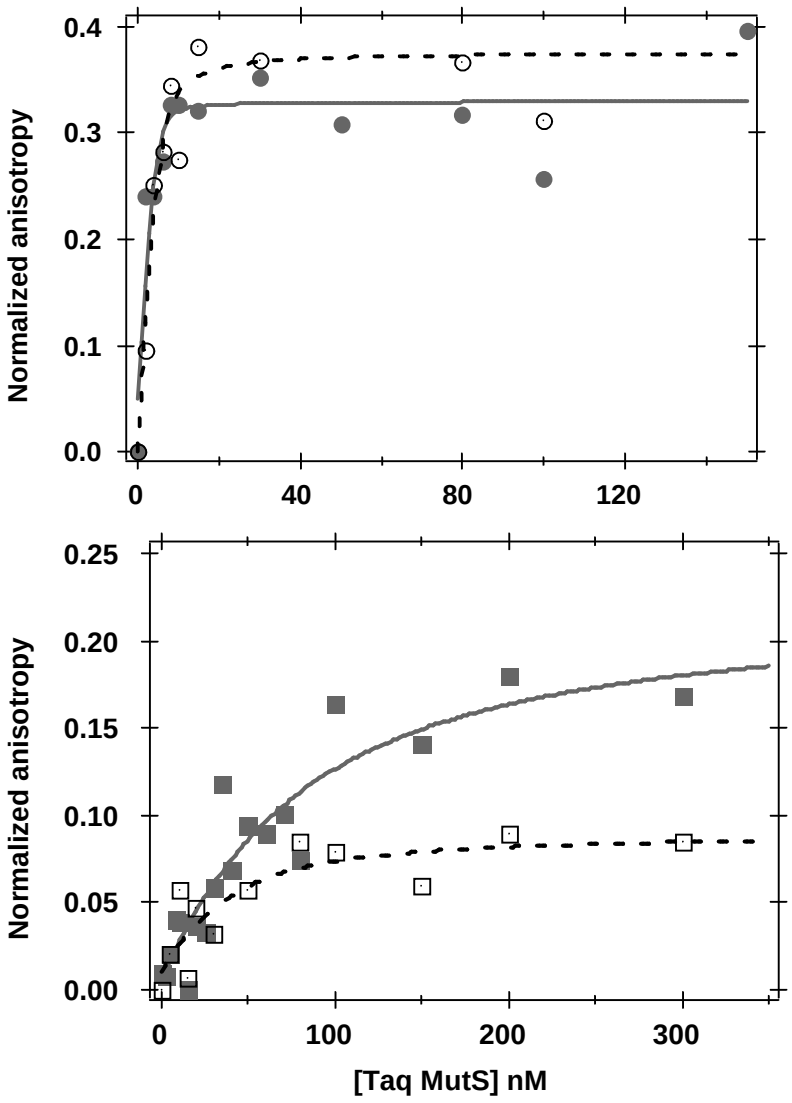

Figure 3.2 Mismatched DNA binding by wild-type *Taq* MutS and *Taq* MutS (E41A)

Sample anisotropy binding isotherms of wild-type *Taq* MutS (solid markers) and *Taq* MutS (E41A) (open markers) to heteroduplex DNA containing a +1 T-bulge (5 nM ΔT, upper panel, circles) and a GT mismatch (30 nM GT, lower panel, squares).

These results are consistent with binding constants determined by AFM, however our results reveal tighter binding to a GT mismatch in comparison to those determined by EMSA. It has been suggested that EMSA is less sensitive to weak or dynamic protein-DNA interactions. As a result, EMSA would produce weaker observed binding constants in comparison to AFM and fluorescence anisotropy which are more sensitive and have reduced dynamic limitations (Yang, Sass et al. 2005). This observation explains why the high affinity binding to ΔT is consistent among the techniques but the weaker binding to GT is more sensitively detected with AFM and fluorescence anisotropy.

EMSA, filter binding assays, and surface plasmon resonance (SPR) have been previously employed to study DNA binding by yMutSα (Alani 1996; Habraken, Sung et al. 1998; Marsischky and Kolodner 1999). Dissociation constants for this protein to GT mismatches and +1 frameshifts (such as a ΔT) have been reported in the literature and are documented in Table 3.1 (Alani 1996; Habraken, Sung et al. 1998; Marsischky and Kolodner 1999). Fluorescence anisotropy binding isotherms of yMutSα to mismatched DNA (Figure 3.3, solid curves) reveal binding constants of 11 ± 2 nM to a ΔT and 2 ± 1 nM to a GT mismatch. These binding constants were determined by the combined average of multiple binding curves (see Materials and Methods). The binding results for yMutSα determined by fluorescence anisotropy were consistent with results previously reported for this protein (Table 3.1) (Alani 1996; Habraken, Sung et al. 1998; Marsischky and Kolodner 1999).

Fluorescence anisotropy results show minimal binding of *Taq* MutS or yMutSα to 24-mer homoduplex DNA substrates (data not shown). MutS proteins have been reported to have high end-binding affinities (Wang, Yang et al. 2003; Yang, Sass et al. 2005)**,** which may likely offer a substantial contribution to the binding affinities for homoduplex DNA

substrates (Alani 1996; Habraken, Sung et al. 1998; Marsischky and Kolodner 1999). The end-labeled fluorescent DNA used in these experiments likely reduces end-binding effects because the fluorophore is occupying one of the two end-binding sites. Additionally, non-specific binding is expected to be reduced for these smaller DNA substrates because there are few non-specific sites to which the protein may bind.

yMutSα (E339A) and Taq MutS (E41A) differentially bind base-base mismatches and base insertion/deletion mismatches

Fluorescence anisotropy was employed to explore the role of the highly conserved Glu residue in the DNA binding motif of MutS and MutSα (E41A in *Taq* MutS and E339 in Msh6) in mismatch binding and discrimination between base insertion/deletion mismatches (ΔT or T-bulge) and base-base mismatches (GT).

Mismatched DNA binding by yMutSα (E339A) was determined by fluorescence anisotropy with the same DNA substrates used to obtain wild-type yMutSα-mismatched DNA binding constants. Preliminary results for binding at room temperature (23°C) were inherently noisy, and binding curves could not be obtained. Our single-molecule FRET assays on wild-type *Taq* MutS (Chapter 2) revealed that these protein-DNA complexes are dynamic, and we expected that these dynamics could be contributing to the noisy anisotropy signal. We reduced the acquisition temperature to 11°C which enabled us to reduce the suspected dynamic motions of the DNA-protein complexes and observe clear binding.

Results show that yMutSα (E339A) binds both a ΔT and a GT mismatch (Figure 3.3, dashed curves), however results are different from the wild-type yMutSα-mismatched DNA binding curves (Figure 3.3, solid curves). For the binding of the yMutSα (E339A) to a ΔT,

the anisotropy signal saturates at half the signal intensity observed for the wild-type, however the calculated binding constants for the two proteins to the DNA substrate are indistinguishable (13 ± 3 nM for yMutSα (E339A) and 11 ± 2 nM for wild-type) (Table 3.1).

Binding isotherms of yMutSα (E339A) to a GT mismatch show weaker binding relative to wild-type (59 ± 25 nM yMutSα (E339A) and 2 ± 1 nM for wild-type yMutSα) (Table 3.1). Anisotropy for yMutSα (E339A) binding the GT mismatch approached saturation at values 70% that of wild-type. The reduced anisotropy plateau values for mismatched DNA-yMutSα (E339A) binding isotherms suggest that these complexes are dynamic (Lakowicz 1999) and will be discussed later in the Chapter.

Mismatch binding curves for *Taq* MutS (E41A) revealed that this mutation maintained wild-type binding affinity for a ΔT, with a dissociation constant estimated to be < 1 nM (Figure 3.2, open circles). Binding of *Taq* MutS (E41A) to a GT mismatch was reduced relative to wild-type (Figure 3.2, open squares), and the anisotropy binding curve displayed only a small increase in anisotropy with increasing protein concentration. As a result, an accurate binding constant could not be determined. Comparison to the wild-type binding curves reveals that MutS (E41A) is capable of binding the GT mismatch, however the binding is weaker and, similar to observations from yMutSα (E339A), the complexes appear to be dynamic based on the reduced anisotropy signal relative to wild-type.

Effects of Glu removal on dynamic DNA bending measured by FRET

It has been suggested that both the electrostatic repulsion between the carboxylate group and the DNA and the hydrogen bond formed between the glutamate and the mismatched base play a role in stabilizing the DNA kinking observed in the mismatched

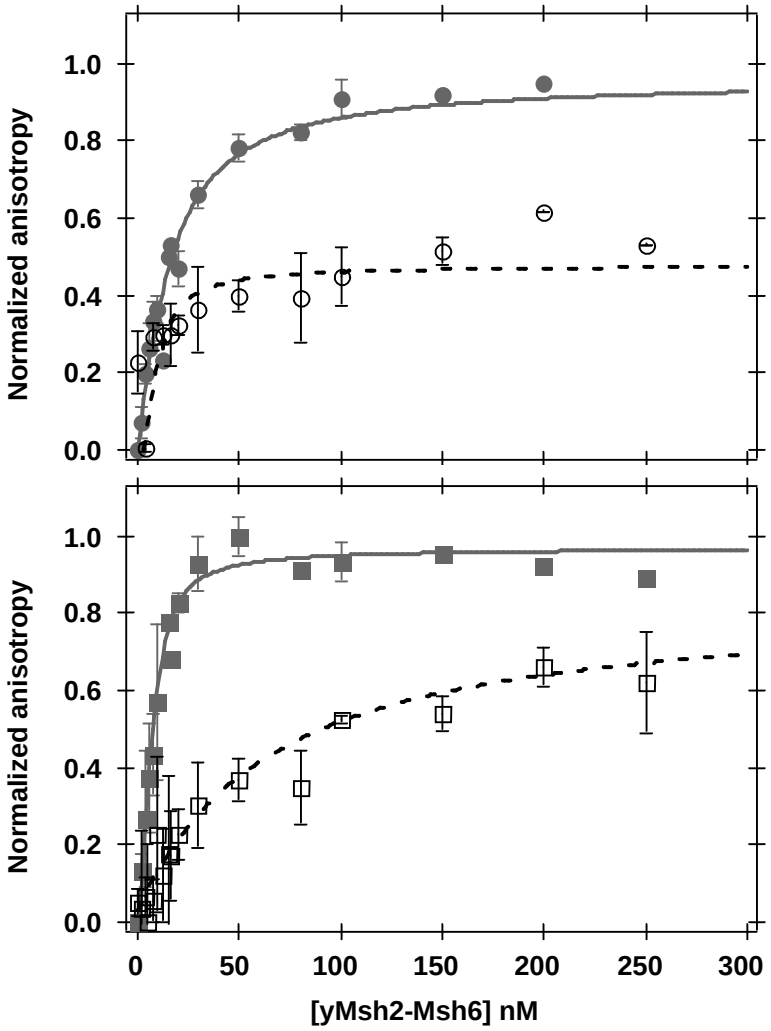

Figure 3.3 Mismatched DNA binding by wild-type yMutSα and yMutSα (E339A)

Average anisotropy binding isotherms of wild-type yMutSα (solid markers) and yMutSα (E339A) (open markers) to 10 nM heteroduplex DNA containing a +1 T-bulge (ΔT, upper panel, circles) and a GT mismatch (lower panel, squares). Anisotropy is normalized from 0 to 1 to demonstrate the differences in saturation anisotropy levels between wild-type yMutSα and yMutSα (E339A) (see Materials and Methods). Standard deviations are determined from the average anisotropy measurement determined at each protein concentration from at least 3 independent binding curves.

	Taq MutS	*Taq* MutS (E41A)	yMutSα	yMutSα (E339A)
ΔT dissociation constants (nM)				
K_d, anisotropy	5 ± 4.9	~ 1	11 ± 2	13 ± 3
K_d, AFM	21 ± 2.3[a]	21 ± 7[e]	-	-
K_d, EMSA	2.2 ± 2.1[b]	2.8 ± 0.6[b]	0.25[c]	-
K_d, filter binding	-	-	0.4[d]	21[d]
K_d, SPR	-	-	~ 3[c]	-
GT mismatch dissociation constants (nM)				
K_d, anisotropy	40 ± 25	ND	2 ± 1	59 ± 25
K_d, AFM	77 ± 7.7[a]	50 ± 16[e]	-	-
K_d, EMSA	310 ± 77[b]	240 ± 30[b]	0.2[d]	-
K_d, filter binding	-	-	19 ± 3.1[d]	-
K_d, SPR	-	-	-	-

Table 3.1 Mismatched DNA binding constants for *Taq* MutS and yMutSα

Mismatched DNA binding constants determined by fluorescence anisotropy for wild-type *Taq* MutS, *Taq* MutS (E41A), wild-type yMutSα, and yMutSα (E339A) and compared with those determined by other techniques.

ND = not determined

[a] denotes constants reported in (Yang, Sass et al. 2005).

[b] denotes constants reported in (Schofield, Brownewell et al. 2001).

[c] denotes constants reported in (Marsischky and Kolodner 1999).

[d] denotes constants reported in (Drotschmann, Yang et al. 2001).

[e] denotes constants reported in (Tessmer and Yang et. al. 2007, manuscript in preparation).

DNA-MutS crystal structures (Schofield, Brownewell et al. 2001). To further explore this hypothesis, we employed single-molecule FRET to monitor mismatched DNA dynamics for *Taq* MutS (E41A) bound to both a ΔT and a GT mismatch. Results observed for the wild-type protein (Chapter 2) revealed a diverse distribution of DNA conformations, with GT-MutS complexes undergoing a number of conformational transitions between many different conformational states while the ΔT-MutS complexes formed a number of stable DNA conformational states lasting for 30 seconds or longer. We were interested to explore how the removal of the highly conserved interaction between glutamate and the mismatched base would affect the dynamics of DNA bending induced by MutS.

Binding of *Taq* MutS (E41A) to a ΔT displayed a binding affinity similar to that observed for the wild-type protein (Table 3.1), suggesting that the Glu residue does not have an important role in ΔT mismatch binding. We used single-molecule FRET to monitor DNA bending for *Taq* MutS (E41A) bound to a ΔT to analyze the role of Glu41 in stabilizing the bent and unbent DNA conformations observed previously (Lamers, Perrakis et al. 2000; Obmolova, Ban et al. 2000; Natrajan, Lamers et al. 2003; Wang, Yang et al. 2003). In the presence of *Taq* MutS (E41A), ΔT mismatched DNA observed by single-molecule FRET had increased dynamics and conformational changes in the DNA relative to that observed for the wild-type protein bound to this substrate (Figure 3.4). For the wild-type protein, fewer than 20% of the observed ΔT-MutS molecules underwent a conformational change during the experimental time trace (100 seconds). In contrast, nearly 50% of the observed E41A-ΔT molecules showed conformational changes during the duration of the experiment.

E41A-ΔT complexes appear to visit high FRET states (FRET > 0.6, more DNA bending) with a higher relative frequency than observed for the wild-type protein bound to

this substrate (Figures 3.4 and 3.5). Additionally, the FRET distribution of states for E41A-ΔT spans a wider FRET range and is overall slightly shifted to higher FRET values, where the most frequented state for the wild-type protein (at FRET ~ 0.35, unbent DNA conformation ***U***) is not the preferred DNA conformation formed for the mutant protein bound to the ΔT.

Single-molecule FRET traces of GT mismatched DNA in the presence of *Taq* MutS (E41A) confirm a weak binding affinity of this mutant protein for a GT mismatch. The DNA in single-molecule FRET traces displays FRET efficiencies of ~ 0.24 (FRET efficiency characteristic of free DNA, Chapter 2) both in the presence and absence of MutS (E41A). In the majority of single-molecule FRET traces in the presence of MutS (E41A), the DNA appeared unbound by protein. When protein binding to the DNA occurred, a very clear shift to higher FRET (MutS-induced DNA bending) was instantaneously observed followed by direct unbinding (Figure 3.6 A and B). However, occasional binding into an intermediate FRET conformation revealed a stable complex that was fairly long-lived (stable for many seconds) in comparison to the high FRET (more bent) state (which typically lasted for 1 second or less) (Figure 3.6).

FRET distributions for single GT-E41A molecules (Figure 3.7) confirm these observations. These distributions document the FRET efficiency sampled for a single MutS-DNA complex at every frame of data acquisition (10 frames/second). The distributions recorded for 2 selected molecules reveal that DNA is typically unbound by MutS (E41A) (Figure 3.7, peaks represented by blue arrows centered at FRET ~ 0.24). However, MutS (E41A) induces bending upon binding a GT mismatch revealing either an unstable bent conformation (Figure 3.7 A, red arrow, FRET ~ 0.60) or a slightly more stable intermediate

bent conformation (Figure 3.7 B, magenta arrow, FRET ~ 0.50). In this case, we estimate conformational stability by the relative number of time frames each FRET conformation occurs.

Preliminary ensemble FRET analysis was performed on E339A-GT and E339A-ΔT complexes. While some bending was observed at low protein concentrations, fluorescence band broadening of TAMRA emission at high protein concentrations, possibly due to non-specific interactions of the protein with the DNA, made results skewed and difficult to analyze. Further work will be dedicated to exploring DNA bending induced by this mutant using single-molecule FRET and comparing to dynamic results obtained for the homologous mutation in *Taq* MutS.

Discussion

Glutamate plays a role in mismatch recognition and discrimination

To explore the importance of the glutamate contact with the mismatch in MutS(α) binding, we determined the mismatch binding constants and properties of this mutation in two MutS homologs: yMutSα (E339A) and *Taq* MutS (E41A).

The anisotropy binding data for yMutSα (E339A) to two mismatches, a ΔT and a GT mismatch, suggest that the glutamate plays an important role in base-base mismatch binding, but binding to a ΔT is unaffected by loss of this amino acid contact. The binding constant for yMutSα (E339A) to a GT mismatch was weaker relative to wild-type binding to the GT mismatch, while the binding constants determined for the wild-type and mutant to a ΔT were

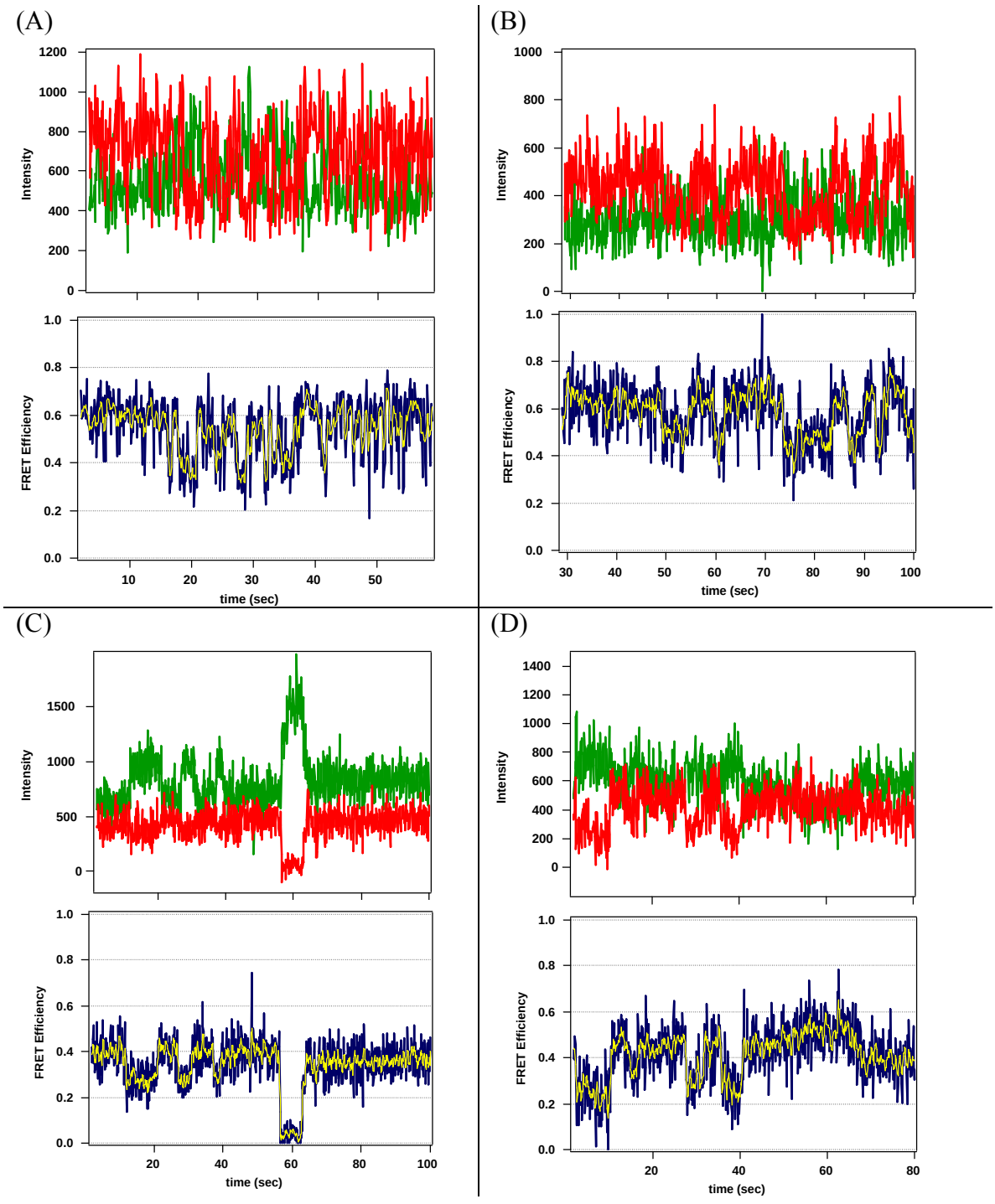
(A)
Intensity
FRET Efficiency
time (sec)
(B)
Intensity
FRET Efficiency
time (sec)
(C)
Intensity
FRET Efficiency
time (sec)
(D)
Intensity
FRET Efficiency
time (sec)

Figure 3.4 DNA bending dynamics of E41A-ΔT complexes

Dynamic FRET traces for *Taq* MutS (E41A) bound to a ΔT. More than half the molecules measured displayed a conformational transition during the experimental time trace, and molecules were inherently more dynamic than for the wild-type protein bound to this mismatch. Additionally, E41A-ΔT complexes visited higher FRET states (more DNA bending) more frequently than was observed for the wild-type protein. Combined, these results suggest that Glu functions in stabilizing both the bent and unbent MutS-DNA conformations.

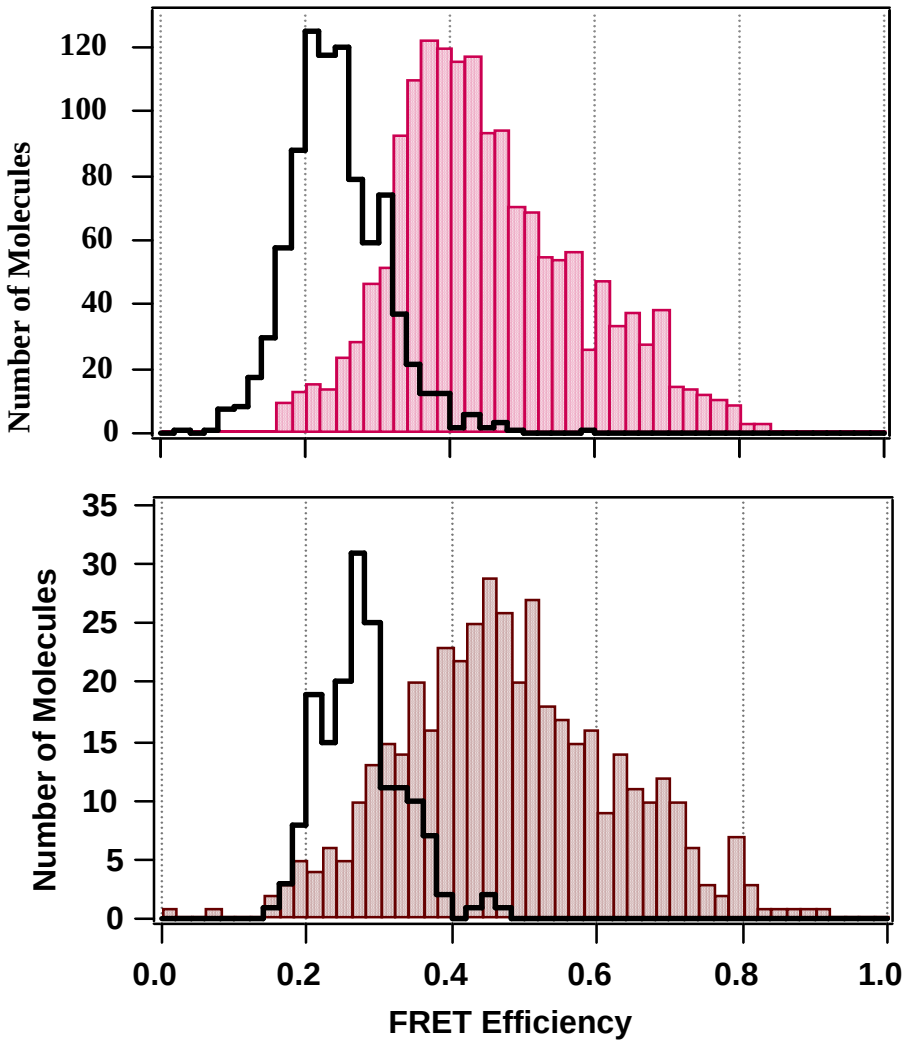
Number of Molecules
120
100
80
60
40
20
0
Number of Molecules
35
30
25
20
15
10
5
0
0.0
0.2
0.4
0.6
0.8
1.0
FRET Efficiency

Figure 3.5 FRET efficiency distributions for ΔT in the presence of wild-type *Taq* MutS and *Taq* MutS (E41A)

FRET efficiency distributions for ΔT DNA in the absence (black cityscape) and presence (colored bars) of wild-type *Taq* MutS (top panel) and *Taq* MutS (E41A) (bottom panel). The FRET distribution for E41A-ΔT is comprised of 445 molecules that did not undergo a conformational change during the time trace (FRET states were stable for 5 seconds or longer). The distribution of states for both the wild-type and the mutant protein are similar, however the mutant distribution is broader and shifted to slightly higher FRET relative to the wild-type protein. E41A-ΔT appears to visit higher FRET states more frequently than the wild-type protein in comparison to the other FRET conformations sampled (further exemplified in single molecule traces represented in Figure 3.4). Additionally, the dominant FRET state at ~ 0.35 in the wild-type distribution is less significant for the mutant. The E41A-ΔT complex was more dynamic than the wild-type MutS-ΔT complex, with more than half the molecules undergoing conformational changes during the experimental time trace for *Taq* MutS (E41A) bound to a ΔT.

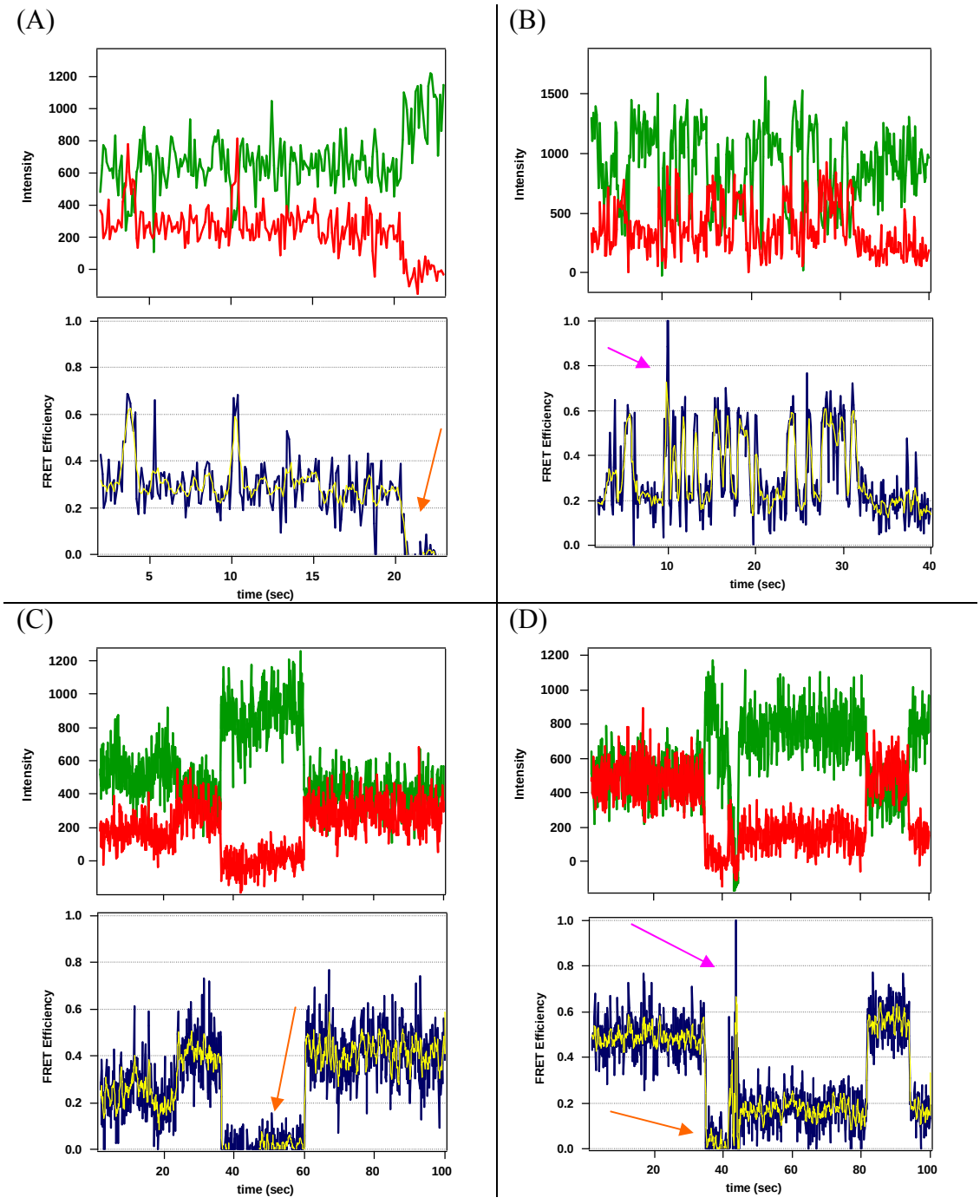
(A)
(B)
(C)
(D)
Intensity
FRET Efficiency
time (sec)

Figure 3.6 DNA bending dynamics of GT mismatched DNA in the presence of *Taq* MutS (E41A)

Dynamic FRET traces for GT mismatched DNA in the presence of *Taq* MutS (E41A). (A) and (B) represent typical traces, where the DNA remains unbound (FRET ~ 0.24) for the majority of the trace until MutS (E41A) rapidly binds into a high FRET conformation (very bent) followed by immediate unbinding. (C) and (D) represent FRET traces where MutS (E41A) appears to bind the GT in an intermediate FRET conformation. This intermediate state is substantially longer-lived than the high FRET conformations represented in (A) and (B). FRET values at zero (orange arrows) represent bleaching and blinking of the FRET acceptor dye. Noise in FRET traces at 10 sec in (B) and 42 sec in (D) (magenta arrows) represent blinking of the FRET donor dye.

(A)

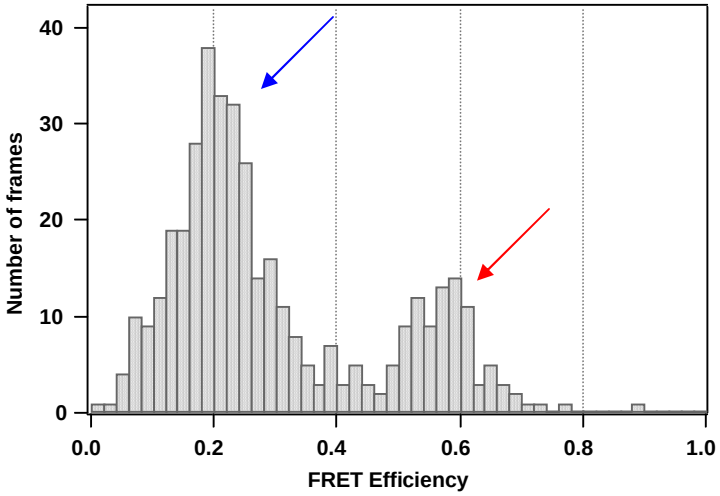
Number of frames
0
10
20
30
40
0.0
0.2
0.4
0.6
0.8
1.0
FRET Efficiency

(B)

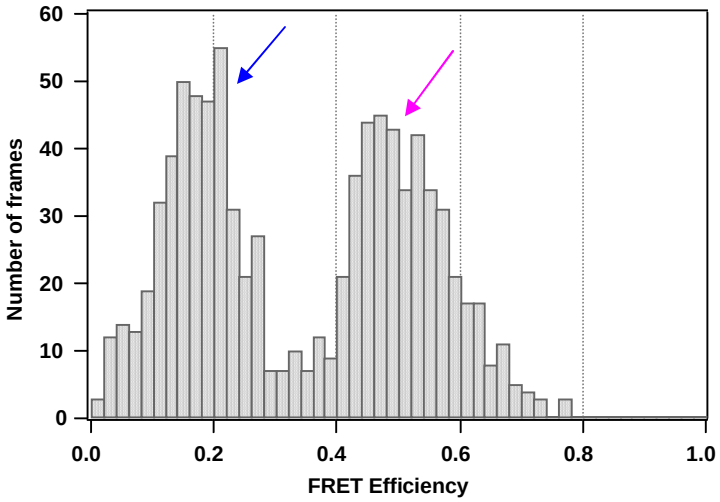
Number of frames
0
10
20
30
40
50
60
0.0
0.2
0.4
0.6
0.8
1.0
FRET Efficiency

Figure 3.7 Single-molecule FRET distributions of GT mismatched DNA in the presence of MutS (E41A)

FRET efficiency distributions for single GT mismatched DNA molecules in the presence of *Taq* MutS (E41A). (A) Distribution of all FRET efficiencies determined in the trace shown in Figure 3.6 B. (B) Distribution of all FRET efficiencies determined in the trace shown in Figure 3.6 C. These distributions record the FRET efficiency at each frame of data acquisition (1 frame every 100 ms) for the FRET trace of a single molecule, therefore this distribution only represents conformations sampled in a single molecule and not in a population of many molecules. This representation confirms the observation that GT mismatched DNA remains unbound the majority of the time trace (blue arrows). However, upon *Taq* MutS (E41A) binding the GT mismatch, two types of conformations ensue: a short-lived conformation at high FRET (~ 0.60) (red arrow in (A)) and longer-lived conformations at intermediate FRET (~ 0.50) (magenta arrow in (B)).

indistinguishable (Table 3.1). Although they result in the same binding constants, the anisotropy curves for the wild-type and the yMutSα (E339A) mutant to ΔT were quite different. The anisotropy signal saturated at a lower level for yMutSα (E339A) binding relative to wild-type binding to the same substrates. Saturation anisotropy was reduced by 50% for E339A-ΔT and 30% for E339A-GT (Figure 3.3), suggesting that the E339A-ΔT and E339A-GT complexes are dynamic.

Fluorescence anisotropy is sensitive to the rotational diffusion of the fluorescent molecule in solution, where freely tumbling molecules exhibit a lower net anisotropy value than molecules interacting with larger binding molecules (ie. DNA bound by MutS). However, if the small fluorescent molecule exhibits dynamic segmental motions (such as DNA bending), the net anisotropy would reflect those motions and be reduced (Lakowicz 1999). As a result, dynamic DNA bending in mismatched DNA bound by MutS would contribute to a reduced net change in anisotropy as was observed for mismatched DNA-E339A complexes. Additionally, single-molecule FRET measurements on the homologous mutation in *Taq* MutS reveal substantially more DNA bending dynamics relative to the wild-type protein on the same mismatched DNA substrates, further supporting the idea that elimination of the interaction between Glu and the mismatch increases dynamics of DNA bending in mismatch-MutS(α) complexes. The relative difference between the saturation anisotropy for E339A-ΔT and E339A-GT (50% E339A-ΔT vs. 70% for E330A-GT relative to wild-type) further reveals that, in comparison, E339A-GT exhibits less DNA bending dynamics or segmental motions than E339A-ΔT complexes.

These results support the suggestion that the interaction between E339 and the mismatch has two primary roles. (1) This contact is essential in keeping yMutSα bound to a

base-base mismatch by stabilizing the MutS-GT complex but is less important for stabilizing the MutS-ΔT complex. Genetic studies have shown that yMutSα (E339A) has completely normal function in repairing base insertion/deletions but displays a mutator phenotype for repairing certain base-base mismatches resulting from G-C to A-T transversions (Holmes, Scarpinato et al. 2007). The discrepancy in binding of the E339A protein to a GT mismatch and a ΔT offers consistency between *in vitro* binding results and *in vivo* genetic findings (Holmes, Scarpinato et al. 2007). (2) The interaction between the Glu and the mismatched base appears to stabilize DNA bending (the suggested initial MutS-DNA recognition complex observed by AFM and X-ray crystallography), where loss of this interaction increases the dynamics of these protein-DNA complexes (Lamers, Perrakis et al. 2000; Obmolova, Ban et al. 2000; Natrajan, Lamers et al. 2003; Wang, Yang et al. 2003; Warren, Pohlhaus et al. 2007). To further investigate these dynamics, we employed single-molecule FRET to monitor mismatched DNA conformational fluctuations induced by *Taq* MutS (E41A).

Glutamate functions in stabilizing the initial mismatch recognition complex and facilitating the formation of the unbent ultimate recognition complex

Fluorescence anisotropy of yMutSα (E339A) suggested that DNA-MutS complexes were dynamic, and we were able to further explore these dynamics by characterizing mismatched DNA bending induced by this mutation in the homologous MutS protein from *Thermus aquaticus (Taq)*. We characterized the DNA bending dynamics of wild-type *Taq* MutS (Chapter 2), therefore we were interested to see how these dynamics would be affected if Glu were removed from the DNA binding motif of MutS.

DNA bending observed by single-molecule FRET revealed that although MutS (E41A) binds a ΔT with wild-type affinity, conformational dynamics of the DNA in E41A-ΔT complexes are increased relative to wild-type. The wild-type protein induced stable DNA conformations that lasted for many seconds (sometimes > 30 seconds); however, the E41A mutant protein induced many more conformational transitions when bound to DNA containing a ΔT (Figure 3.4). Additionally, the E41A-ΔT complexes visited higher FRET states (more bending) with greater frequency than observed in single molecule traces for the wild-type MutS-ΔT complexes (Chapter 2). These results suggest that the Glu *does not* play a role in the recognition of ΔT by MutS (revealed from tight DNA binding affinity) or in bending DNA containing a ΔT (revealed by visits to high FRET, or highly bent DNA conformations), consistent with previous observations (Tessmer and Yang, manuscript in preparation). However, the increased dynamics of these complexes suggest that this residue does function in stabilizing DNA distortion induced at the mismatch site, as previously suggested (Drotschmann, Yang et al. 2001; Schofield, Brownewell et al. 2001). These dynamics are consistent with the reduced anisotropy signal, presumably the result of dynamic DNA bending, that we observe for mismatch binding by yMutSα (E339A).

The FRET efficiency distribution of states for E41A-ΔT also revealed a larger breadth of conformations sampled in comparison to the wild-type (Figure 3.5). The most populated conformation for the wild-type protein is the unbent, low FRET state at FRET ~ 0.35 (conformation ***U***, Chapter 2). In contrast, E41A-ΔT visited higher FRET states more frequently and this low FRET, unbent conformation less frequently in comparison to wild-type-ΔT complexes. This difference is evident both in the FRET efficiency distribution and in single-molecule FRET traces. We believe that the low FRET conformation at 0.35 may

represent the unbent ultimate recognition complex observed by AFM and proposed in the DNA bending model (Wang, Yang et al. 2003). Our wild-type results predicted that the free energy barrier for the transition between DNA bending and unbending at a ΔT was low, explaining why the unbent conformation is more stable in ΔT-MutS complexes than in GT-MutS complexes. Elimination of negative charge from Glu results in a decrease in the formation of this unbent conformation in comparison to the wild-type protein suggesting that the Glu interaction contributes to reduced free energy barrier for the transition from bending to unbending. As a result, Glu does appear to facilitate the formation of the unbent DNA-MutS conformation, consistent with previous propositions (Lebbink, Georgijevic et al. 2006) (Tessmer and Yang, manuscript in preparation).

Single-molecule FRET measurements for MutS (E41A) interactions with a GT mismatch confirmed the weak binding observed from fluorescence anisotropy measurements. The mismatched DNA appeared to be unbound by MutS (E41A) the majority of the time. However, sudden binding and unbinding events were observed (Figure 3.6 A and B) as well as the formation of stable intermediate FRET conformations (Figure 3.6 C and D). The data show that when MutS (E41A) binds a GT mismatch and induces significant bending (high FRET), it is likely to unbind the DNA immediately. This result is in contrast to the wild-type MutS-GT DNA bending dynamics, where this bent conformation is the most stable of all conformations sampled (conformation ***B***, lifetime of 12 sec, Chapter 2).

However, when MutS (E41A) binds the GT mismatch in an intermediate bent state (medium FRET), the complexes are more stable, and the protein often stays bound in this conformation for a few seconds (Figure 3.6 C and D). This result is also different in comparison to the wild-type bending results, where the intermediate FRET conformations

(***U*, I,*** and ***B****) were *less stable* than the high FRET, bent conformation (***B***). The FRET efficiency range of this stable intermediate conformation is consistent with the FRET range of the unstable transition intermediate observed for the wild-type MutS-GT complexes (conformation ***U****, τ = 0.75 sec). The free energies of transitions for wild-type GT-MutS complexes revealed that ***U**** acts as a transition intermediate between bending and unbending (Chapter 2). Stability of this conformation in MutS (E41A) suggests that Glu is essential in allowing the DNA to complete its conformational transition from bent to unbent. In the absence of the Glu residue, complexes are unable to form the unbent DNA conformation and get 'stuck' in an intermediate conformation during their transition path from bending to unbending. This observation is also supported by the fact that we rarely observe the unbent conformation in E41A-GT complexes.

AFM distributions of DNA bending by *Taq* MutS (E41A) bound to a GT mismatch revealed two distinct populations of complexes centered at bend angles of ~20° and ~70°, with clear shifts to higher angles relative to the wild-type protein (Tessmer and Yang, manuscript in preparation). Tessmer and Yang, et. al., proposed that the conformation at 20° represented E41A-GT complexes that were 'trapped' in an intermediate conformation between bending and unbending and that Glu functioned in the formation of the unbent state. The intermediate FRET conformation that we directly observe in these complexes and its high relative stability are very consistent with this suggestion.

The combined DNA binding and bending results for *Taq* MutS (E41A) at a GT mismatch suggest that the glutamate is important for base-base mismatch recognition and stabilizing the MutS-GT complex. Upon occasional GT binding, bending is induced; however, this bent conformation is very unstable and results in the release of MutS from the

DNA within ~ 1 to 2 seconds. The Glu residue is therefore essential for the formation of a stable initial mismatch recognition MutS-GT DNA complex. This observation suggests that formation of the hydrogen bond between Glu and the mismatch is one of the first steps in mismatch recognition, consistent with conclusions drawn from observations of AFM images of these complexes (Tessmer and Yang, manuscript in preparation).

DNA bending dynamics of MutS (E41A), in comparison to wild-type, suggest that the Glu has a role in stabilizing nearly all observed bent and unbent conformations (Chapter 2, conformations ***U, I, B, MB***, and ***SB***) while destabilizing the intermediate conformations in GT-MutS complexes (***U**** and ***B****). Replacing Glu with Ala appears to directly reverse this trend in stabilities, where the intermediate conformation ***U**** becomes the most stable DNA conformation and the others appear to become less stable (determined by the increase in dynamics among these conformations). These results suggest that Glu facilitates *both* bending and unbending at both the ΔT insertion mismatch and the GT base-base mismatch.

We propose that similar dynamics may occur for mismatched DNA-yMutSα (E339A) complexes based on tight binding affinities but reduced net anisotropy signal. Future work will entail using single-molecule FRET to study the conformational dynamics of this protein bound to multiple types of mismatches. However, results shown here reveal that these complexes are dynamic and appear to follow a similar dynamic trend to *Taq* MutS (E41A). Although there are experimental difficulties to overcome when working with the yeast MutS homolog, results will be interesting.

Can DNA bending dynamics tell us something about mismatch repair in vivo?

In vivo genetic studies revealed that yMutSα (E339A) maintains complete functionality in frameshift repair (which the ΔT substrate represents) and transition mismatch repair with loss of repair of base-base mismatches resulting in G-C to T-A transversions (Holmes, Scarpinato et al. 2007). In conjunction with *in vivo* observations, our DNA binding results revealed weaker binding of this mutant to base-base mismatches in comparison to binding to base insertion/deletions. Weak mismatch binding by MutS(α), therefore, appears to be linked to loss of MMR *in vivo*. However, DNA binding is not the only part of the story, and it has been previously suggested that DNA binding does not necessarily dictate repair efficiency because even mismatches bound weakly by MutS are repaired *in vivo* (Jiricny, Su et al. 1988). The work presented here invokes questions regarding what role DNA conformational dynamics may serve in DNA mismatch repair.

The DNA bending model (Figure 3.1) hypothesizes that DNA bending and unbending serve as signaling strategies employed by MutS to get repair underway (Wang, Yang et al. 2003). Results in Chapter 2 led to the proposition that dynamic conformational sampling of MutS-DNA complexes could also have a part in governing mismatch repair initiation, and perhaps significant occupancy in the unbent conformation ***U*** is necessary for efficient signaling of mismatch repair.

Although E41A-ΔT complexes frequently occupy bent DNA conformations, these complexes are very dynamic and continue to sample the unbent DNA conformation with reasonable frequency (for several seconds or longer). If similar conformational dynamics occur for the homologous mutation in yMutSα, this observation may explain why this Glu-

to-Ala mutation does not eliminate repair of frameshifts *in vivo* (Holmes, Scarpinato et al. 2007).

We observe very different DNA conformational dynamics for E41A-GT complexes. These complexes were very unstable and did not appear to occupy the unbent conformation that we observe in the wild-type MutS-GT complexes. Once again, if we hypothesize that similar conformational dynamics occur for the homologous mutation in yMutSα, this observation may explain why the Glu-to-Ala mutation eliminates repair of base-base mismatches *in vivo* (Holmes, Scarpinato et al. 2007).

Lebbink and coworkers suggested that the hydrogen bond between the glutamate and the GT mismatch in *E. coli* was essential in inducing a conformational change in MutS to an ATP-bound sliding clamp MutS conformation that functions in signaling repair (Lebbink, Georgijevic et al. 2006). The DNA bending model suggests that DNA unbending also facilitates the formation of this MutS sliding clamp, thus signaling the ATPase activity of MutS and repair initiation. Therefore, the inability of *Taq* MutS (E41A)-GT complexes to sample the unbent DNA conformation is consistent with all of these previous *in vitro* and *in vivo* observations (Wang, Yang et al. 2003; Lebbink, Georgijevic et al. 2006; Holmes, Scarpinato et al. 2007).

Conclusions

We sought to measure mismatched DNA binding and bending by MutS from two organisms, bacteria and yeast, to determine what effect, if any, the mutation of a conserved Glu in the DNA binding motif would have on mismatch recognition and DNA conformational flexibility and dynamics. Results revealed that the Glu has a similar function

in both bacteria and yeast, helping to form a stable MutS(α)-GT complex but less necessary in stabilizing the MutS(α)-ΔT complex. These results, which complement *in vivo* observations (Lebbink, Georgijevic et al. 2006; Holmes, Scarpinato et al. 2007), reveal that formation of a stable MutS(α)-mismatch complex is likely important for MMR to proceed, however prior studies have revealed that DNA binding can not be the only factor that contributes to DNA mismatch repair *in vivo* (Jiricny, Su et al. 1988).

Our results show that mismatched DNA-MutS(α) (EA) complexes are very dynamic, with DNA conformational fluctuations increased considerably relative to the wild-type MutS-DNA complexes. The dynamics of mismatched DNA-MutS complexes may govern mismatch repair signaling and offer a link between MutS-DNA structure and mismatch repair efficiency that is not revealed in crystal structures alone.

We propose, in line with the DNA bending model, that the ability to sample an unbent DNA conformation may be fundamental in initiating mismatch repair. As a result, more dynamic MutS-DNA complexes may sample the unbent conformation less frequently and still be repaired (ie. E41A-ΔT) while others are incapable of sampling the unbent conformation and are less able to signal repair efficiently (ie. E41A-GT), resulting in refractory or decreased mismatch repair *in vivo*.

While additional work will be done to explore DNA dynamics of a host of MutS mutants, the results presented here begin to offer insight to the role of DNA dynamics in DNA mismatch repair. Future work will entail not only studying the effects of mutations in MutS on DNA bending but also exploring the roles of sequence context of the mismatch in DNA binding, dynamics, and equilibrium. Moreover, these methods may be exploited to studying DNA dynamics of a host of different mismatched DNA substrates as well as

damaged DNA substrates, which may offer insight into the role of DNA dynamics in DNA damage response.

Acknowledgements

I would like to thank Drs. Yong Yang, Ingrid Tessmer, and Shannon Holmes for sharing their interesting MutS(α) results and encouraging me to pursue the DNA binding and bending experiments described in this chapter. I would like to thank Dr. Ashutosh Tripathy (UNC Macromolecular Interactions Facility) and Dr. Tom Hollis (Wake Forest University) for use of the fluorometers to perform fluorescence anisotropy experiments. I would also like to thank Vanessa Van Vranken for stimulating discussions of these results and for assistance in single-molecule FRET experiments and data analysis.

Materials and Methods

Proteins and Oligonucleotides

Thermus aquaticus (*Taq*) MutS was purified as previously described (Biswas, Ban et al. 1999; Clark, Cook et al. 1999; Schofield, Nayak et al. 2001). Wild-type *Saccharomyces cerevisiae* Msh2-Msh6 and Msh2-Msh6 (E339A) were a generous gift of our collaborators at NIH-NIEHS (Alan Clark, Shannon Holmes, Tom Kunkel). *Taq* MutS (E41A) was a generous gift of our collaborators at NIH-NIDDK (Chungwei Du, Peggy Hsieh).

DNA oligonucleotides used in fluorescence experiments are listed in Table 5.1. HPLC-purified single-stranded oligonucleotides and complementary strands were purchased from MWG Biotech and Integrated DNA Technologies. The DNA substrate used in fluorescence anisotropy binding assays (Figure 5.1 A) contained TAM-24 annealed to ΔT-24,

GT-24, or GC-24 to generate a 24 base pair duplex DNA fragment containing a ΔT, a GT base-base mismatch, or GC homoduplex DNA, respectively. Duplex DNA substrates were made by combining the appropriate single-stranded oligonucleotides and annealing in MutS binding buffer containing 20 mM Tris-HCl pH 7.8, 100 mM sodium acetate (NaOAc), and 5 mM magnesium chloride ($MgCl_2$) at 65°C for 20 minutes followed by slow cooling to room temperature. Annealed substrates were stored at 4°C until use.

DNA substrates for single-molecule FRET experiments contained TAM-50 annealed to Cy5-ΔT, Cy5-GT, or Cy5-GC to generate a 19 base pair duplex DNA at the 3' end of the 50-mer fragment containing a ΔT, a GT base-base mismatch, or GC homoduplex DNA, respectively (Figure 5.2 A). Oligonucleotides were annealed in MutS binding buffer (see above) in a 1:1 ratio at 65°C for 20 minutes followed by slow cooling to 55°C. At this point, an additional complementary strand (Comp-31) was added and annealed to complete the remaining duplex DNA. The substrate was allowed to slowly cool to room temperature and stored on ice or at 4°C.

Fluorescence anisotropy binding assays

Binding of MutS and yMutSα to heteroduplex and homoduplex DNA was monitored by equilibrium fluorescence anisotropy measurements obtained with a Jobin-Yvon Fluorolog-3 fluorometer (23°C and 11°C) and a Tecan Safire II microarray plate reader (23°C). TAMRA was excited at 535 nm, and polarized emission was measured at 582 nm. Duplex DNA (ranging in concentration from 5 nM to 100 nM) was incubated with increasing protein concentrations for 5 minutes in binding buffer (20 mM Tris-HCl pH 7.8, 100 mM NaOAc, 5 mM $MgCl_2$) before each measurement was acquired. Every data point was

determined from the average of 10 measurements on the sample. Anisotropy was calculated using the instrument software with corrections for dark and background counts and was measured as a function of protein concentration.

Fluorescence anisotropy binding data analysis

The anisotropy data points were first normalized by setting the initial anisotropy value for free DNA (A_o) to 0 following the equation $A_i = (A_i\text{-}A_o)/A_o$ (Eq. 3.1), where A represents the anisotropy measurement and the corresponding subscript represents the protein concentration for that measurement. The yMutSα binding data were then scaled to an equivalent saturation anisotropy of 1 (A_{max}) for comparison. For yMutSα, a minimum of 3 binding curves were combined by averaging the anisotropy value at each protein concentration to create an average binding curve for the respective protein-DNA substrate. Binding curves were fit by a weighted non-linear regression binding isotherm using

$$A = A_{\max} \cdot \frac{K_D + P_{tot} + D_{tot} - \sqrt{(K_D + P_{tot} + D_{tot})^2 - 4D_{tot}P_{tot}}}{2D_{tot}} \qquad \text{(Eq. 3.2)}$$

where A is the normalized anisotropy, P_{tot} is the total added protein concentration, D_{tot} is the total dsDNA concentration, A_{max} is the saturation anisotropy, and K_d is the dissociation constant. For concentration points with only two measurements, the standard error was set at a value 50% larger than the largest standard error on the respective curve for weighted curve fitting. Finally, the curves were scaled relative to one another to reflect apparent differences in the saturation anisotropy. Dissociation constants reported for yMutSα were determined from the average binding curve, while those for *Taq* MutS were determined by the average

K_d determined for at least 4 independent binding curves determined at varied DNA concentrations.

Single-molecule fluorescence microscopy

Slide and sample preparation

Quartz microscope slides and flow channels were prepared as previously described (Weninger, Bowen et al. 2003). Slides were thoroughly cleaned by 15 minute incubations in a bath sonicator in the following series of solvents: alconox, acetone, ethanol, 1 M KOH, ethanol, 1 M KOH. Slides were rinsed and stored in water and flamed under a propane torch to dry immediately before use. Flow channels were created in the slides by adhering a no. 1.5 coverslip to the slide using Scotch double-sided tape as a spacer. Edges were sealed with epoxy. Samples were inserted into the channels through small holes that had been drilled in the quartz slide prior to cleaning.

The quartz surface was treated first with biotinylated-BSA (1 mg/mL, 5 minute incubation) followed by streptavidin (0.1 mg/mL, 5 minute incubation), similar to methods previously described (McKinney, Freeman et al. 2005). Annealed biotinylated, fluorescently-labeled, mismatched DNA was added to the treated surfaces at 10 to 30 pM for 5 minutes, and the unbound DNA was rinsed away with chilled buffer. Samples were imaged at room temperature in the above buffer with the addition of enzymatic oxygen scavenging components (2% glucose, 1% β-mercaptoethanol, 0.1 mg/mL glucose oxidase, 0.025 mg/mL catalase) to enhance fluorophore lifetime and triplet state quencher cyclooctatetraene (~50 μM) to reduce dye blinking.

The protein was allowed to bind the DNA for at least 5 minutes prior to image collection. Fluorescence images were collected both in the absence and presence of protein for accurate comparison of protein-induced conformational changes in the DNA.

TIR Fluorescence Microscopy

Data were collected using a prism-type total internal reflection fluorescence (TIRF) laser microscope as described (Weninger, Bowen et al. 2003; Bowen, Weninger et al. 2005). Two lasers were directed onto the prism, one at 532 nm to directly excite the FRET donor (TAMRA) and one at 635 nm to directly excite the FRET acceptor (Cy5) at the quartz-solution interface. Fluorescence emission was collected through a 60x 1.2 NA water immersion objective and split by a 645 nm dichroic mirror into short and long wavelength paths. These paths were filtered for TAMRA and Cy5 emissions using HQ 585/70 and HQ 700/75 bandpass filters, respectively. The respective spectrally-resolved emissions were relayed as dual images on an intensified charge-coupled device camera. Images were exposed at 10 frames per second and collected using software written in-house (Keith Weninger, NCSU).

Observed intensities of single-molecules were integrated with software written in-house (Keith Weninger, NCSU) to obtain individual fluorescence emission time traces as described (Bowen, Weninger et al. 2005). Emission traces were background corrected, and FRET efficiencies were calculated from the respective donor and acceptor emissions as $E = (I_A)/(I_D + I_A)$, where E is the energy transfer and I_D and I_A are the intensities of the donor fluorophore and the acceptor fluorophore respectively. Further details on Materials and Methods can be found in Chapter 5.

References

Alani, E. (1996). "The Saccharomyces cerevisiae Msh2 and Msh6 proteins form a complex that specifically binds to duplex oligonucleotides containing mismatched DNA base pairs." Mol Cell Biol **16**(10): 5604-15.

Biswas, I., C. Ban, et al. (1999). "Oligomerization of a MutS mismatch repair protein from Thermus aquaticus." J Biol Chem **274**(33): 23673-8.

Bowen, M. E., K. Weninger, et al. (2005). "Single-molecule studies of synaptotagmin and complexin binding to the SNARE complex." Biophys J **89**(1): 690-702.

Carey, J. (1991). "Gel retardation." Methods Enzymol **208**: 103-17.

Clark, A. B., M. E. Cook, et al. (1999). "Functional analysis of human MutSalpha and MutSbeta complexes in yeast." Nucleic Acids Res **27**(3): 736-42.

Drotschmann, K., W. Yang, et al. (2001). "Asymmetric recognition of DNA local distortion. Structure-based functional studies of eukaryotic Msh2-Msh6." J Biol Chem **276**(49): 46225-9.

Habraken, Y., P. Sung, et al. (1998). "ATP-dependent assembly of a ternary complex consisting of a DNA mismatch and the yeast MSH2-MSH6 and MLH1-PMS1 protein complexes." J Biol Chem **273**(16): 9837-41.

Holmes, S. F., K. D. Scarpinato, et al. (2007). "Specialized mismatch repair function of Glu339 in the Phe-X-Glu motif of yeast Msh6." DNA Repair (Amst) **6**(3): 293-303.

Jiricny, J., S. S. Su, et al. (1988). "Mismatch-containing oligonucleotide duplexes bound by the E. coli mutS-encoded protein." Nucleic Acids Res **16**(16): 7843-53.

Junop, M. S., G. Obmolova, et al. (2001). "Composite active site of an ABC ATPase: MutS uses ATP to verify mismatch recognition and authorize DNA repair." Mol Cell **7**(1): 1-12.

Kunkel, T. A. and D. A. Erie (2005). "DNA mismatch repair." Annu Rev Biochem **74**: 681-710.

Lakowicz, J. R. (1999). Topics in Fluorescence Spectroscopy. New York, Kluwe Academic/Plenum Publishers.

Lamers, M. H., A. Perrakis, et al. (2000). "The crystal structure of DNA mismatch repair protein MutS binding to a G x T mismatch." Nature **407**(6805): 711-7.

Lebbink, J. H., D. Georgijevic, et al. (2006). "Dual role of MutS glutamate 38 in DNA mismatch discrimination and in the authorization of repair." Embo J **25**(2): 409-19.

Lohman, T. M. and W. Bujalowski (1991). "Thermodynamic methods for model-independent determination of equilibrium binding isotherms for protein-DNA interactions: spectroscopic approaches to monitor binding." Methods Enzymol **208**: 258-90.

Malkov, V. A., I. Biswas, et al. (1997). "Photocross-linking of the NH2-terminal region of Taq MutS protein to the major groove of a heteroduplex DNA." J Biol Chem **272**(38): 23811-7.

Marsischky, G. T. and R. D. Kolodner (1999). "Biochemical characterization of the interaction between the Saccharomyces cerevisiae MSH2-MSH6 complex and mispaired bases in DNA." J Biol Chem **274**(38): 26668-82.

McKinney, S. A., A. D. Freeman, et al. (2005). "Observing spontaneous branch migration of Holliday junctions one step at a time." Proc Natl Acad Sci U S A **102**(16): 5715-20.

Myszka, D. G. (2000). "Kinetic, equilibrium, and thermodynamic analysis of macromolecular interactions with BIACORE." Methods Enzymol **323**: 325-40.

Natrajan, G., M. H. Lamers, et al. (2003). "Structures of Escherichia coli DNA mismatch repair enzyme MutS in complex with different mismatches: a common recognition mode for diverse substrates." Nucleic Acids Res **31**(16): 4814-21.

Obmolova, G., C. Ban, et al. (2000). "Crystal structures of mismatch repair protein MutS and its complex with a substrate DNA." Nature **407**(6805): 703-10.

Schofield, M. J., F. E. Brownewell, et al. (2001). "The Phe-X-Glu DNA binding motif of MutS. The role of hydrogen bonding in mismatch recognition." J Biol Chem **276**(49): 45505-8.

Schofield, M. J., S. Nayak, et al. (2001). "Interaction of Escherichia coli MutS and MutL at a DNA mismatch." J Biol Chem **276**(30): 28291-9.

Selmane, T., M. J. Schofield, et al. (2003). "Formation of a DNA mismatch repair complex mediated by ATP." J Mol Biol **334**(5): 949-65.

Wang, H., Y. Yang, et al. (2003). "DNA bending and unbending by MutS govern mismatch recognition and specificity." Proc Natl Acad Sci U S A **100**(25): 14822-7.

Warren, J. J., T. J. Pohlhaus, et al. (2007). "Structure of the Human MutSalpha DNA Lesion Recognition Complex." Mol Cell **26**(4): 579-92.

Weninger, K., M. E. Bowen, et al. (2003). "Single-molecule studies of SNARE complex assembly reveal parallel and antiparallel configurations." Proc Natl Acad Sci U S A **100**(25): 14800-5.

Yamamoto, A., M. J. Schofield, et al. (2000). "Requirement for Phe36 for DNA binding and mismatch repair by Escherichia coli MutS protein." Nucleic Acids Res **28**(18): 3564-9.

Yang, Y., L. E. Sass, et al. (2005). "Determination of protein-DNA binding constants and specificities from statistical analyses of single molecules: MutS-DNA interactions." Nucleic Acids Res **33**(13): 4322-34.

CHAPTER FOUR

ENSEMBLE AND SINGLE-MOLECULE FRET REVEAL MISMATCHED DNA BENDING INDUCED BY YEAST MSH2-MSH6 (yMutSα)

Introduction

Eukaryotic MMR is significantly more complex than the homologous prokaryotic systems, with multiple homologs of each repair protein functioning interchangeably based on the nature of the mismatch (Acharya, Wilson et al. 1996). Msh2-Msh6 (MutSα) is the eukaryotic MutS homolog that functions most similarly to *E. coli* and *Taq* MutS. Msh6 contains the same conserved Glu-X-Phe binding motif that functions in mismatch recognition by MutS (discussed in Chapter 3) and has been shown to asymmetrically bind small insertion/deletion loops and base-base mismatches in the same manner as prokaryotic MutS homodimers (Acharya, Wilson et al. 1996; Drotschmann, Yang et al. 2001; Schofield, Brownewell et al. 2001; Warren, Pohlhaus et al. 2007).

The primary objective of the work described here is to investigate DNA bending at a mismatch induced by yMutSα to determine if the DNA bending model of mismatch initiation proposed for prokaryotes could be applied to a eukaryotic DNA mismatch repair system. Fluorescence resonance energy transfer (FRET) measurements were obtained to monitor ensemble bending of mismatched DNA by yMutSα. Single-molecule FRET experiments

were further pursued to observe the dynamics of yMutSα-mismatched DNA complexes. The results presented here support the potential application of the DNA bending model to eukaryotic MMR initiation (Lamers, Perrakis et al. 2000; Obmolova, Ban et al. 2000; Junop, Obmolova et al. 2001; Schofield, Nayak et al. 2001; Selmane, Schofield et al. 2003; Wang, Yang et al. 2003).

Results and Discussion

yMutSα DNA bending measured by ensemble FRET

Eukaryotic mismatch repair proteins have been extensively studied, however little is known about the structure-function properties of many of the eukaryotic mismatch repair homologs. Crystal structures, AFM, and FRET have clearly shown that *E. coli* and *Taq* MutS induce bending in mismatched DNA at the mismatch site (Lamers, Perrakis et al. 2000; Obmolova, Ban et al. 2000; Wang, Yang et al. 2003), and moderate bending was recently observed in the human MutSα-mismatched DNA crystal structure (Warren, Pohlhaus et al. 2007). The bent MutS-DNA complex is hypothesized to play a significant role in mismatch recognition, specificity, and repair. Here we show evidence of eukaryotic MutS homolog *S. cerevisiae* Msh2-Msh6, or yMutSα, inducing DNA bending in two mismatched DNA substrates: a ΔT and a GT mismatch.

We first employed ensemble FRET to observe changes in DNA bending induced by yMutSα. Figure 4.1 shows the fluorescence spectra of GT mismatched DNA in the absence and presence of yMutSα. A decrease in FRET donor intensity at 582 nm and an increase in FRET acceptor intensity at 660 nm are observed. Figure 4.2 shows the absolute changes in

emission of the FRET donor (squares) and the FRET acceptor (circles) for three DNA substrates: a GT mismatch (A), a ΔT (B), and homoduplex DNA (C), for increasing concentrations of yMutSα.

From the intensity changes we were able to estimate the average bend angle of all MutS-DNA complexes in solution. Average bending was calculated based on the change in FRET donor intensity from free DNA to DNA bound by yMutSα (described in Materials and Methods and Chapter 5). The average bending of these two mismatches induced by yMutSα at room temperature was determined to be 25° ± 6° and 40° ± 8° for the ΔT and GT mismatch, respectively. Deviations are calculated from three independent measurements and do not account for errors in the donor-acceptor distance calculations or the documented error in R_o for the FRET dye pair (described in Materials and Methods). FRET results for homoduplex DNA in the presence of yMutSα show little to no fluorescence intensity changes (Figure 4.2 C), indicating that bending induced by yMutSα is mismatch specific as has been shown for the prokaryotic homologs (Chapter 2) (Wang, Yang et al. 2003).

yMutSα DNA bending measured by single-molecule FRET

To further explore the dynamics of DNA bending induced by yMutSα, we employed single-molecule FRET to measure conformational fluctuations of the DNA in real-time upon yMutSα binding. The mismatched DNA substrates used for single-molecule FRET were the same as those used for ensemble FRET experiments, however the DNA was 31 base-pairs longer and biotinylated at one end for surface binding (described in Chapter 2, Figure 2.1). Single-molecule FRET trajectories for DNA in the presence of yMutSα for a GT mismatch and a ΔT are shown in Figure 4.3. Typical FRET time traces indicated that molecules were

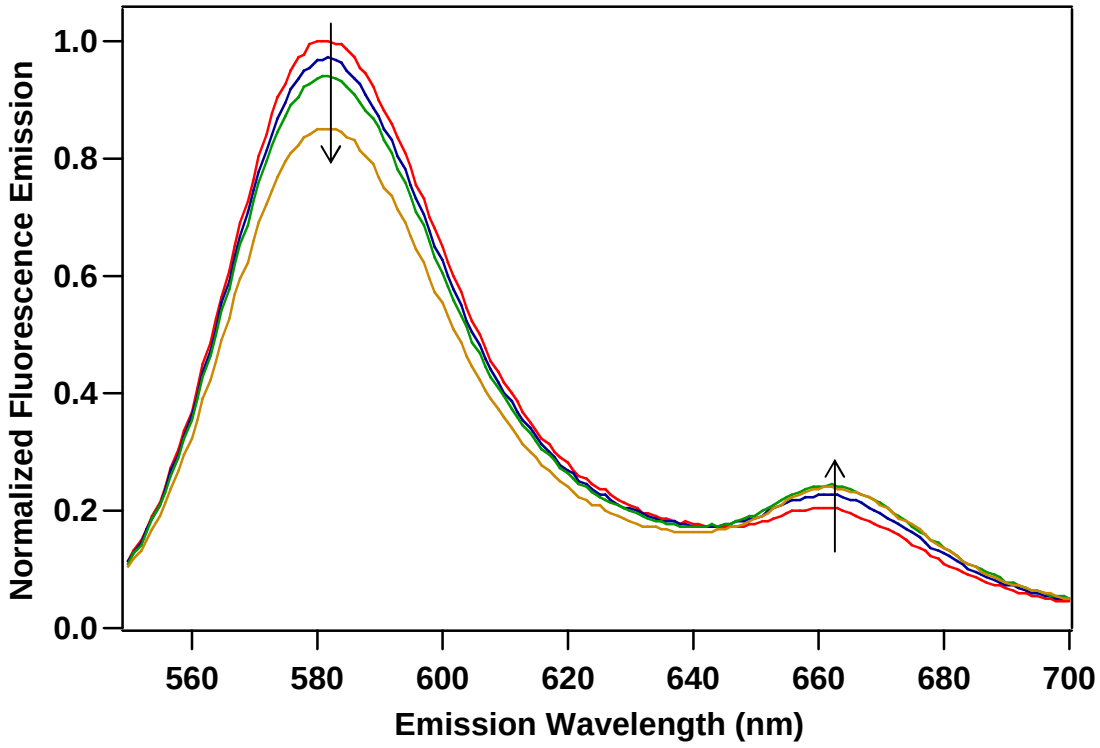

Figure 4.1 Ensemble FRET revealing DNA bending induced by yMutSα

Fluorescence spectra of 10 nM GT mismatch dsDNA (FRET substrate Figure 5.1 D) upon the addition of yMutSα. The arrows indicate increasing concentration of yMutSα from 0 nM (red curve) to 60 nM (orange curve). Blue and green curves represent the addition of 8 nM and 20 nM yMutSα, respectively. The FRET donor emission decreases upon the addition of protein, and the FRET acceptor emission subsequently increases, clearly showing energy transfer between the two fluorophores and thus DNA bending induced by the protein. Normalized emissions at 582 nm as a function of protein concentration were used in determining the average bend angle.

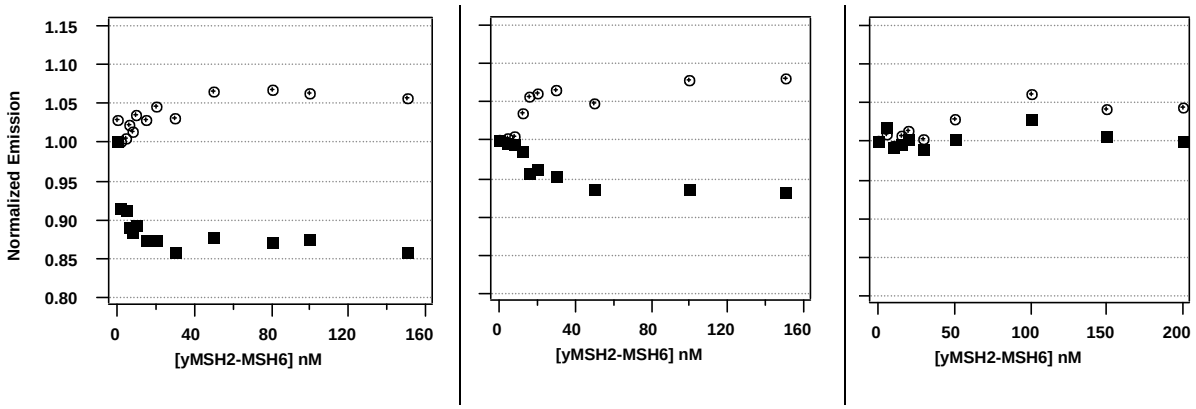

Figure 4.2 Normalized FRET donor and acceptor emissions for yMutSα

Normalized fluorescence emission of the FRET donor (solid squares, emission 582 nm) and the FRET acceptor (open circles, emission 660 nm) as a function of yMutSα (yMsh2-Msh6) concentration for three different DNA substrates: (A) GT mismatch; (B) +1 T-bulge; and, (C) homoduplex DNA. Emission values are normalized for all three substrates by dividing the emission value at each point by that for free DNA (0 nM yMsh2-Msh6). This normalization allows us to directly visualize changes in donor and acceptor emission with respect to one another as well as allowing for comparison of extent of FRET for all substrates. Negative FRET (donor decrease at 582 nm) is more dominant and the signal less noisy than positive FRET (acceptor increase at 660 nm), therefore the extent of negative FRET is more reliable for comparison of FRET between substrates and is subsequently used to calculate average bend angles. yMutSα did not bind to homoduplex DNA, and this result is represented here by no change in FRET (C).

	yMutSα	*Taq* MutS
Average bend angle, ΔT	25° ± 6°	40° ± 2°
Average bend angle, GT	40° ± 8°	39° ± 7°

Table 4.1 Average DNA bend angles for MutS(α) determined by ensemble FRET

Mismatched DNA average bend angles as determined by ensemble fluorescence resonance energy transfer for *Taq* MutS and yMutSα.

not dynamic, staying in a single FRET conformation for the duration of the time trace (Figure 4.3, top panel). Fewer than 10% of the DNA molecules (GT and ΔT) in the presence of yMutSα underwent a conformational change during the time traces (Figure 4.3, bottom panel), indicating that while bending is induced at the mismatch, conformational fluctuations between multiple conformational states were unlikely to occur on the time scale of the experiments (100 seconds).

Distributions of FRET conformations for free DNA and DNA in the presence of yMutSα for both mismatches are shown in Figure 4.4. We observe bending in GT mismatched DNA induced by yMutSα directly from the FRET distribution of states, where the distribution in the presence of yMutSα is shifted to higher FRET (or more bent) conformations than the distribution in the absence of yMutSα (Figure 4.4 A).

In contrast, for ΔT in the presence of yMutSα, the distribution of FRET states is nearly identical to that of free DNA (Figure 4.4 B). The breadth of the distribution is slightly broader in the presence of protein, and there is an increase in skew on the high FRET side of the distribution, both suggesting that the protein might be interacting with the DNA. Ensemble FRET results revealed that less bending is induced at a ΔT than a GT mismatch, therefore the single-molecule FRET distributions are consistent with this finding. In addition, crystal structures of human MutSα reveal ~ 45° bending in the DNA compared with ~ 60° bending observed in the crystal structures of prokaryote MutS homologs, consistent with our observation of less bending of these mismatched DNA substrates in comparison to bending induced by *Taq* MutS (Chapter 2) (Lamers, Perrakis et al. 2000; Obmolova, Ban et al. 2000; Natrajan, Lamers et al. 2003; Warren, Pohlhaus et al. 2007).

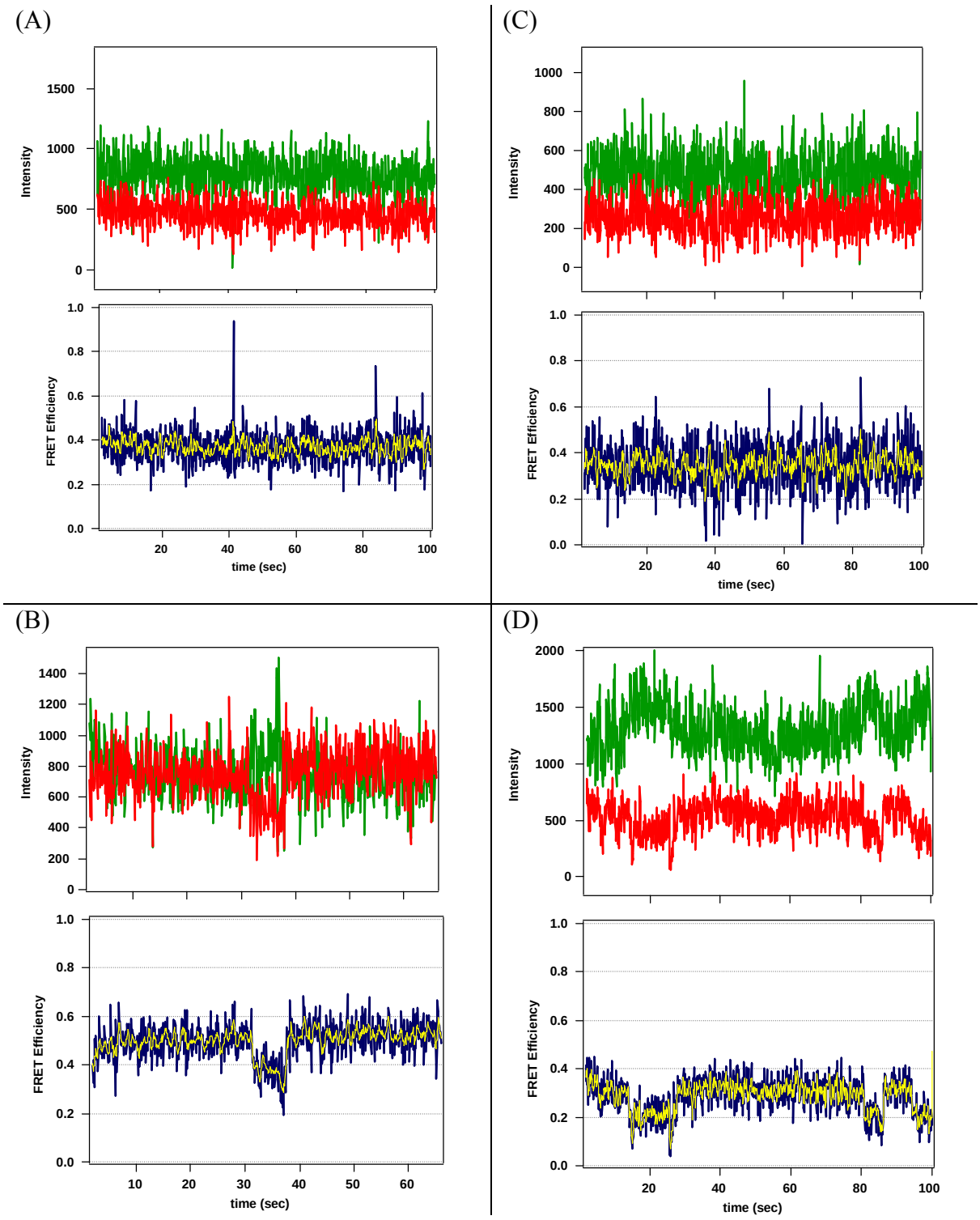
(A)
Intensity
1500
1000
500
0
FRET Efficiency
1.0
0.8
0.6
0.4
0.2
0.0
20
40
60
80
100
time (sec)
(C)
Intensity
1000
800
600
400
200
0
FRET Efficiency
1.0
0.8
0.6
0.4
0.2
0.0
20
40
60
80
100
time (sec)
(B)
Intensity
1400
1200
1000
800
600
400
200
0
FRET Efficiency
1.0
0.8
0.6
0.4
0.2
0.0
10
20
30
40
50
60
time (sec)
(D)
Intensity
2000
1500
1000
500
0
FRET Efficiency
1.0
0.8
0.6
0.4
0.2
0.0
20
40
60
80
100
time (sec)

Figure 4.3 Single-molecule FRET traces of mismatched DNA-yMutSα complexes

Single-molecule FRET trajectories for DNA in the presence of yMutSα for two mismatches: a GT base-base mismatch (A and B) and a +1 T-bulge (C and D). Typical FRET time traces indicated that molecules were not dynamic, staying in a single FRET conformation for the duration of the time trace (A and C). Fewer than 10% of the molecules measured demonstrated some conformational change during the time trace (B and D).

(A)

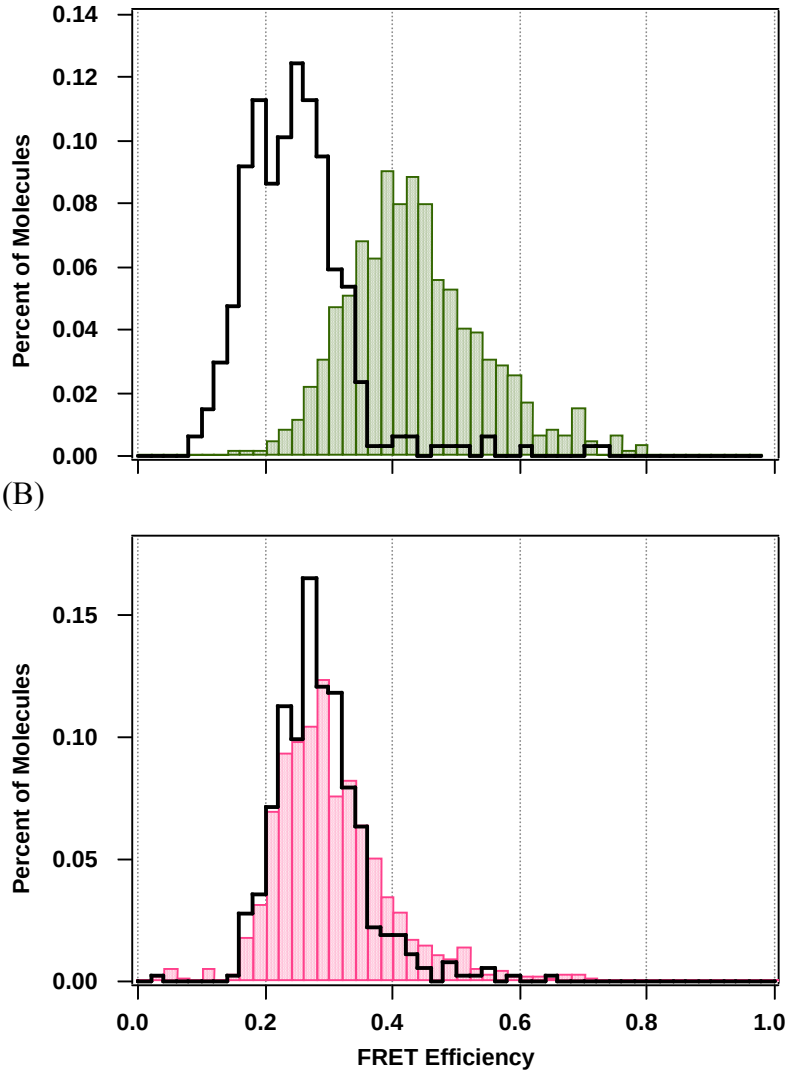

Figure 4.4 FRET efficiency distributions of mismatched DNA-yMutSα complexes

Single-molecule FRET efficiency distribution of states for GT mismatched (A) and T-bulge DNA (B) in the absence of yMutSα (black cityscape) and presence of yMutSα (colored bars). The distributions are represented as percent of molecules for comparison. Histogram for GT mismatch is comprised of free DNA (n=337) and DNA in the presence of yMutSα (n=556). Histogram for T-bulge is comprised of free DNA (n=364) and DNA in the presence of yMutSα (n=1135).

When molecules were closely analyzed, conformational changes among multiple low FRET states were observed in a subset of molecules (Figure 4.3 D), dynamics that are not observed in the absence of yMutSα. Taken together, these results suggest that yMutSα may be inducing a conformational change in ΔT DNA, however our FRET assay does not offer the distance resolution necessary to resolve these moderately bent conformations from free DNA. Future work will entail employing this FRET assay with a different FRET dye pair that will offer more distance sensitivity for the reduced bending observed for yMutSα bound to a ΔT.

Conclusions and Future Directions

Ensemble and single-molecule FRET was employed to measure yMutSα-induced DNA bending at a mismatched DNA base pair. DNA bending induced by yMutSα is clearly observed at both a GT mismatch and a ΔT using ensemble FRET, providing evidence relating the DNA bending model to eukaryotic mismatch repair. While this work is preliminary, it sets the foundation for a host of work using ensemble and single-molecule fluorescence techniques to study DNA mismatch repair initiation by yMutSα.

Because little bending was observed for ΔT DNA in the presence of yMutSα, it would be beneficial to modify the fluorescent dye pair to adjust the Förster distance of the FRET pair and thus the distance sensitivity of the experiment. By increasing the Förster distance, the FRET distribution peaks centered at 0.25 would be shifted to intermediate FRET values ranging anywhere from 0.3 to 0.7, and greater distance resolution could be achieved. An additional approach to this problem would entail labeling yMutSα where the

protein could be colocalized to the DNA while DNA bending was being observed. It is most likely that a combination of modified FRET dyes and yMutSα labeling will be the best approach to solving this problem.

This work represents an exciting beginning to using fluorescence to better understand DNA mismatch repair in eukaryotes and lends itself to studying other interactions related to the repair process, including DNA conformational changes induced by MutS mutants, conformational changes in the presence of ATP and MutL, MutS-MutL multimer stoichiometries, interactions of MutS and MutL with accessory proteins, studies of conformational dynamics of DNA with oxidative damage, and so on. The possibilities are vast.

Acknowledgements

I would to thank Susan Doyle for sharing purified yMutSα protein with me to perform the experiments described in this chapter and Dr. Haifa Johns for allowing me to use the undergraduate laboratory fluorometer for ensemble FRET measurements.

Materials and Methods

Proteins and Oligonucleotides

Thermus aquaticus (*Taq*) MutS was purified as previously described (Biswas, Ban et al. 1999; Clark, Cook et al. 1999; Schofield, Nayak et al. 2001). Wild-type *Saccharomyces cerevisiae* Msh2-Msh6 was purified by Susan Doyle (Erie Lab) with the help of our collaborators at NIH-NIEHS (Alan Clark, Tom Kunkel).

DNA oligonucleotides used in fluorescence experiments are listed in Table 5.1. Single-stranded oligonucleotides and complementary strands were purchased HPLC-purified from MWG Biotech and Integrated DNA Technologies. Figure 5.1 D represents the primary DNA substrate used in fluorescence assays to measure ensemble DNA bending induced by MutS and yMutSα. The ensemble FRET DNA substrate contained TAM-24 anealed to Cy5-ΔT, Cy5-GT, or Cy5-GC to generate a 19 base-pair duplex DNA fragment (with a 5 base 5' single-stranded overhang) containing a ΔT, a GT base-base mismatch, or GC homoduplex DNA, respectively. Duplex DNA substrates were made by combining the appropriate single-stranded oligonucleotides and annealing in buffer containing 20 mM Tris-HCl pH 7.8, 100 mM sodium acetate (NaOAc), and 5 mM magnesium chloride ($MgCl_2$) at 65°C for 20 minutes followed by slow cooling to room temperature. Annealed substrates were stored at 4°C until use.

DNA substrates for single-molecule FRET experiments contained TAM-50 anealed to Cy5-ΔT, Cy5-GT, or Cy5-GC to generate a 19 base-pair duplex DNA at the 3' end of the 50-mer fragment containing a ΔT, a GT base-base mismatch, or GC homoduplex DNA, respectively (Figure 5.2 A). Oligonucleotides were annealed in MutS binding buffer in a 1:1 ratio at 65°C for 20 minutes followed by slow cooling. When the temperature reached 55°C, an additional complementary strand (Comp-31) was added and annealed to complete the remaining duplex DNA. The substrate was allowed to slowly cool to room temperature and stored on ice or at 4°C.

Ensemble fluorescence resonance energy transfer (FRET) measurements

FRET measurements were obtained with a Jobin-Yvon Fluorolog-3 fluorometer with TAMRA excitation at 535 nm and FRET emission measured between 550 nm and 700 nm (TAMRA emission maximum at 582 nm, Cy5 emission maximum at 660 nm). TAMRA and Cy5 were selected as the FRET pair to monitor DNA bending induced by MutS proteins due to their large Förster radius (R_o) and optimal spectral properties. The R_o value, or inter-dye distance where energy transfer efficiency is 50%, for this donor-acceptor pair was experimentally determined from a single-molecule distance-dependent study to be 65 Å (± 5 Å) for these dyes tethered to DNA (Deniz, Dahan et al. 1999) and was used to determine relative inter-dye distances before and after MutS was added to the DNA substrates in these experiments.

Energy transfer (E) at inter-dye distance *r* is defined as $E(r) = (1 / (1 + (R_o/r)^6))$ (Eq. 4.1) (Lakowicz 1999). Changes in energy transfer efficiency may be determined by changes in absolute fluorescence intensity following the equation $E = (1 - (I_{da} / I_d))$ (Eq. 4.2), where I_{da} is the absolute fluorescence intensity of the FRET donor in the presence of a FRET acceptor and I_d, the fluorescence intensity of the FRET donor in the absence of acceptor (Lakowicz 1999). For the ensemble FRET DNA probe in Figure 5.1 D, I_d was determined as the fluorescence intensity of TAMRA in the absence of MutS and I_{da}, in the presence of MutS. Assuming the DNA duplex is nearly linear and that the mismatch does not introduce distortion in the DNA (addressed in Chapter 2, Figure 2.3), the inter-dye distance in the absence of MutS (r_1) was calculated to be 71.8 Å for the 19 base-pair dye separation using a helical model of DNA described previously for fluorescence resonance energy transfer (Clegg, Murchie et al. 1993; Jares-Erijman and Jovin 1996; Deniz, Dahan et al. 1999). The inter-dye distance in the presence of MutS (r_2) at saturation was calculated from Equations

(4.1) and (4.2) and the acquired intensity measurements. The fluorescence intensity of TAMRA in the absence of Cy5 was monitored as a function of MutS concentration, and fluctuations in this signal were applied as correction factors to FRET intensity measurements. The average induced bend angle was estimated from r_2 and the segmental lengths between the fluorophores and the mismatch site using the Law of Cosines. Although exact bend angles and distances may not be precisely determined due to various considerations in the relative orientations of the dyes, we use these calculations for comparison of extent of bending induced by MutS and MutSα for multiple DNA substrates.

Single-molecule fluorescence microscopy

Slide and sample preparation

Quartz microscope slides and flow channels were prepared as previously described (Weninger, Bowen et al. 2003). Slides were thoroughly cleaned by 15 minute incubations in a bath sonicator in the following series of solvents: alconox, acetone, ethanol, 1 M KOH, ethanol, 1 M KOH. Slides were rinsed and stored in water and flamed under a propane torch to dry immediately before use. Flow channels were created in the slides by adhering a No. 1.5 coverslip to the slide using Scotch double-sided tape as a spacer. Edges were sealed with epoxy. Samples were inserted into the channels through small holes that had been drilled in the quartz slide prior to cleaning.

The quartz surface was treated first with biotinylated-BSA (1 mg/mL, 5 minute incubation) followed by streptavidin (0.1 mg/mL, 5 minute incubation) similar to methods previously described (McKinney, Freeman et al. 2005). Annealed biotinylated, fluorescently-labeled mismatched DNA substrates were added to the treated surfaces at 10 to

30 pM for 5 minutes, and the unbound DNA was rinsed away with chilled buffer. Samples were imaged at room temperature in the above buffer with the addition of enzymatic oxygen scavenging components (2% glucose, 1% β-mercaptoethanol, 0.1 mg/mL glucose oxidase, 0.025 mg/mL catalase) to enhance fluorophore lifetime and triplet state quencher cyclooctatetraene (~50 μM) to reduce dye blinking.

MutSα was allowed to bind the DNA for at least 5 minutes before data collection. Fluorescence images were collected both in the absence and presence of protein.

TIR Fluorescence Microscopy

Data were collected using a prism-type total internal reflection fluorescence (TIRF) laser microscope as described (Weninger, Bowen et al. 2003; Bowen, Weninger et al. 2005). Two lasers were directed onto the prism, one at 532 nm to directly excite the FRET donor (TAMRA) and one at 635 nm to directly excite the FRET acceptor (Cy5) at the quartz-solution interface. Fluorescence emission was collected through a 60x 1.2 NA water immersion objective and split by a 645 nm dichroic mirror into short and long wavelength paths. These paths were filtered for TAMRA and Cy5 emissions using HQ 585/70 and HQ 700/75 bandpass filters, respectively. The respective spectrally-resolved emissions were relayed as dual images on an intensified charge-coupled device camera. Images were exposed at 10 frames per second and collected using software written in-house (Keith Weninger, NCSU).

Observed intensities of single-molecules were integrated with software written in-house (Keith Weninger, NCSU) as described to obtain individual fluorescence emission time traces (Bowen, Weninger et al. 2005). Emission traces were background corrected, and

FRET efficiencies were calculated from the respective donor and acceptor emissions as $E = (I_A)/(I_D + I_A)$, where E is the energy transfer and I_D and I_A are the intensities of the donor fluorophore and the acceptor fluorophore respectively. Further details on Materials and Methods can be found in Chapter 5.

References

Acharya, S., T. Wilson, et al. (1996). "hMSH2 forms specific mispair-binding complexes with hMSH3 and hMSH6." Proc Natl Acad Sci U S A **93**(24): 13629-34.

Biswas, I., C. Ban, et al. (1999). "Oligomerization of a MutS mismatch repair protein from Thermus aquaticus." J Biol Chem **274**(33): 23673-8.

Bowen, M. E., K. Weninger, et al. (2005). "Single-molecule studies of synaptotagmin and complexin binding to the SNARE complex." Biophys J **89**(1): 690-702.

Clark, A. B., M. E. Cook, et al. (1999). "Functional analysis of human MutSalpha and MutSbeta complexes in yeast." Nucleic Acids Res **27**(3): 736-42.

Clegg, R. M., A. I. Murchie, et al. (1993). "Observing the helical geometry of double-stranded DNA in solution by fluorescence resonance energy transfer." Proc Natl Acad Sci U S A **90**(7): 2994-8.

Deniz, A. A., M. Dahan, et al. (1999). "Single-pair fluorescence resonance energy transfer on freely diffusing molecules: observation of Forster distance dependence and subpopulations." Proc Natl Acad Sci U S A **96**(7): 3670-5.

Drotschmann, K., W. Yang, et al. (2001). "Asymmetric recognition of DNA local distortion. Structure-based functional studies of eukaryotic Msh2-Msh6." J Biol Chem **276**(49): 46225-9.

Jares-Erijman, E. A. and T. M. Jovin (1996). "Determination of DNA helical handedness by fluorescence resonance energy transfer." J Mol Biol **257**(3): 597-617.

Junop, M. S., G. Obmolova, et al. (2001). "Composite active site of an ABC ATPase: MutS uses ATP to verify mismatch recognition and authorize DNA repair." Mol Cell **7**(1): 1-12.

Lakowicz, J. R. (1999). Topics in Fluorescence Spectroscopy. New York, Kluwe Academic/Plenum Publishers.

Lamers, M. H., A. Perrakis, et al. (2000). "The crystal structure of DNA mismatch repair protein MutS binding to a G x T mismatch." Nature **407**(6805): 711-7.

McKinney, S. A., A. D. Freeman, et al. (2005). "Observing spontaneous branch migration of Holliday junctions one step at a time." Proc Natl Acad Sci U S A **102**(16): 5715-20.

Natrajan, G., M. H. Lamers, et al. (2003). "Structures of Escherichia coli DNA mismatch repair enzyme MutS in complex with different mismatches: a common recognition mode for diverse substrates." Nucleic Acids Res **31**(16): 4814-21.

Obmolova, G., C. Ban, et al. (2000). "Crystal structures of mismatch repair protein MutS and its complex with a substrate DNA." Nature **407**(6805): 703-10.

Schofield, M. J., F. E. Brownewell, et al. (2001). "The Phe-X-Glu DNA binding motif of MutS. The role of hydrogen bonding in mismatch recognition." J Biol Chem **276**(49): 45505-8.

Schofield, M. J., S. Nayak, et al. (2001). "Interaction of Escherichia coli MutS and MutL at a DNA mismatch." J Biol Chem **276**(30): 28291-9.

Selmane, T., M. J. Schofield, et al. (2003). "Formation of a DNA mismatch repair complex mediated by ATP." J Mol Biol **334**(5): 949-65.

Wang, H., Y. Yang, et al. (2003). "DNA bending and unbending by MutS govern mismatch recognition and specificity." Proc Natl Acad Sci U S A **100**(25): 14822-7.

Warren, J. J., T. J. Pohlhaus, et al. (2007). "Structure of the Human MutSalpha DNA Lesion Recognition Complex." Mol Cell **26**(4): 579-92.

Weninger, K., M. E. Bowen, et al. (2003). "Single-molecule studies of SNARE complex assembly reveal parallel and antiparallel configurations." Proc Natl Acad Sci U S A **100**(25): 14800-5.

CHAPTER FIVE

MATERIALS AND METHODS

DNA substrates

Fluorescently-labeled single-stranded oligonucleotides and complementary strands were purchased HPLC-purified from MWG Biotech and Integrated DNA Technologies. A catalog of DNA oligonucleotides used in bulk and single-molecule fluorescence experiments are listed in Table 5.1. All oligonucleotides are listed as single-stranded fragments. Single-stranded DNA (ssDNA) was stored at -80°C in water until needed. Stocks were thawed on ice, then to room temperature, then heated to 65°C for 10 minutes to melt the DNA prior to annealing.

Duplex DNA substrates were made by combining the appropriate single-stranded oligonucleotides and annealing in buffer containing 20 mM Tris-HCl pH 7.8, 100 mM sodium acetate (NaOAc), and 5 mM magnesium chloride ($MgCl_2$) at 65°C for 20 minutes followed by slow cooling until the sample reached room temperature (standard conditions unless otherwise noted). Annealed substrates were stored at 4°C until use.

Fluorescence anisotropy DNA substrates

DNA substrates for fluorescence anisotropy experiments contained TAM-24 hybridized to ΔT-24, GT-24, AC-24, or GC-24 to generate a 24 base-pair DNA fragment containing a +1 T-bulge (ΔT), a GT base-base mismatch, an AC base-base mismatch, or GC homoduplex DNA, respectively (Figure 5.1 A). These oligonucleotides were annealed by the above conditions in a 1:1.1 ratio (labeled:unlabeled oligonucleotide). In addition, Cy5-tethered oligos were also designed with fluorescence anisotropy capability. Fluorescence anisotropy was performed using Cy5 by hybridizing Comp-24 to one of the 5 Cy5 oligonucleotides (Cy5-ΔT, Cy5-GT, Cy5-GC, Cy5-CC, or Cy5-AC) to generate a 19 base-pair duplex fragment containing ΔT, a GT mismatch, GC homoduplex DNA, a CC mismatch, or an AC mismatch, respectively (Figure 5.1 B). TAMRA-tethered duplex DNA substrates were typically the preferred substrate for anisotropy due to the increased detector sensitivity at this fluorescence emission range (582 nm).

Ensemble FRET DNA substrates

DNA substrates for ensemble FRET experiments were designed where two different inter-fluorophore separation distances could be employed: one with an inter-dye separation of 19 base-pairs and one with a separation of 24 base-pairs (Figure 5.1 C). The 19 base-pair FRET DNA substrate contained TAM-24 hybridized to Cy5-ΔT, Cy5-GT, Cy5-CC, Cy5-AC, or Cy5-GC to generate a 19 base-pair duplex DNA fragment (with a 5 base 5' single-stranded overhang) containing a ΔT, a GT mismatch, a CC mismatch, an AC mismatch, or GC homoduplex DNA, respectively (Figure 5.1 D). The 24 base-pair FRET DNA substrate contained TAM-Cy5-dual hybridized to ΔT-24, GT-24, AC-24, or GC-24 to generate the

same mismatches, only with an inter-fluorophore distance increased by 5 base-pairs. Oligonucleotides were annealed in a 1:1 ratio in the aforementioned buffer under the same temperature conditions.

Single-molecule FRET DNA substrates

DNA substrates for single-molecule FRET experiments contained TAM-50 hybridized to Cy5-ΔT, Cy5-GT, Cy-AC, or Cy5-GC to generate a 19 base-pair duplex DNA at the 3' end of the 50-mer fragment containing a ΔT, a GT mismatch, an AC mismatch, or GC homoduplex DNA, respectively (Figure 5.2 A). Oligonucleotides were annealed in buffer containing 20 mM Tris-HCl pH 7.8, 100 mM NaOAc, and 5 mM $MgCl_2$ in a 1:1 ratio at 65°C for 20 minutes followed by slow cooling. When the temperature reached 55°C, an additional complementary strand (Comp-31) was added and annealed to complete the remaining duplex DNA. The substrate was allowed to slowly cool to room temperature.

DNA substrates for single-molecule FRET controls were designed to generate the same mismatched substrates with only one of the two FRET dyes (donor-only or acceptor-only substrates, Figure 5.2 B-C). The donor-only DNA substrate (donor control) was prepared by annealing TAM-50 to ΔT-50, GT-50, or GC-50 to generate a 50-mer fragment containing a ΔT, a GT mismatch, or GC homoduplex DNA, respectively, with only the FRET donor at the 3' end and biotin at the 5' end (Figure 5.2 B). The acceptor-only DNA substrate (acceptor control) was prepared by annealing Bio-50 to Cy5-ΔT, Cy5-GT, or Cy5-GC to generate a 19 base-pair duplex DNA at the 3' end of the 50-mer fragment containing a ΔT, a GT mismatch, or GC homoduplex DNA, respectively. Oligonucleotides were annealed under the aforementioned conditions at 65°C for 20 minutes followed by slow cooling.

oligonucleotide	Sequence and modification (5’ to 3’)
TAM-24	TAC CTC ATC TCG AGC GTG CCG ATA-TAMRA
TAM-Cy5-24dual	Cy5-TAC CTC ATC TCG AGC GTG CCG ATA-TAMRA
Cy5-ΔT	TAT CGG CAC GTC TCG AGA TG-Cy5
Cy5-GT	TAT CGG CAC GTT CGA GAT G-Cy5
Cy5-GC	TAT CGG CAC GCT CGA GAT G-Cy5
Cy5-CC	TAT CGG CAC CCT CGA GAT G-Cy5
Cy5-AC	TAT CGG CAC ACT CGA GAT G-Cy5
ΔT-24	TAT CGG CAC GTC TCG AGA TGA GGT A
GT-24	TAT CGG CAC GTT CGA GAT GAG GTA
GC-24	TAT CGG CAC GCT CGA GAT GAG GTA
AC-24	TAT CGG CAC ACT CGA GAT GAG GTA
Comp-24	TAC CTC ATC TCG AGC GTG CCG ATA
TAM-50	Biotin-TGT CGG GGC TGG CTT AAG GTG TGA AAT ACC TCA TCT CGA GCG TGC CGA TA-TAMRA
Comp-31	AGG TAT TTC ACA CCT TAA GCC AGC CCC GAC A
Bio-50	Biotin-TGT CGG GGC TGG CTT AAG GTG TGA AAT ACC TCA TCT CGA GCG TGC CGA TA
GC-50	TAT CGG CAC GCT CGA GAT GAG GTA TTT CAC ACC TTA AGC CAG CCC CGA CA
GT-50	TAT CGG CAC GTT CGA GAT GAG GTA TTT CAC ACC TTA AGC CAG CCC CGA CA
ΔT-50	TAT CGG CAC GTC TCG AGA TGA GGT ATT TCA CAC CTT AAG CCA GCC CCG ACA
BioComp-30	Biotin-TGT CGG GGC TGG CTT AAG GTG TGA AA
T5’	GAC GCT AGC GT(6MI) CG CTC GTC GAG ATG AGG T
T3’	GAC GCT AGC (6MI)TG CGG CTC GTC GAG ATG AGG T
BF-100	ACC TCA TCT CGA CGA GCC GCC GCT AGC GTC
BF-109	ACC TCA TCT CGC GAG CCG CAC GCT AGC GTC
BF-120	ACC TCA TCT CGA CGA GCC GCA CGC TAG CGT C
BF-200	ACC TCA TCT CGA CGA GCC GTA CGC TAG CGT C
BF-209	ACC TCA TCT CGG CGA GCC GCA CGC TAG CGT C

Table 5.1 Oligonucleotides used in bulk and single-molecule fluorescence experiments

Catalog of oligonucleotides used in bulk and single-molecule fluorescence experiments. The location of the mismatch is underlined.

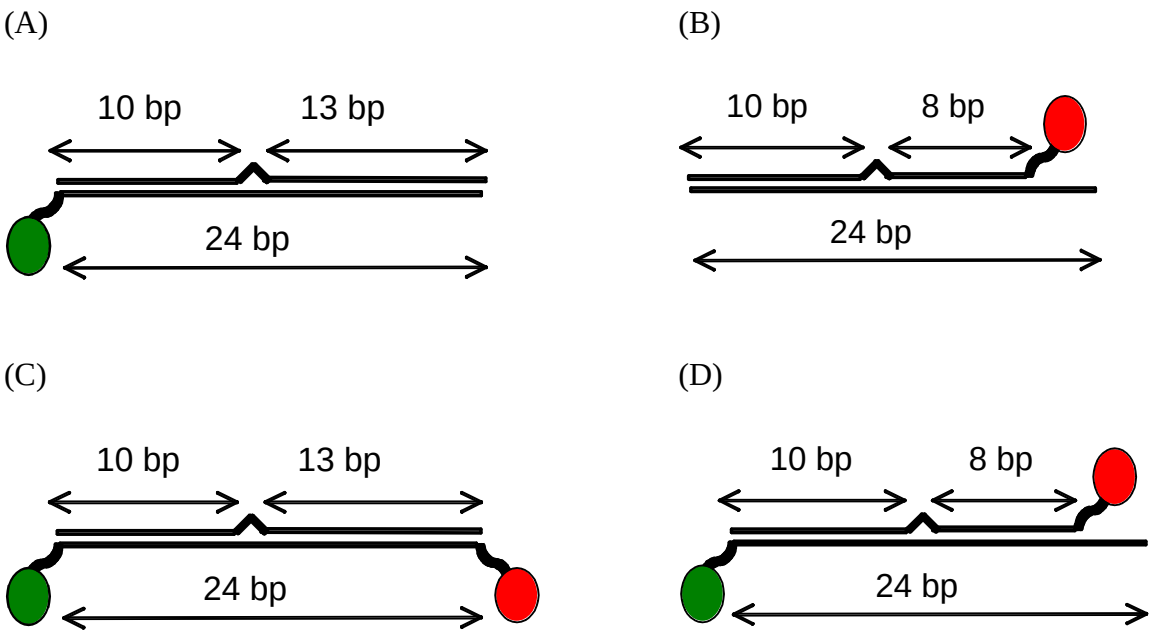

Figure 5.1 DNA substrates for fluorescence anisotropy and ensemble FRET

DNA substrates used in fluorescence anisotropy (A and B) and ensemble FRET experiments (C and D). The green oval represents the FRET donor (TAMRA, excited at 532 nm). The red oval represents the FRET acceptor (Cy5, excited at 635 nm). The triangle emerging from the DNA represents the location of the mismatch.

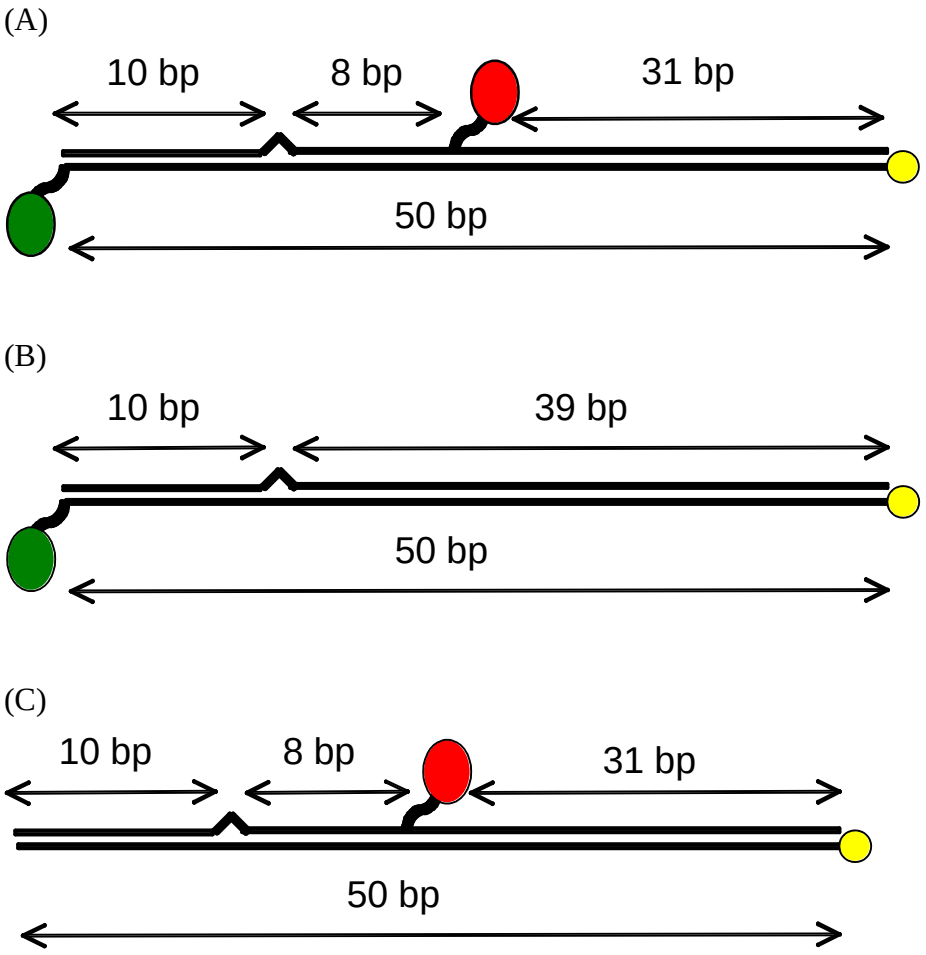

Figure 5.2 DNA substrates for single-molecule FRET

DNA substrates for single-molecule FRET experiments. (A) FRET substrate, (B) FRET donor control, (C) FRET acceptor control. The green oval represents the FRET donor (TAMRA, excited at 532 nm), and the red oval represents the FRET acceptor (Cy5, excited at 635 nm). The yellow circle represents the biotinylation site on the DNA.

When the temperature reached 55°C, Comp-31 was added and annealed to complete the acceptor-only duplex DNA (Figure 5.2 C).

Base-flipping fluorescent base analog DNA substrates

Single-stranded DNA substrates containing 6-methyl isoxanthopterin (6MI) were purchased gel-purified from Fidelity Systems, Inc. Two unique sequences were purchased with different respective locations of the fluorescent probe: T5' sequence, with the fluorescent base analog immediately 5' a cytosine and 3' a thymine; and, T3' sequence, with the fluorescent base analog immediately 3' a cytosine and 5' a thymine (Table 5.1).

Complementary strands were purchased HPLC purified from Integrated DNA Technologies, Inc. T5' or T3' oligonucleotides were hybridized to BF-100, BF-109, or BF-120 to generate double-stranded DNA containing a ΔT immediate 5' or 3' to the 6MI site (T5'-100 or T3'-100), a ΔT 8 or 10 bases away from the 6MI site (T5'-109 or T3'-109) (experimental controls), or homoduplex DNA (T5'-120 or T3'-120).

Duplex DNA with a GT mismatch at the 6MI site and a GT mismatch 7 or 9 bases away from the 6MI site (experimental control) were made by annealing T5' with BF-200 or BF-209, respectively.

Ensemble fluorescence experimental methods

Fluorescence anisotropy binding assays

Binding of MutS and yMutSα to heteroduplex and homoduplex DNA was monitored by equilibrium fluorescence anisotropy measurements obtained with a Jobin-Yvon

Fluorolog-3 fluorometer (23°C and 11°C) and a Tecan Safire II microarray plate reader (23°C). TAMRA was excited at 535 nm, and polarized emission was measured at 582 nm. Duplex DNA (ranging in concentration from 5 nM to 100 nM) was incubated with increasing protein concentrations for 5 minutes in binding buffer (20 mM Tris-HCl pH 7.8, 100 mM NaOAc, 5 mM $MgCl_2$) before each measurement was acquired. Anisotropy was calculated using the instrument software with corrections for dark and background counts and was measured as a function of protein concentration.

Fluorescence binding data analysis

The anisotropy data points were first normalized by setting the initial anisotropy value for free DNA (A_o) to 0 following the equation $A_i = (A_i - A_o)/A_o$ (Eq. 5.1), where A represents the anisotropy measurement and the corresponding subscript represents the protein concentration for that measurement. The yMutSα binding data were then normalized to an equivalent saturation anisotropy of 1 (A_{max}) for comparison. For yMutSα, a minimum of 3 binding curves were combined by averaging the anisotropy value at each protein concentration to create an average binding curve for the respective protein-DNA substrate. Binding curves were fit by a weighted non-linear regression binding isotherm using

$$A = A_{\max} \cdot \frac{K_D + P_{tot} + D_{tot} - \sqrt{(K_D + P_{tot} + D_{tot})^2 - 4D_{tot}P_{tot}}}{2D_{tot}} \qquad \text{(Eq. 5.2)}$$

where A is the normalized anisotropy, P_{tot} is the total added protein concentration, D_{tot} is the total dsDNA concentration, A_{max} is the saturation anisotropy, and K_d is the dissociation constant. For concentration points with only two measurements, the standard error was set at a value 50% larger than the largest standard error on the respective curve for weighted curve

fitting. Finally, the curves were relatively scaled to reflect apparent differences in the saturation anisotropy. Dissociation constants reported for yMutSα were determined from the average binding curve, while those for *Taq* MutS were determined by the average K_d determined for at least 4 independent binding curves determined at varied DNA concentrations.

Ensemble fluorescence resonance energy transfer (FRET) measurements

FRET measurements were obtained with a Jobin-Yvon Fluorolog-3 fluorometer with TAMRA excitation at 535 nm and FRET emission measured between 550 nm and 700 nm (TAMRA emission maximum at 582 nm, Cy5 emission maximum at 660 nm). TAMRA and Cy5 were selected as the FRET pair to monitor DNA bending induced by MutS proteins due to their large Förster radius (R_o) and optimal spectral properties. For this donor-acceptor pair, the R_o value, or inter-dye distance where energy transfer efficiency is 50%, was experimentally determined from a single-molecule distance-dependent study to be 65 Å (± 5 Å) for these dyes tethered to DNA (Deniz, Dahan et al. 1999) and was used to determine relative inter-dye distances before and after MutS was added to DNA substrates in these experiments.

Energy transfer (E) at inter-dye distance *r* is defined as $E(r) = (1 / (1 + (r/R_o)^6))$ (Eq. 5.3) (Lakowicz 1999). Changes in energy transfer efficiency may be determined by changes in absolute fluorescence intensity following the equation $E = (1 - (I_{da} / I_d))$ (Eq. 5.4), where I_{da} is the absolute fluorescence intensity of the FRET donor in the presence of a FRET acceptor and I_d, the fluorescence intensity of the FRET donor in the absence of acceptor (Lakowicz 1999). For the FRET DNA probes in Figure 5.1, I_d was determined as the

fluorescence intensity of TAMRA in the absence of MutS and I_{da}, in the presence of MutS. Assuming the DNA duplex is nearly linear, the inter-dye distance in the absence of MutS (r_1) was calculated to be 86.2 Å for the 24 base-pair dye separation and 71.8 Å for the 19 base-pair dye separation using a helical model of DNA described previously for fluorescence resonance energy transfer (Clegg, Murchie et al. 1993; Jares-Erijman and Jovin 1996; Deniz, Dahan et al. 1999). The inter-dye distance in the presence of MutS (r_2) at saturation was calculated from Equations (5.3) and (5.4) and the acquired intensity measurements. The fluorescence intensity of TAMRA in the absence of Cy5 was monitored as a function of MutS concentration, and fluctuations in this signal were applied as correction factors to FRET intensity measurements. The average induced bend angle was estimated from r_2 and the segmental lengths between the fluorophores and the mismatch site using the Law of Cosines. Although exact bend angles and distances may not be precisely determined due to various considerations in the relative orientations of the dyes, we use these calculations simply for comparison of extent of bending induced by MutS for multiple DNA substrates.

Single-molecule FRET experimental methods

Slide and sample preparation

Quartz microscope slides and flow channels were prepared as previously described (Weninger, Bowen et al. 2003). New quartz slides (1" x 3" x 1 mm, G. Finkenbeiner, Inc.) were drilled using 220G diamond point drill bits (part 115005, Starlite) to create a series of holes that would ultimately be used as sample flow channels (Figure 5.4 A-B). Slides were then thoroughly cleaned by 15 minute incubations in a bath sonicator in the following series of solvents: alconox, acetone, ethanol, 1 M KOH, ethanol, 1 M KOH. Slides were rinsed

(A)

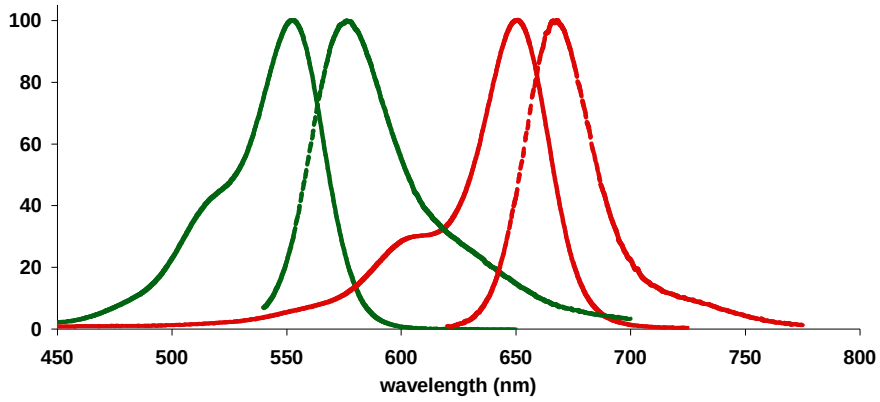

(B)

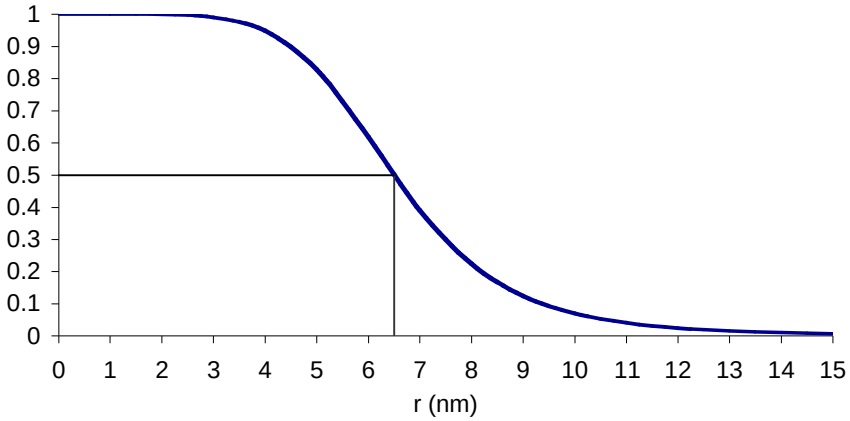

Figure 5.3 Absorption and emission profiles for TAMRA and Cy5

(A) Fluorescence absorption (solid lines) and emission (dashed lines) spectra of TAMRA (FRET donor, green) and Cy5 (FRET acceptor, red). The overlap of the donor emission and the acceptor absorption make this a good FRET pair with a Forster distance, or distance where energy transfer is 50%, experimentally determined to be ~6.5 nm (65 Å).

(B) Plot of dependence of energy transfer efficiency (E) on inter-dye distance (r, in nm). The Forster distance is marked at E = 0.5, or 50%. The best distance sensitivity between the two dyes, therefore, may be measured in the range between 4 and 8 nm.

and stored in water and flamed under a propane torch to dry immediately before use. Flow channels were created in the slides by adhering a No. 1.5 coverslip (VWR 48393 230) to the slide using Scotch double-sided tape as a spacer (Figure 5.4 A). Edges were sealed with epoxy (Figure 5.4 B). Samples were inserted into the channels through the small holes that had been drilled in the quartz slide prior to cleaning.

Biotin-BSA-coated surfaces were made by treating the quartz surface first with biotinylated-BSA (Sigma A8549, 1 mg/mL, 5 minute incubation) followed by streptavidin (Invitrogen S888, 0.1 mg/mL, 5 minute incubation) similar to methods previously described (McKinney, Freeman et al. 2005). Annealed biotinylated, fluorescently-labeled mismatched DNA substrates were added to the treated surfaces at 10 to 30 pM for 5 minutes, and the unbound DNA was rinsed away with chilled MutS binding buffer. Figure 5.5 is a cartoon representation of the surface. Samples were imaged at room temperature in MutS binding buffer (20 mM Tris-HCl pH 7.8, 100 mM NaOAc, and 5 mM $MgCl_2$) with the addition of enzymatic oxygen scavenging components to enhance fluorophore lifetime.

Optimal oxygen scavenging buffer was made by first supplementing binding buffer with 2% glucose (Sigma G7528) and triplet state quencher cyclooctatetraene (COT, Aldrich 138924, ~50 μM) (which functions to reduce dye blinking). This solution was 0.2 μm syringe-filtered. A 100x glucose oxidase/catalase (GOX/CAT) stock solution (20 mg/mL GOX (Sigma G6641), 5 mg/mL CAT (Sigma C3515)) was prepared in 100 μL MutS binding buffer supplemented with 1% β-mercaptoethanol (BME, Fluka 63689). This stock solution was filtered using a 0.2 μm nanosep microspin filter and stored at 4°C for up to 3 days. Immediately prior to imaging, 1x MutS binding buffer containing glucose and COT was

supplemented with 1% BME and GOX/CAT to generate a final buffering solution containing 0.2 mg/mL glucose oxidase and 0.05 mg/mL catalase.

MutS was allowed to bind the DNA for 5 minutes before image collection. Images were collected both in the presence and absence of MutS for every reaction. The concentration of MutS was also adjusted to measure variations in kinetics.

Biotin-PEG surface preparation

Biotin-PEG (polyethylene glycol) surfaces were also employed to tether biotinylated DNA while reducing interactions of MutS with the surface. To generate these surfaces, freshly drilled and solvent-cleaned slides were flamed under a propane torch to dry and subjected to an additional sonication in acetone for 15 minutes. No. 1.5 coverslips were placed in a porcelain slide holder (thoroughly cleaned with water and acetone) and sonicated in acetone for 15 minutes.

All glass slide tubs, slide holders, and supplies were thoroughly cleaned by rinsing with 1M KOH, water, and liberally with acetone. Three rectangular tubs and complementary slide holder were used for quartz slide reactions, while beakers and porcelain coverslip holders were used for coverslip reactions. Three baths were prepared as follows: bath #1 contained 200 mL of clean acetone; bath #2 contained 1% volume/volume silane (3-aminopropyl triethoxy silane, Vectabond SP-1800) in 200 mL clean acetone; and, bath #3 contained 200 mL of clean ddH_2O. Freshly sonicated quartz slides were placed in the slide carriage, and the slides were plunged into bath #2 and allowed to react for 5 minutes. The solution was agitated intermittently with a glass pipette. After the 5 minute reaction, the slides were removed from bath #2 and transferred to bath #1 to rinse away excess silane. The

(A)

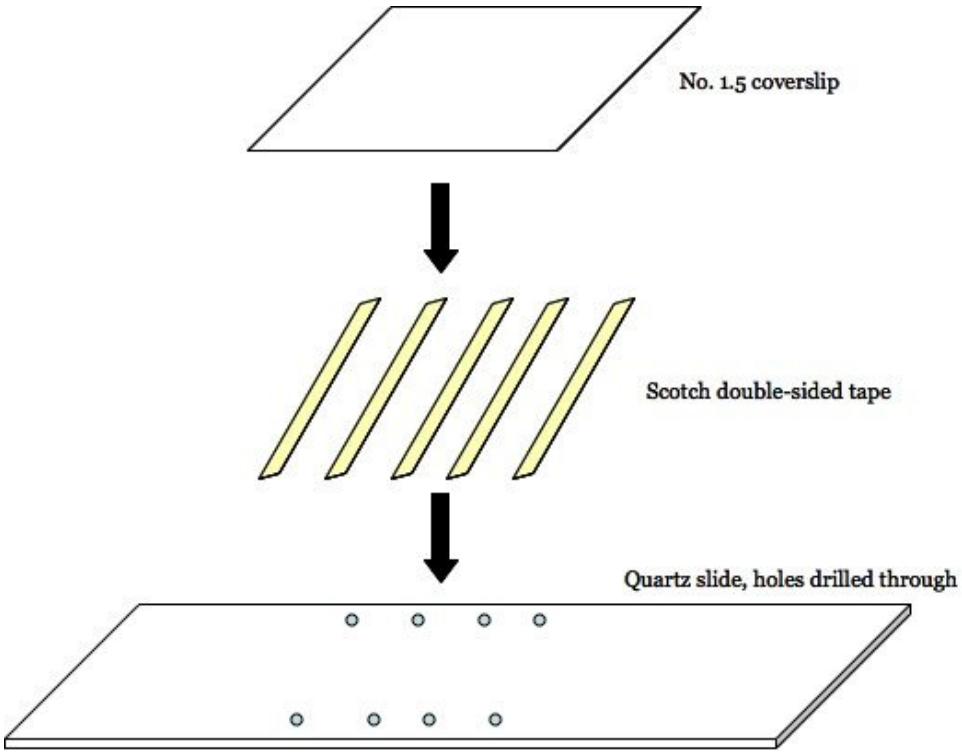

(B)

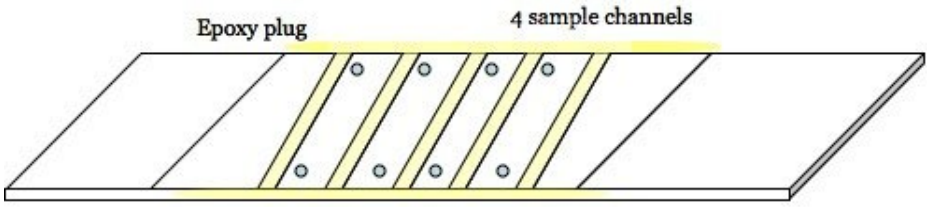

Figure 5.4 Microscope sample slide preparation

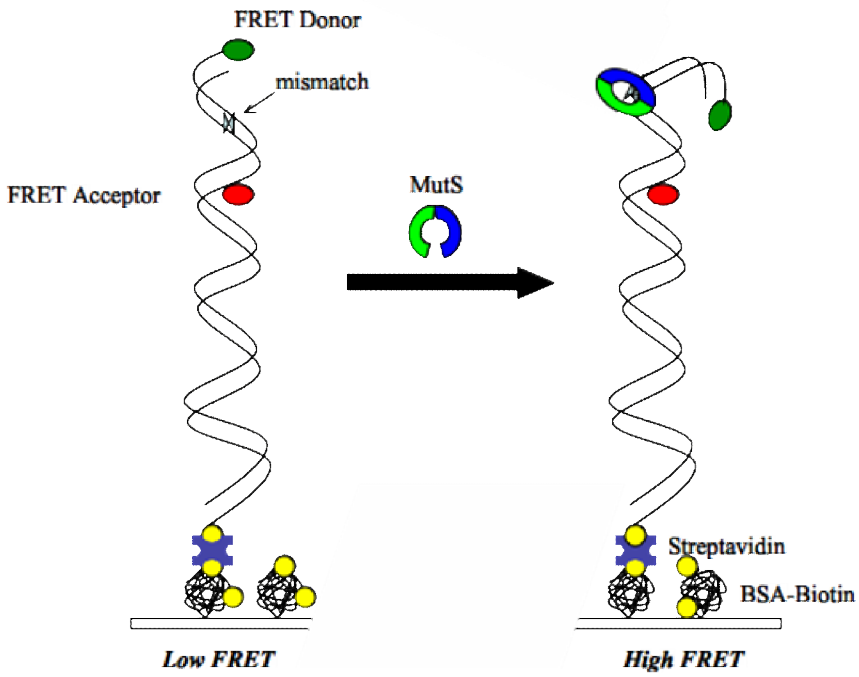

Figure 5.5 Cartoon representation of single-molecule FRET surface assembly and experiment

The green and red ovals represent the FRET donor and acceptor, respectively. Upon the binding of MutS (represented as the blue and green donut), and induced bending, the FRET donor and acceptor become closer in proximity, and energy transfer is increased.

slides were then transferred to bath #3 to quench the silane reaction. The slides were removed from the carriage and rinsed individually with water. Excess water was shaken away, and slides were allowed to dry on chemwipes. The same silane reaction procedure was performed on the coverslips, only reactions were carried out in glass beakers. Coverslips were also rinsed thoroughly and allowed to air-dry on chemwipes.

A 0.1 M sodium bicarbonate solution was prepared and allowed to chill on ice. Biotin-PEG solutions were prepared by mixing amine-reactive PEG with biotin-modified PEG to make ~0.1 to 1.0% biotin-PEG. This was achieved by resuspending NHS-PEG (N-hydroxysuccinimide ester-polyethylene glycol) and biotin-PEG in sodium bicarbonate solution at 100 mg/mL and 1 mg/mL, respectively. The amine reaction begins immediately upon suspension of these solutions in buffer, therefore this solution was mixed quickly, and 50-100 μL was deposited on the dried quartz slide immediately. A coverslip was sandwiched on top of the quartz slide. The slides were placed in an empty, clean pipette tip box (with water added at the bottom to keep the slides hydrated) and allowed to react in a dark place for up to 1 hour.

Upon completion of the PEG reaction, the slides were removed from the box and the coverslips were carefully pulled away from the quartz slide horizontally (without direct lifting) using tweezers. The slides and coverslips were thoroughly rinsed with nanopure water to remove excess unreacted PEG. The slides and coverslips were allowed to dry (PEG side facing UP) on chemwipes. Modified slides were stored in a plastic slide holder in a dark place for up to two weeks.

Vesicle encapsulation for single-molecule FRET

An alternative to directly tethering single DNA or protein molecules to a surface to perform single-molecule TIRF experiments is to encapsulate the fluorescent molecule of interest in a biotinylated-lipid vesicle. This has been employed previously to study conformational fluctuations of single-protein molecules during folding/unfolding transitions (Rhoades, Gussakovsky et al. 2003).

Biotinylated lipid was mixed with (egg) phosphatidyl choline lipid (Avanti polar lipids) to generate a 0.1% biotinylated-lipid solution (in chloroform) of ~ 20 mg/mL. Exactly 10 μL of this lipid mixture was place in the bottom of a glass culture test-tube. The lipid was dried under an stream of Argon, with the tube being continually rotated during drying to ensure the formation of a thin lipid film at the bottom of the tube. This rotation was necessary to avoid clumping of the lipid at the bottom of the tube. The tube was placed in a vacuum chamber for 15 to 30 additional minutes to remove excess chloroform residue from the lipid.

The fluorescent sample to be encapsulated was diluted to ~ 500 pM to create a sample solution of 600 μL total volume. This solution was added to the thin lipid film, swirled, and vortexed to mix. The cloudy solution was sonicated in an ice water bath (5 x 5 sec pulses) to break-up any elongated to onion-like membrane structures that may have formed during vortexing. The water bath during sonication is essential to prevent the vesicles from overheating.

The solution was syringe-filtered using glass syringes and custom frits (Avanti polar lipids). Two rubber O-rings were placed in the appropriate indentions in the two white frits and dampened with nanopure water. Two filter support papers (Avanti #610014) were

placed centered on top two rubber O-rings. A filtering membrane (Whatman Nucleopore track-etched membrane, 0.05 μm x 19 mm (Lot #4351006)) was placed centered over one of the two filter supports. The white frits are designed to slide into a custom bolt. One frit was placed in the bolt, and the other was carefully sandwiched on top, taking care not to displace the filter support papers from the center of the O-ring. This works well when done sideways. A white washer was placed in the bolt's complementary nut, and the nut was screwed onto the bolt tightly to create seal in the membrane between the two frits.

The bolt is designed to adapt to glass syringes on both sides. The solution is inserted to the bolt on side 1 and removed on side 2. The vesicle/fluorescent sample was drawn into one of two glass syringes, and the syringes were adhered to both sides of the bolt holding the fritted-membrane. The sample was pushed through side 1 of the membrane and collected through the syringe on side 2. The sample was pushed through the membrane, back-and-forth between the two syringes for at least 21 passes. The solution will begin to appear less cloudy and will eventually turn clear. Once totally clear, the solution was removed from the bolt through the syringe on side 2. It is important that the solution is not collected from the same syringe in which it was originally inserted. The sample was transferred to a sterile eppendorf tube. The syringes, white frits, O-rings, the nut, and the bolt were cleaned by rinsing 10 times with water and 10 times with absolute ethanol and allowed to air dry.

To separate vesicle-encapsulated fluorescent molecules from free fluorescent molecules in the solution, the solution was run through a size exclusion gravity column (Sepharose CL4B, Nap5 type). The column was pre-calibrated to determine the void volume and the volumes in which vesicles and free fluorescent molecule eluted. The column was rinsed 3 times with water then 3 times with buffer. About 100 μL of the vesicle sample was

loaded onto the column. Once loaded, buffer was run through the column. At this junction, fractions were collected as the solution eluted from the column. About 200 μL fractions were collected, and calibration measurements predict the fractions in which the vesicle sample resides. Vesicles containing fluorescent molecules elute from this column first, and free fluorescent molecules, which get caught in the sepharose, elute last.

The final fractions containing vesicle-encapsulated fluorescent molecules could then be diluted accordingly and tethered to a clean glass surface using the biotin-BSA-streptavidin coating described above.

Site-directed mutagenesis of Taq MutS for single-molecule colocalization

We were interested in pursuing multi-color fluorescence experiments that would enable us to use single-molecule fluorescence measurements to colocalize our protein (in this case *Taq* MutS) to our fluorescently-labeled DNA bound to the surface. In order to do this, it was necessary to place a fluorescent label on the protein so that its presence could be monitored using fluorescence microscopy. Unique protein-labeling sites are typically generated by cloning a non-native cysteine residue at the surface of the protein for labeling with a maleimide-reactive fluorophore. Native cysteine residues must be cloned out of the gene, therefore this method only works for a limited number of cysteine residues in the protein sequence. *Taq* MutS has one cysteine located at position 42 in the DNA binding motif. This residue is fairly buried and did not efficiently react with maleimide-reactive fluorophores. As a result, we did not clone this residue out of the gene sequence since it posed no labeling interference.

We performed site-directed mutagenesis to insert a non-native cysteine on the protein surface. A number of mutant MutS sequences were cloned, including mutations at the C-terminal of the enzyme (A769C, A779C, and L774C) and mutations near the sides of the enzyme in domain IV (E315C, G367C, and S376C). None of these mutant proteins survived expression and purification. We believe that these mutations induced folding problems that resulted in degradation, seemingly represented by fractionation patterns revealed in SDS-PAGE.

Coincidentally, a group from Korea had generated a double mutant *Taq* MutS clone to perform site-specific fluorescent labeling: C42A/T469C (Cho, Chung et al. 2007). Cho et. al. generously donated that cloned gene to us, and the protein was expressed and purified as described (Cho, Chung et al. 2007).

TIR Fluorescence Microscopy

Data were collected using a prism-type total internal reflection fluorescence (TIRF) laser microscope as described (Figure 5.6 A) (Weninger, Bowen et al. 2003; Bowen, Weninger et al. 2005). Two lasers were directed onto the prism, one at 532 nm to directly excite the donor dye (TAMRA) and one at 635 nm to directly excite the acceptor dye (Cy5) at the quartz-solution interface. Fluorescence emission was collected through a 60x 1.2 numerical aperature (NA) water immersion objective and split by a 645 nm dichroic mirror into short and long wavelength paths (Optical Insights Dual-View beam-splitter). These paths were filtered for TAMRA and Cy5 emissions using HQ 585/70 and HQ 700/75 bandpass filters, respectively. The respective spectrally-resolved emissions were relayed as dual images on an intensified charge-coupled device camera (Roper Scientific Cascade II

512B) (Figure 5.6 B). Images were exposed at 10 frames per second and collected using software written in-house by our collaborator (Keith Weninger, NCSU).

Typical experiments entailed an alternating laser excitation scheme whereby the molecules were first briefly subjected to red laser excitation to locate all viable FRET acceptor dyes. After this flash of red excitation, the molecules were subjected to green laser excitation for times ranging from 45 seconds to 150 seconds. Energy transfer was only calculated during green excitation. The molecules were once again subjected to red laser excitation at the completion of the experiment for appropriate background corrections. A sample single molecule trace, including excitation scheme, is shown in Figure 5.7.

Data Analysis

Observed intensities of single-molecules were integrated with software written in-house as described to obtain individual fluorescence emission time traces (Figure 5.6 B, 5.7) (Bowen, Weninger et al. 2005). Emission traces were background corrected, and FRET efficiencies were calculated from the respective donor and acceptor emissions as $E = (I_A)/(I_D + I_A)$ (Eq. 5.5), where E is the energy transfer and I_D and I_A are the intensities of the donor fluorophore and the acceptor fluorophore respectively (Figure 5.7).

Dynamic FRET efficiency traces were analyzed using an edge detection algorithm (written by our collaborators in the Computer Science Department (UNC)) to separate FRET transitions and calculate the average FRET efficiency and lifetime of each step as well as the sequence of FRET transitions. Step edges were convolved by the derivative of the Gaussian function as originally described by Canny (Canny 1986). This analysis is described in further detail in Appendix B. For FRET edge analysis, scale spaces were modified with

(A)

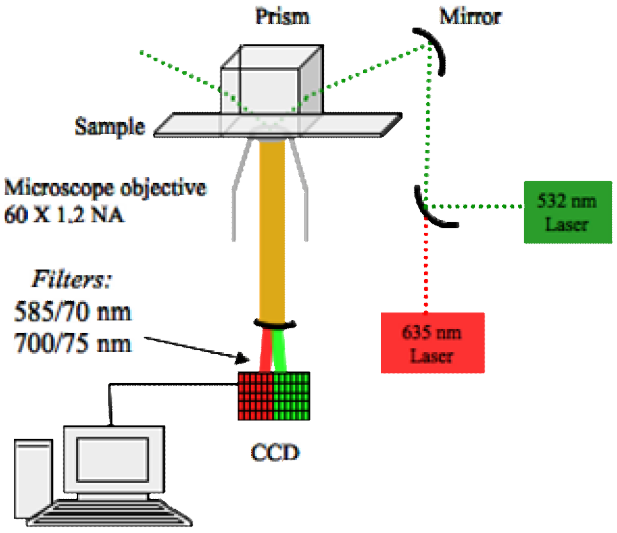

(B)

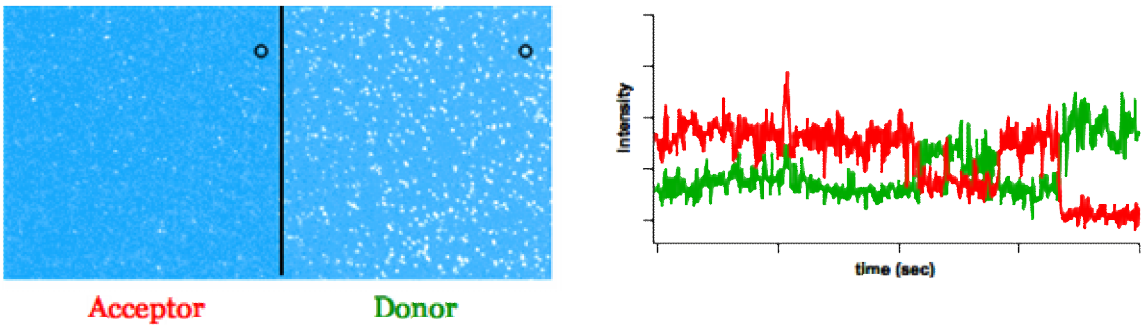

Figure 5.6 Schematic of single-molecule TIRF microscope

(A) Schematic of single-molecule TIRF microscope set-up. (B) Sample image of the surface as detected by the high resolution CCD camera. The left and right sides are geometrically mapped images of the same area on the surface only filtered separately to select for FRET donor emission (right side) and FRET acceptor emission (left side). To the right are representative time traces (FRET donor is the green trace, FRET acceptor is the red trace) obtained by selection of individual molecule from the surface (shown as black circles on the sample image).

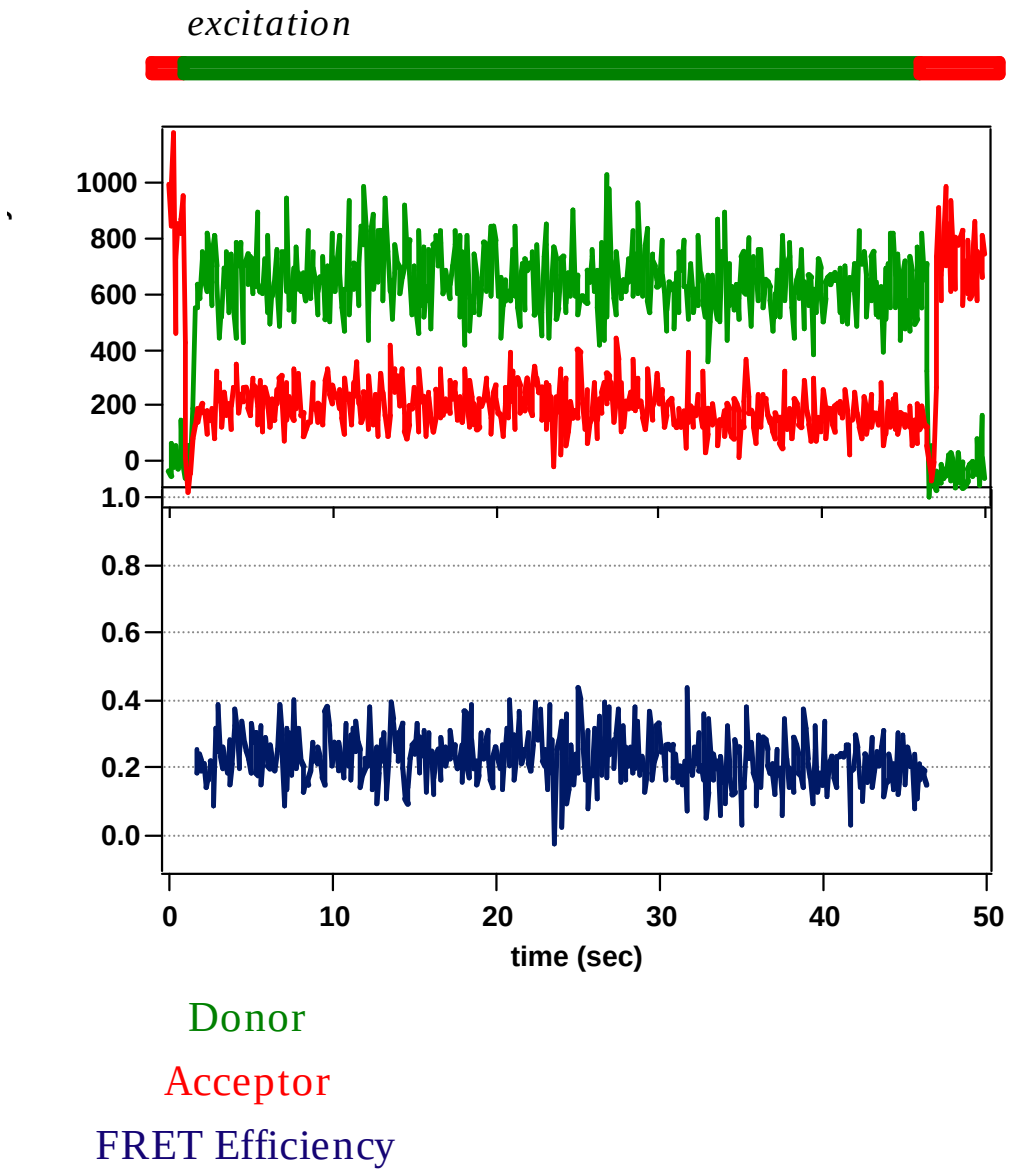

Figure 5.7 Sample single-molecule trace with laser excitation scheme

The green trace represents the FRET donor emission, and the red trace represents the FRET acceptor emission. The blue trace represents the calculated FRET energy transfer efficiency for the duration of the trace where $E = (I_A)/(I_A + I_D)$.

varying thresholds to eliminate false transition edges due to noise fluctuations in the data. Average FRET efficiencies were calculated for each step, with the first and last 4 frames at the transition edges being excluded from the average. This exclusion eliminated points at the transition edge in the average. Lifetimes at each FRET efficiency and transition sequences were also extracted. Lifetimes associated with transitions to or from a dark state (due to dye blinking) or associated with the first and last conformations in the FRET trace were eliminated from the lifetime analysis. Figure B.4 is a representative result from a FRET edge analysis on a time trace for a single DNA molecule bound by MutS.

Base-flipping fluorescence experimental methods

Glassware cleaning procedure (adopted from (Berger))

All solutions were prepared in ultra-clean, protein-free glassware. This was achieved through a rigorous cleaning and filtering process. All glassware and glass storage vials were cleaned thoroughly with Alconox to remove particulate residue then rinsed 20 times with deionized water and twice with MilliQ water to remove deionized water. The glassware was then rinsed with one volume of 2 M nitric acid to degrade any present protein contaminants, then rinsed twice with MilliQ water. The nitric acid was then neutralized by a rinse with 2 volumes of 1 M sodium hydroxide. The glassware was finally rinsed 20 times with MilliQ water. Items not used immediately were dried at 160°C for one hour and stored covered for no longer than 7 days.

Buffer preparation

A glass microanalysis vacuum filtration system with a fritted glass support and 25 mm filter diameter (Fisher Scientific) was thoroughly cleaned by the procedure outlined above. The glass frit was rinsed with MilliQ water, which was discarded. A 0.10 μm pore nitrocellulose mixed ester filter (Fisher Scientific, E01WP02500) was then placed on the glass frit and rinsed with MilliQ water. MilliQ water was then filtered through the nitrocellulose filter, de-gassed, and stored in 20 mL portions in glass vials cleaned by the procedure outlined above. This filtered water was used immediately to make buffer solutions.

Stocks of each buffer component (10x concentration) were made and stored at room temperature for up to 30 days. Approximately 50 mL of 200 mM Tris-HCl (pH 7.8), 50 mL of 50 mM magnesium chloride, and 50 mL of 1 M sodium acetate were made in cleaned glass bottles. Each solution was then filtered with a Nalgene bottle top filter unit (Catalog No. 0001650020, 0.20 μm polyethersulfone membrane) to remove undissolved solid.

Buffer at 1x concentration was made with filtered MilliQ water and discarded after one day. Buffer at 1x concentration was made from the 10x stock components (*Taq* MutS binding buffer: 20 mM Tris-HCl pH 7.8, 5 mM magnesium chloride, 100 mM sodium acetate). Several milliliters of this buffer were used to rinse a fresh 0.10 μm nitrocellulose filter, and the 1x buffer was filtered and de-gassed in the glass microanalysis vacuum filtration system described. Protein dialysis and all experiments were performed with the same 1x buffer solution.

Protein preparation

Taq MutS was expressed and purified by our collaborators at the National Institute of Health as previously described (Biswas, Obmolova et al. 2001). Protein was stored at -80°C in 20 mM Hepes-NaOH (pH 7.8), 10% glycerol, 1 mM EDTA, 0.5 mM DTT, and 150 mM NaCl until use. Prior fluorescence studies have shown that the components of this storage buffer adversely affect the fluorescence intensity of the solution, generating large background signals that may mask the change in signal induced by the analyte (Figure AIII.2).

To eliminate this background, MutS storage buffer was exchanged with 1x binding buffer using a Microcon centrifugal filter (50 kDa nominal molecular weight limit, YM-50). The filter was first rinsed with 1x filtered buffer prior to buffer exchanging. Protein samples were rinsed at least 3 times with filtered buffer to remove any residual storage buffer components. A volume of buffer equal to the original volume of protein stock was added to the filter, the filter was inverted, and the protein was removed by centrifugation at 3,000x g-force for 5 minutes.

The resultant protein concentration was determined by Bradford assay. In separate tubes, 3 μL of MutS before dialysis and 3 μL of MutS after dialysis were diluted to 100 μL with 150 mM NaCl, with the blank containing only 100 μL of NaCl. To these, 1 mL of Coomassie Brilliant Blue solution was added, and the solutions were vortexed and allowed to sit at room temperature for 2 minutes. Absorbances of the samples were measured at 595 nm with a UV spectrometer in a 1 cm pathlength cuvette. The protein concentration before dialysis was 1.4 mg/mL (determined following purification via a full Bradford Assay with a BSA standard), and the linear dependence of absorbance and concentration allowed the determination of the protein concentration following dialysis.

Cuvette Cleaning

Quartz cuvettes (315 μL volume capacity, Starna Cells, Inc. 3-3.45-Q-3) were used for all fluorescence measurements. Cuvettes were cleaned daily by submersion in 250 mL of 1% Hellmanex II cleaning solution (Hellma Cells, Inc.) at 37°C for 30 minutes. The cuvettes were then thoroughly rinsed with MilliQ water inside and out and allowed to air-dry at room temperature. Between samples, cuvettes were rinsed 5 times with 70% ethanol, 30 times with MilliQ water, then with 1 volume of buffer.

Fluorescence Instrumentation

Fluorescence intensity measurements were acquired with a Jobin Yvon Horiba Fluoromax-3 (Serial No. 3255) equipped with a Xenon lamp. Excitation and emission monochromators were calibrated daily by user manual specifications. Samples were excited with 350 nm light, and fluorescence emission was measured from 370 nm to 520 nm. Excitation and emission monochromator slit widths were set to 6.0 nm. Measurements were acquired at a rate of 1 nm per second.

Temperature controlled fluorescence spectra were acquired with a Jobin Yvon Horiba Fluorolog equipped with a Xenon lamp and a temperature control box. Experimental parameters were identical to those listed above, however experiments were performed at 23°C and/or 50°C to monitor temperature sensitivity of the fluorescence intensity.

Experimental Conditions

Spectra of MilliQ water and ultra-clean buffer were collected daily to ensure that the solutions were free of particulate contaminants and other species that would enhance background fluorescence. Exactly 300 μL of 200 nM dsDNA was added to the cuvette, and the cuvette was inverted to remove any small bubbles that would affect light scattering. MutS was added in varying concentrations to the dsDNA samples, and the solution incubated at room temperature for 5 to 10 minutes before the fluorescence data were collected. This method was applied to all DNA samples.

Fluorescence spectra were normalized to set the maximum emission (at 427 nm) equal to one. This allowed for comparative changes in intensity to be more easily distinguished. The emission spectra were corrected for the buffer background by subtracting the buffer emission spectrum from the fluorescence emission spectrum of the sample.

References

Berger, M. D. Appendix A: Tryptophan Fluorescence in RecA Protein-Obtaining quality fluorescence spectra with The RecA protein. Biochemistry and Cell Biology. Houston, Rice University.

Biswas, I., G. Obmolova, et al. (2001). "Disruption of the helix-u-turn-helix motif of MutS protein: loss of subunit dimerization, mismatch binding and ATP hydrolysis." J Mol Biol **305**(4): 805-16.

Bowen, M. E., K. Weninger, et al. (2005). "Single-molecule studies of synaptotagmin and complexin binding to the SNARE complex." Biophys J **89**(1): 690-702.

Canny, J. (1986). "A computational approach to edge detection." IEEE Trans. Pattern Anal. Mach. Intell. **8**(6): 679-698.

Cho, M., S. Chung, et al. (2007). "A simple fluorescent method for detecting mismatched DNAs using a MutS-fluorophore conjugate." Biosens Bioelectron **22**(7): 1376-81.

Clegg, R. M., A. I. Murchie, et al. (1993). "Observing the helical geometry of double-stranded DNA in solution by fluorescence resonance energy transfer." Proc Natl Acad Sci U S A **90**(7): 2994-8.

Deniz, A. A., M. Dahan, et al. (1999). "Single-pair fluorescence resonance energy transfer on freely diffusing molecules: observation of Forster distance dependence and subpopulations." Proc Natl Acad Sci U S A **96**(7): 3670-5.

Jares-Erijman, E. A. and T. M. Jovin (1996). "Determination of DNA helical handedness by fluorescence resonance energy transfer." J Mol Biol **257**(3): 597-617.

Lakowicz, J. R. (1999). Topics in Fluorescence Spectroscopy. New York, Kluwe Academic/Plenum Publishers.

McKinney, S. A., A. D. Freeman, et al. (2005). "Observing spontaneous branch migration of Holliday junctions one step at a time." Proc Natl Acad Sci U S A **102**(16): 5715-20.

Rhoades, E., E. Gussakovsky, et al. (2003). "Watching proteins fold one molecule at a time." Proc Natl Acad Sci U S A **100**(6): 3197-202.

Weninger, K., M. E. Bowen, et al. (2003). "Single-molecule studies of SNARE complex assembly reveal parallel and antiparallel configurations." Proc Natl Acad Sci U S A **100**(25): 14800-5.

APPENDIX A

FRET: MATHEMATICAL BACKGROUND AND THEORY

Fluorescence resonance energy transfer requires that the donor and the acceptor molecule be in resonance such that there is an overlap between the emission band of the donor and the absorption band of the acceptor. This overlap is denoted by the coupling coefficient, J, following the equation:

$$J = \frac{\int F(\lambda) \cdot \varepsilon(\lambda) \cdot \lambda^4 d\lambda}{\int F(\lambda) d\lambda}$$

where $F(\lambda)$ is the fluorescence intensity of the donor fluorophore at wavelength λ (in units of cm), and $\varepsilon(\lambda)$ is the extinction coefficient of the acceptor fluorophore at wavelength λ (in units of $cm^{-1}M^{-1}$).

Förster described the energy transfer rate as:

$$k = \frac{1}{\tau_d} \cdot \left(\frac{R_o}{r} \right)^6$$

where τ_d is the fluorescence lifetime of the donor in the absence of the acceptor molecule, r is the distance between the centers of the donor and the acceptor molecules, and R_o is the "Förster energy transfer distance" or the "critical energy transfer distance." This is the distance where the energy transfer is equivalent to the fluorescence decay rate, or where the energy transfer efficiency is 50%.

The critical transfer distance R_o is related to several properties including the spectroscopic properties of the donor and the acceptor and spatial orientation factors. This distance is mathematically defined as:

$$R_o^{\,6} = \left(8.785e^{-5}\right) \cdot \frac{\kappa^2 \cdot \phi_d \cdot J}{n^4}$$

where J is the coupling constant as mentioned above; ϕ_d is the quantum yield of the donor molecule in the absence of the acceptor; n is the index of refraction of the medium (1.4 for FRET in an aqueous solution); and, κ^2 is the orientation factor.

The orientation factor has strong angular dependence between the donor and the acceptor molecules, following the relationship:

$$\kappa^2 = \left(\cos\alpha - 3\cos\beta\cos\gamma\right)^2$$

where α is the angle between the donor and acceptor transition moments, β is the angle between the donor transition moment and the line adjoining the centers of the donor and acceptor molecules, and γ is the angle between the acceptor transition moment and the line adjoining the centers of the donor and acceptor molecules. In general, κ^2 lies between the values of 0 and 4. For the circumstance where the donor and acceptor molecules have free rotation in time, or rotation faster than the donor excited state lifetime, κ^2 is known to have an exact value of 2/3.

The distance between the donor and acceptor fluorophores is experimentally determined following the relationship:

$$E_{FRET} = \frac{1}{1+\left(\frac{r}{R_o}\right)^6} = 1 - \frac{I_{da}}{I_d} = 1 - \frac{\tau_{da}}{\tau_d}$$

where I_{da} (τ_{da}) is the intensity (decay lifetime) of the donor fluorophore in the presence of the acceptor fluorophore in a FRET experiment, and I_d (τ_d) is the intensity (decay lifetime) of the donor in the absence of the acceptor fluorophore (the reference measurement).

The relationship between the FRET energy transfer efficiency and the distance between the donor and acceptor molecules is shown in Figure 1.2. The general distance information obtained from FRET energy measurements may be relative measurements or average measurements depending on the system being studied and the uncertainty in the variables that comprise the calculation of R_o.

APPENDIX B

CHAPTER TWO SUPPLEMENTAL RESULTS

Gaussian derivative kernal to analyze dynamic FRET traces

In order to characterize all FRET efficiencies sampled, acquire their dwell times, and record transition trajectories, we employed a custom analysis script (written by Brian Eastwood, Russell Taylor Laboratory, UNC Department of Computer Science) to measure FRET transitions based on a Gaussian derivative kernal. A sample of this analysis on a single GT-MutS FRET trajectory is shown in Figure B.1.

The fundamental basis of this analysis method is to distinguish between noise in the signal and significant transition events. Signal processing theory provides an efficient method to make this distinction, where the derivative of the Gaussian function serves as an ideal edge detector (Canny 1986). In one dimension, *x*, the Gaussian derivative function is defined as:

$$\frac{dG(x;\sigma)}{dx} = -\frac{\exp\left(\frac{-x^2}{2\sigma^2}\right)\cdot x}{\sqrt{2\pi}\cdot\sigma^3}$$

Edge detection involves filtering the signal with a discrete Gaussian derivative kernal and searching for extrema in the resulting signal. The filtering operation can be performed by multiplying the Fourier transforms of the signal and the filter kernal (Canny 1986). For a function I (x):

$$I'(x) = F^{-1}\left[F(I(x))\cdot F\left(\frac{dG(x;\sigma)}{dx}\right)\right]$$

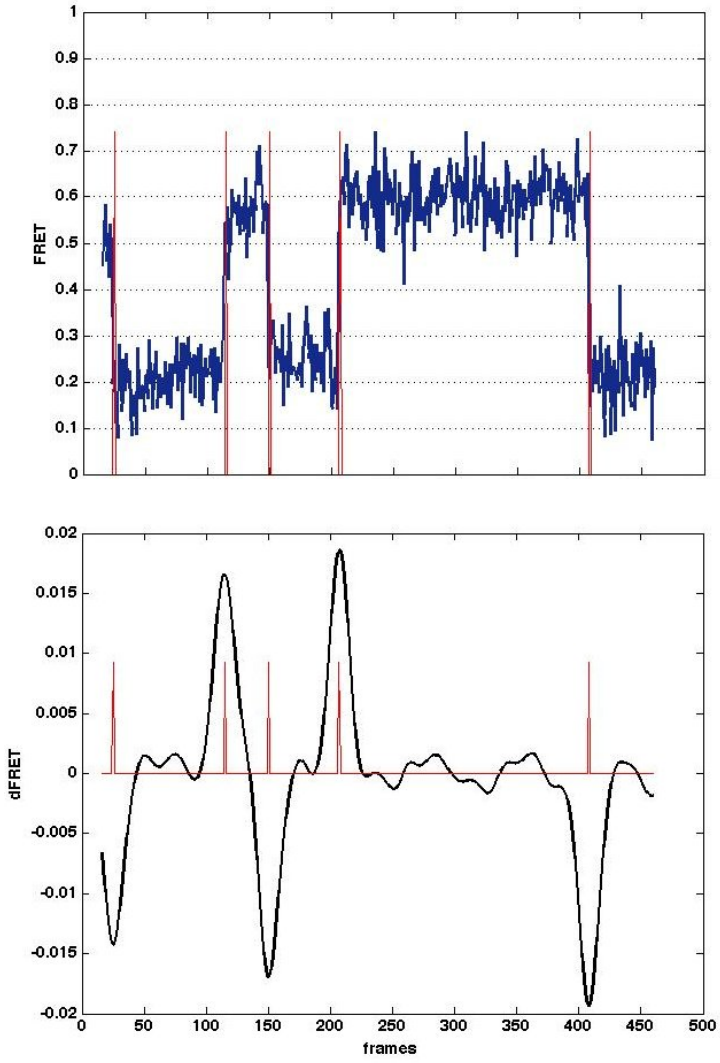

Figure B.1 Sample trace representing Gaussian derivative kernal analysis to determine transition edges in FRET traces

Top: Single-molecule FRET trajectory (blue trace) with transitions. Bottom: Calculated derivative of the FRET efficiency trace (black trace). The red tick marks represent the location of local extrema in dFRET using a Gaussian derivative kernal dictating the location of transition edges.

where F and F^{-1} designate the Fourier and inverse Fourier transforms, respectively. Maxima in the filtered signal correspond to positive (increasing) edges, while minima correspond to negative (decreasing) edges (Figure B.1). The Gaussian derivative filter not only detects edges but also smoothes signal features in proportion to the Gaussian function's scale parameter, σ.

Choice of the scale parameter is essential in signal processing because every point in a noisy signal looks like an edge in the absence of scale consideration. As described in (Canny 1986), the Gaussian derivative filter selects at most one maximum in the filtered signal within an interval of scale parameter. This means a Gaussian derivative with a large scale parameter can be used to detect significant edges in signal containing a high degree of noise. Using a large scale parameter, however, limits the accuracy to which one can determine the position of an edge.

To resolve this trade-off between sensitivity to noise and accuracy, we used a multi-scale approach to analyze our FRET data. We computed the scale-space deriviative of the signal by processing with multiple Gaussian derivatives of increasing scales. We obtained a rough estimate of edge positions by detecting the maxima at the most coarse scale. The estimate is refined by tracing the maxima back through scale-space.

This analysis provided us with each FRET efficiency sampled in a given FRET trace as well the time the molecule spent at that FRET efficiency ('dwell time') and the transition sequence.

Transition density plot analysis and 2D Gaussian peak fitting

Transition density plots documenting the conformational transitions observed in mismatched DNA-MutS complexes were generated as shown in Figures 2.5 and 2.8. An example of the deconvolution of ΔT-MutS transition peaks is shown in Figure B.2. A contour image of the TDP was generated (Figure B.2 A), and unique areas of density were extracted to regenerate a contour image of the individual peak (an example of a single peak shown in Figure B.2 B). This 3-dimensional array was fit to a 2D Gaussian function following the equation:

$$z = z_o + A\exp\left[\frac{-1}{2(1-cor^2)}\cdot\left(\left(\frac{x-x_o}{x_{width}}\right)^2+\left(\frac{y-y_o}{y_{width}}\right)^2-\frac{2\cdot cor\cdot(x-x_o)\cdot(y-y_o)}{x_{width}\cdot y_{width}}\right)\right]$$

where x_o, y_o, and z_o are the offsets in the *x*, *y*, and *z* dimensions; x_{width} and y_{width} are the breadths of the Gaussians in both the x and y dimensions; *A* is the peak amplitude, and, *cor* is a correlation parameter representing deviation from the x-y orthogonal (angular skew in the peak). The 2D Gaussian fit result produced a probability density array (shown as an overlay in Figure B.2 C). The density arrays for the fits of each separated peak were summed to generate the density plots shown in Figures 2.5 C.

This analysis method was also performed on GT-MutS transitions as shown in Figure B.4. The sum of the 2D Gaussian peak fits is shown as the TDP in Figure 2.8 C.

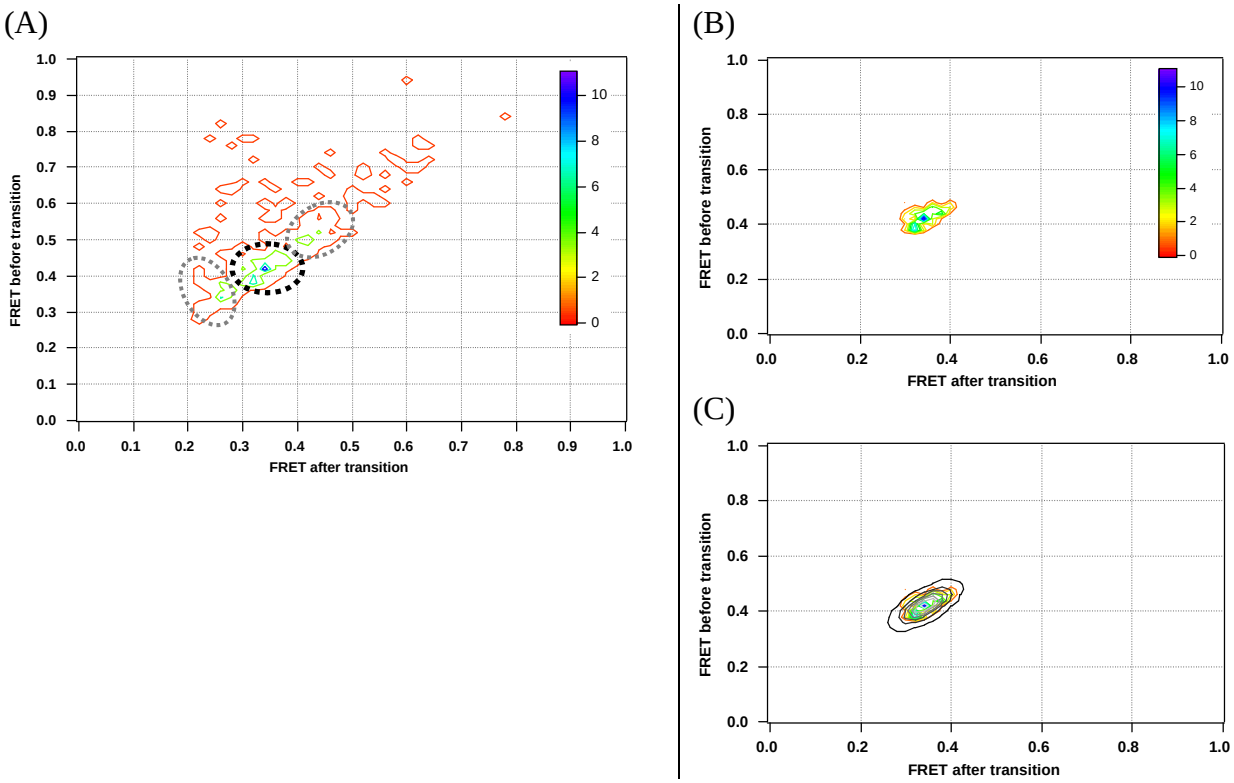

Figure B.2 Analysis method employed to extract unique conformational transitions from transition density plots

(A) Contour image of all ΔT-MutS complexes transitioning from high FRET to low FRET (representing only the density above the diagonal line in Figure 2.5). Individual peaks are loosely enclosed in dashed circles. The peak enclosed by the black dashed circle is represented as a contour image in (B). The peak was fit to a 2D Gaussian function, and the result of the fit is shown overlaid in gray in (C). The skew in the peak toward the diagonal is the result of heterogeneous broadening as previously described by Ha and coworkers.

Lifetime analysis to isolate unique GT-MutS conformations

We employed lifetime analysis to identify the number of unique conformational species within the FRET distribution of all states sampled. Lifetimes have been used to identify and characterize different chemical species among various FRET states or within a single FRET conformation (Zhuang, Kim et al. 2002). To extract the number of states using lifetimes, we grouped the observed FRET efficiencies (with corresponding dwell times) in different FRET ranges and plotted frequency versus the dwell time in that FRET range. The exponential fit to frequency versus dwell time provides the kinetic rate of the conformation (fit parameter $1/\tau$), and the inverse (τ) represents the 'lifetime' of the state. A single exponential fit represents a single lifetime, or conformational species, within that range of FRET efficiencies. Accordingly, a double exponential fit would produce two kinetic rates and two lifetimes implying that two conformational species comprise the range of FRET efficiencies (Zhuang, Kim et al. 2002). Using this analysis, we were able to extract 6 unique FRET conformational states from the FRET efficiency distribution for GT-MutS complexes.

We were able to separate the high FRET state and the low FRET state by removing FRET values lying within the overlapped region of a double Gaussian fit of the FRET efficiency distribution. These two Gaussian curves overlap between FRET 0.30 and 0.60. As a result, dwell times corresponding to all FRET values less than 0.30 were combined as a single state, and dwell times corresponding to all FRET values greater than 0.60 were combined as a single state. The combined dwell times of all FRET states between 0 and 0.29 converged to a single exponential of τ = 2.3 seconds (Figure B.4 A, conformation representing free DNA). The combined dwell times of all FRET states from 0.61 to 1.0

converged to a single exponential at τ = 12 seconds (Figure B.4 E, bent DNA conformation ***B***).

Dwell times associated with FRET values between these two FRET states falling in the overlapped region of the double Gaussian fit were further analyzed to determine if additional species could be resolved by characteristic lifetimes. FRET values in this region were grouped in small segments of FRET efficiencies (FRET +/- 0.005) and expanded as lifetimes converged to the same values.

Dwell times associated with FRET values between 0.30 and 0.40 converged to a single exponential with τ = 1.5 seconds (Figure B.4 B, unbent DNA conformation ***U***). Dwell times associated with FRET values from 0.41 to 0.50 fit to a double exponential decay and thus comprise two species with lifetimes τ_1 = 0.75 seconds and τ_2 = 6.6 seconds (Figure B.4 C, conformations ***U**** and ***I***). While these species are indistinguishable by FRET efficiency, unique lifetimes confirm that these are two unique conformations within a single FRET state (Zhuang, Kim et al. 2002). Finally, a double exponential fit of dwell times associated with FRET values from 0.51 to 0.60 yielded two states with decay constants of τ_1 = 1.5 seconds and τ_2 = 15 seconds (Figure B.4 D, conformations ***B**** and ***B***). The similarity of the longer lifetime (τ_2) to that of conformation ***B*** (12 seconds vs. 15 seconds) suggests that this is not a unique state but contains species from conformation ***B***. However, the state with the shorter lifetime (conformation ***B****) appears to be unique.

Our documented lifetime of the FRET state representing unbound, free DNA (FRET 0 to ~ 0.29) is consistent with kinetic studies where the expected lifetime of the unbound state at this MutS concentration (200 nM) is 1.7 seconds based on the mismatch binding rate of $k_{on} = 3 \times 10^6\ M^{-1}sec^{-1}$ (Jacobs-Palmer and Hingorani 2007). We were able to differentiate

(A) Dwell times associated with FRET efficiencies from 0 to 0.29 (free DNA)

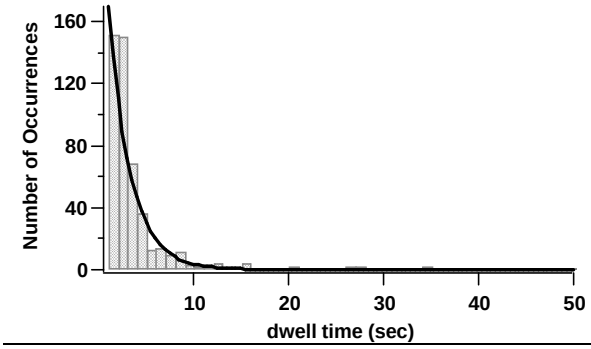

(B) Dwell times associated with FRET efficiencies from 0.30 to 0.40 (conformation U)

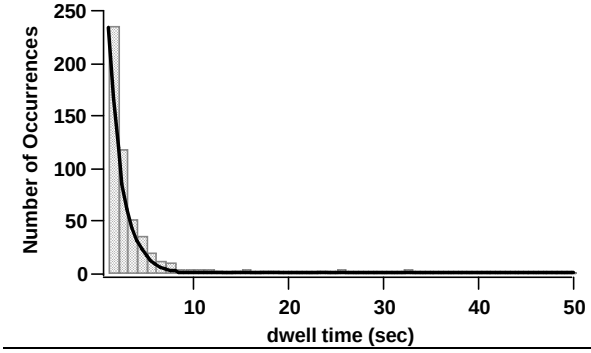

(C) Dwell times associated with FRET efficiencies from 0.41 to 0.50 (conformations U* and I)

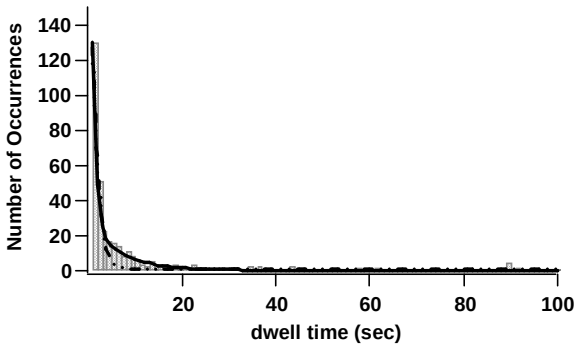

(D) Dwell times associated with FRET efficiencies from 0.51 to 0.60 (conformations B* and B)

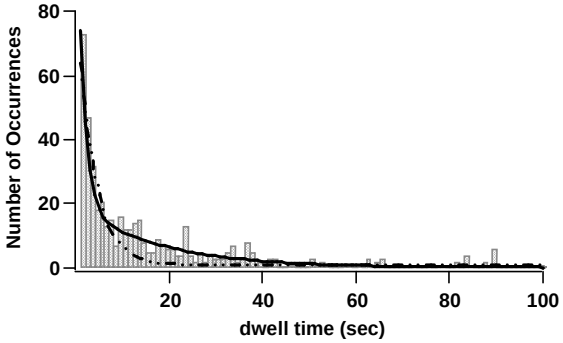

(E) Dwell times associated with FRET efficiencies from 0.61 to 1.0 (conformation B)

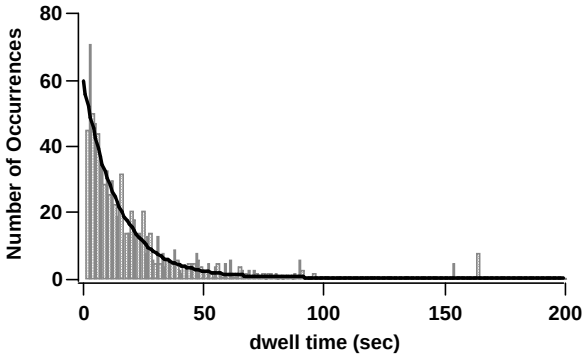

Figure B.3 Lifetime analysis of GT-MutS FRET conformations

Dwell times of individual FRET states for GT-MutS complexes (2992 FRET efficiencies sampled in 1095 molecules). (A) and (E) show dwell times in the lowest and highest FRET efficiency ranges outside of the overlapped region of the double gaussian fit to the FRET efficiency distribution (denoted as free DNA and conformation ***B***), respectively. These data converge to a single exponential decay with τ = 2.3 sec for free DNA and τ = 12 sec for conformation ***B***. (B) through (D) show the dwell times in the intermediate FRET states lying within the overlapped region of the double Gaussian distribution. (B) shows dwell times associated with FRET efficiencies from 0.30 to 0.40 converging to a single exponential with decay constant τ = 1.5 sec (conformation ***U***). (C) represents dwell times associated with FRET efficiencies from 0.41 to 0.50. The dwell time distribution converges to two unique lifetimes (τ1 = 0.75 sec and τ2 = 6.6 sec), indicating that this FRET state contains two conformational species (conformations ***U**** and ***I***) unique from conformations ***U***, ***B***, and free DNA, likely serving as transition intermediates. Convergence to two lifetimes implies that two unique chemical species comprise this state. Dwell times associated with FRET efficiencies between 0.51 and 0.60 (shown in (D)) converge to a double exponential with lifetimes τ1 = 1.5 sec and τ2 = 15 sec (conformations ***B**** and ***B***). The longer lifetime is consistent with conformation ***B***, implying that these conformations are the same species. The conformation with the shorter lifetime (conformation ***B****) appears to be unique. Single exponential decay fits are shown as dashed lines in (C) and (D) for reference.

(A)

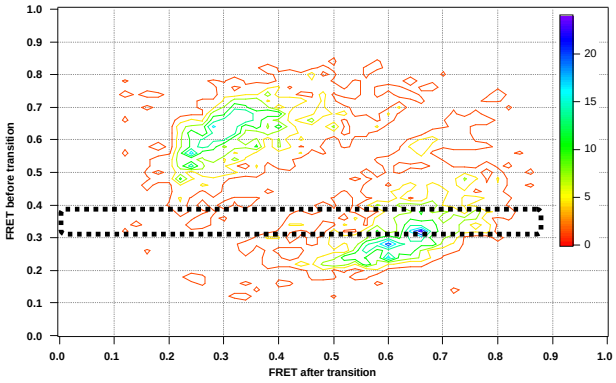
FRET before transition
FRET after transition
0.0
0.1
0.2
0.3
0.4
0.5
0.6
0.7
0.8
0.9
1.0
0
5
10
15
20

(B)

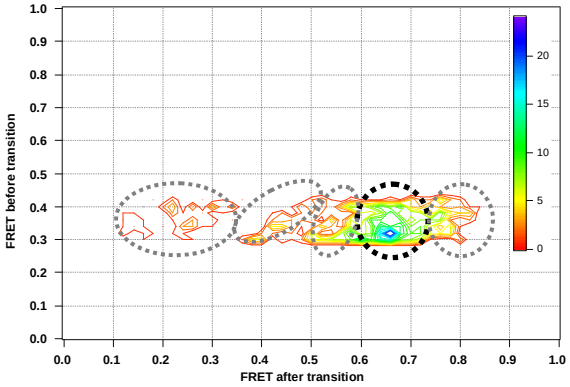
FRET before transition
FRET after transition
0.0
0.1
0.2
0.3
0.4
0.5
0.6
0.7
0.8
0.9
1.0
0
5
10
15
20

(C)

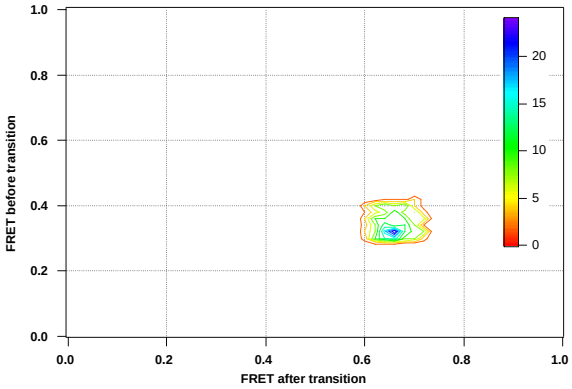
FRET before transition
FRET after transition
0.0
0.2
0.4
0.6
0.8
1.0
0
5
10
15
20

(D)

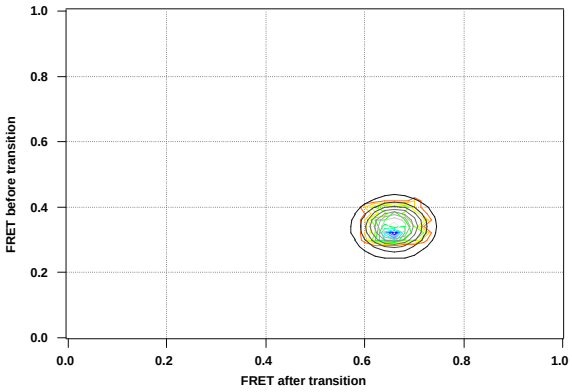
FRET before transition
FRET after transition
0.0
0.2
0.4
0.6
0.8
1.0

Figure B.4 Sample 2D Gaussian fitting of GT-MutS conformational transitions

Analysis method employed to extract unique conformational transitions from transition density plots. (A) Contour image of all GT-MutS conformational transitions of those shown in Figure 2.8. A cross-section of selected transitions based on lifetime analysis is enclosed in the dashed box and shown in (B). The conformations in this FRET range converged to a single lifetime of 1.5 seconds. Individual peaks chosen by discrete areas of density are enclosed in circles. These peaks were separated, as shown in (C), and subsequently fit to a 2D Gaussian distribution. The result of the fit of the peak in (C) is shown overlaid in gray in (D).

this conformation from conformation ***U*** (unbent GT-MutS complexes) by performing the experiment at a lower MutS concentration. These results showed an increase in the lifetime of the FRET state associated with free DNA, while the lifetime of the remaining GT-MutS conformations were unchanged (Table 2.1).

Combined transitions and lifetimes show that GT-MutS conformations U, B*, and I are unique intermediate conformations*

We used transition densities to further differentiate between intermediate FRET conformations that were comprised of two unique species as determined by two unique lifetimes for the state. We investigated transitions to and from FRET conformations ***U****, ***I***, and ***B**** to confirm that these states were unique, and we further looked at transitions of FRET conformation ***B*** in the mixed FRET range (0.51 to 0.60) to confirm that this was the same conformation as determined by lifetime for FRET conformations > 0.60.

The lifetime decay curves were deconvoluted into single exponential decays, and a cutoff time was employed based on these deconvoluted curves to separate conformations comprising the short lifetime states (either ***U**** or ***B****) from the conformations comprising the long lifetime states (either ***I*** or ***B***). For FRET states ***U**** and ***I***, the cutoff time was determined to be 3 seconds. As a result, all FRET values in this range with dwell times of 3 seconds or less were assigned as conformation ***U****, and all FRET values in this range with dwell times longer than 3 seconds were assigned as conformation ***I***. For FRET states ***B**** and ***B***, the cutoff time was determined to be 4 seconds. Therefore, all FRET values in this range with dwell times of 4 seconds or less were assigned as conformation ***B****, and all FRET values in this range with dwell times longer than 4 seconds were assigned as conformation ***B***. These

cutoff times were robust to within a few seconds, as results were minimally affected when these cutoff times were altered within a 1 to 2 second range in either direction.

Transition density plots of these separated transitions revealed that transition state ***U**** (τ = 0.75 sec) preferentially transitions to and from high FRET conformations (***B*** or ***SB***) (Figure B.5 A and B.6 A). A fraction of binding and unbinding transitions were observed, but these transitions were not typical and occurred in fewer than 20% of transitions measured to or from this conformation. Transition density plots of transitions to and from intermediate state ***I*** (τ = 6.6 sec) revealed that this conformation has an equal probability of transitioning to a lower FRET conformation (conformation ***U*** or unbinding) as it does to a higher FRET conformation (***B*** or ***SB***) (Figure B.5 B and B.6 B).

Unique transition densities were also observed when transitions corresponding to FRET states ***B**** and ***B*** were separated based on lifetime. Transition density plots revealed that transition state ***B**** (τ = 1.5 sec) is capable of transitioning to and from both lower and higher FRET conformations (Figure B.5 C and B.6 C). Between 60 and 65% of the observed transitions from or to conformation ***B*** were to or from a lower FRET state (conformation ***U*** or unbinding), while the remaining 35 to 40% of the transitions were to or from a high FRET state (***B*** or ***SB***). Transition densities for the bent DNA conformation ***B*** (τ = 12 sec) revealed dominant transitions due to binding and unbinding of MutS to and from the DNA or conformational transitions to or from conformation ***U*** (80 to 90% of the transitions) (Figure B.5 D and B.6 D). This result was expected because this conformation, although mixed with FRET conformation ***B****, was determined to be the same as the high FRET state ***B*** based on lifetime, and similar transitions confirm this conclusion.

The results from this analysis were used to determine the number of transitions comprising each conformational transition peak and were used to determine the transition probabilities of each of these conformational transitions.

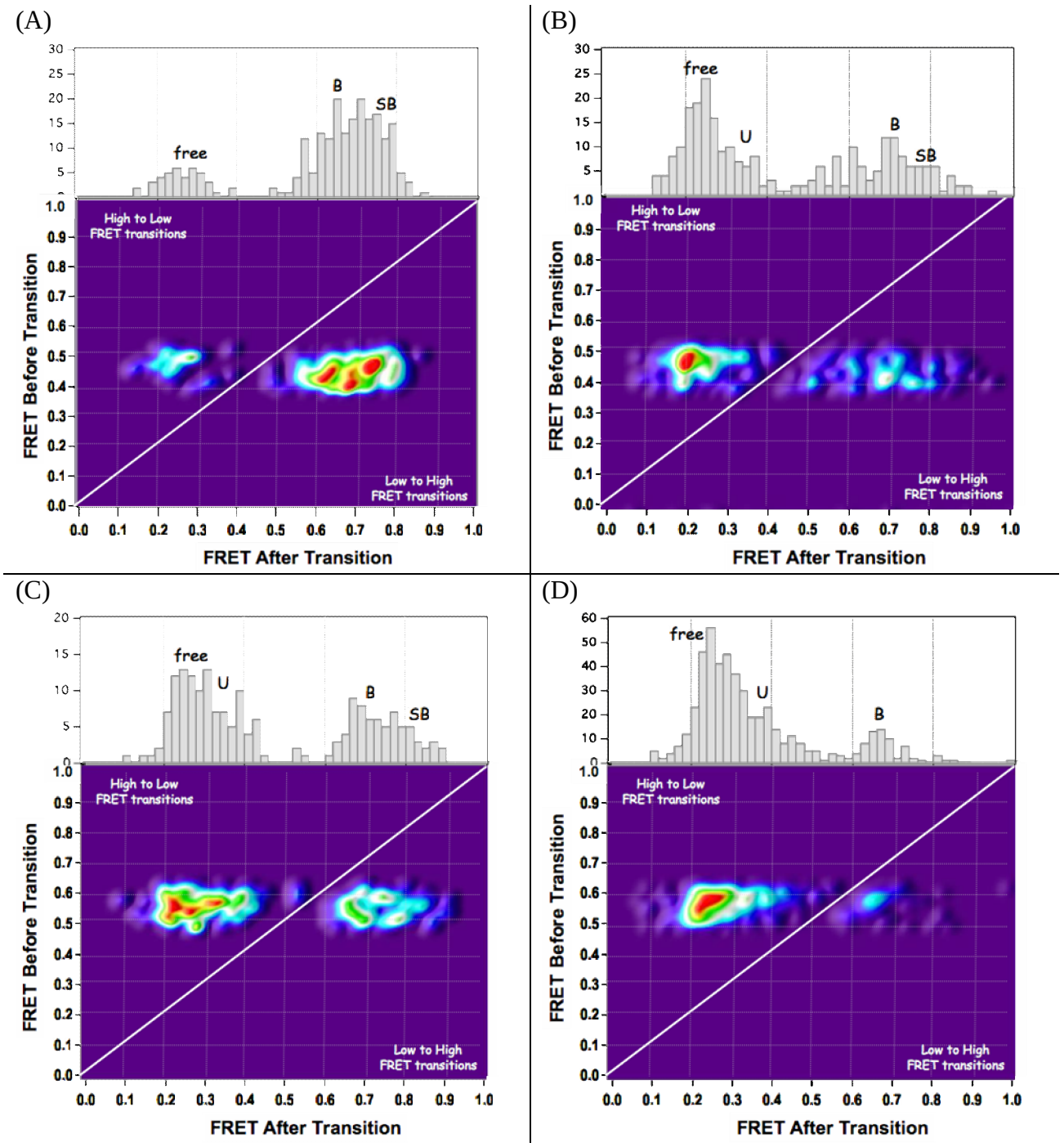
(A)
free
B
SB
High to Low FRET transitions
Low to High FRET transitions
FRET Before Transition
FRET After Transition
(B)
free
U
B
SB
High to Low FRET transitions
Low to High FRET transitions
FRET Before Transition
FRET After Transition
(C)
free
U
B
SB
High to Low FRET transitions
Low to High FRET transitions
FRET Before Transition
FRET After Transition
(D)
free
U
B
High to Low FRET transitions
Low to High FRET transitions
FRET Before Transition
FRET After Transition

Figure B.5 Transition densities of FRET intermediates separated by lifetime

Transition density plots showing FRET states that transition from FRET conformation ***U**** (A), from FRET conformation ***I*** (B), from FRET conformation ***B**** (C), and from FRET conformation ***B*** (D). Two-dimensional FRET distributions showing the conformations are included to show the relative number of times each FRET state occurs.

(A)

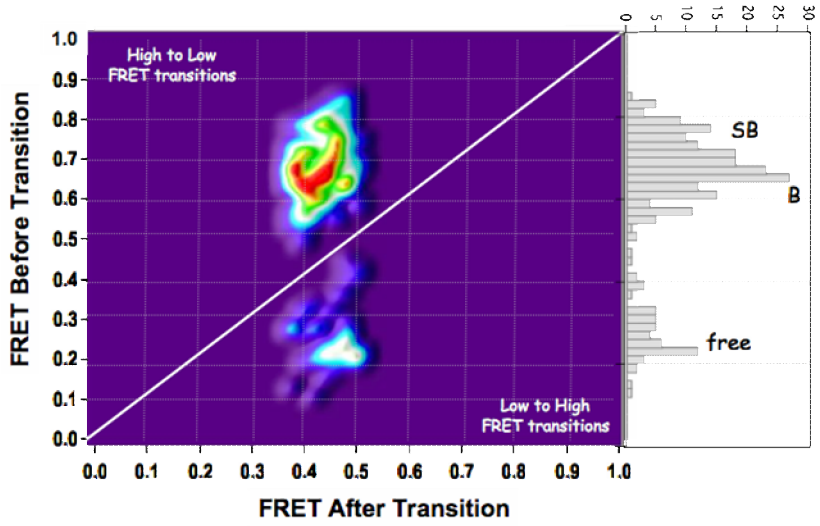
High to Low
FRET transitions
Low to High
FRET transitions
FRET Before Transition
FRET After Transition
SB
B
free

(B)

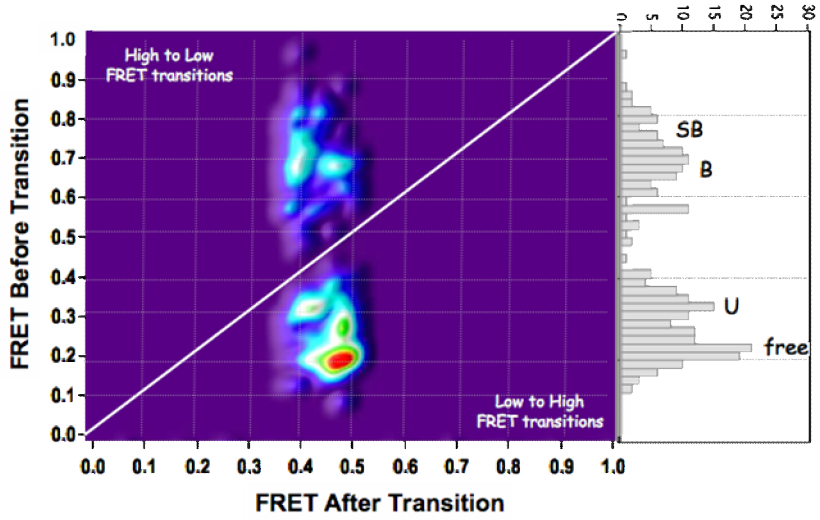
High to Low
FRET transitions
Low to High
FRET transitions
FRET Before Transition
FRET After Transition
SB
B
U
free

(C)

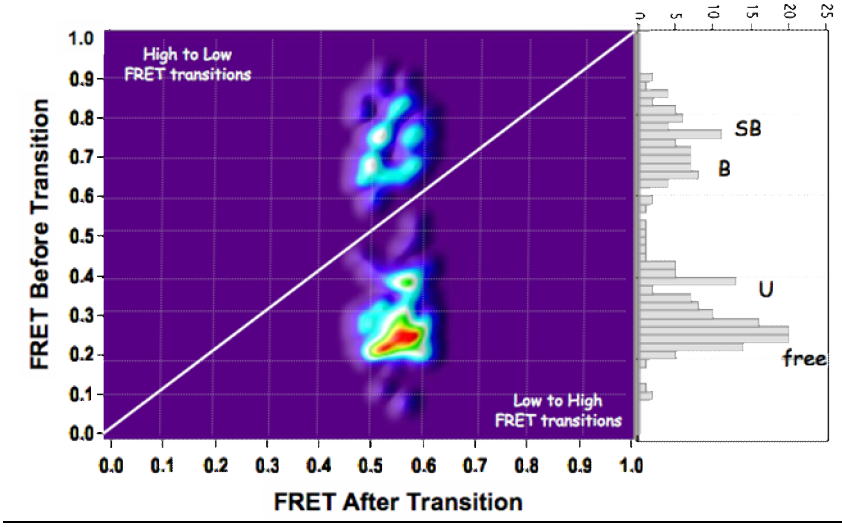
High to Low
FRET transitions
Low to High
FRET transitions
FRET Before Transition
FRET After Transition
SB
B
U
free

(D)

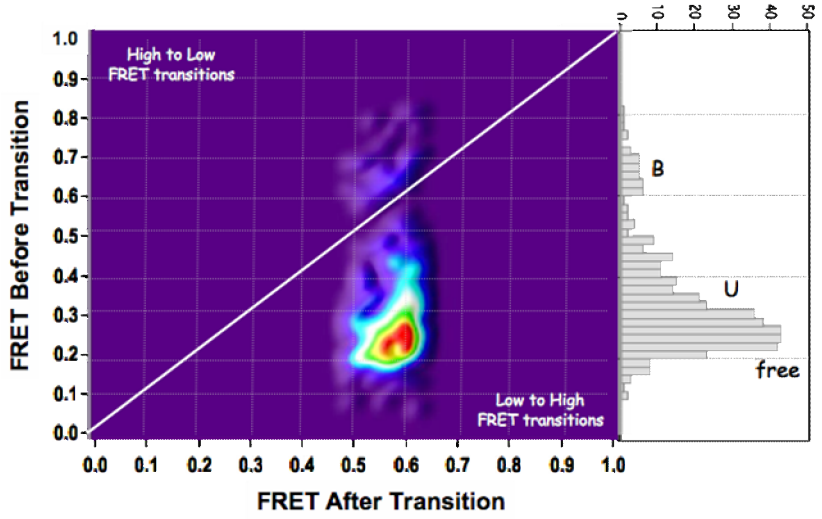
High to Low
FRET transitions
Low to High
FRET transitions
FRET Before Transition
FRET After Transition
B
U
free

Figure B.6 Transition densities of FRET intermediates separated by lifetime

Transition density plots showing conformational transitions to FRET state ***U**** (A), to FRET state ***I*** (B), to FRET state ***B**** (C), and to FRET state ***B*** (D). FRET distribution of states is shown as an adjacent histogram for reference. Results reveal that conformation ***U**** typically transitions from a higher FRET state (such as conformation ***B***), while conformation ***I*** has an equal probability of transitioning from a lower FRET state (***U*** or free DNA) or a higher FRET state (***B*** or ***SB***). Results also reveal that conformation ***B**** has a 60 to 65% probability of transitioning from a lower FRET state (***U*** or free DNA) and a 35 to 40% chance of transitioning from a higher FRET state (***B*** or ***SB***). In contrast, transitions to conformation F are typically from a lower FRET state (***U*** or free DNA).

References

Canny, J. (1986). "A computational approach to edge detection." IEEE Trans. Pattern Anal. Mach. Intell. **8**(6): 679-698.

Jacobs-Palmer, E. and M. M. Hingorani (2007). "The effects of nucleotides on MutS-DNA binding kinetics clarify the role of MutS ATPase activity in mismatch repair." J Mol Biol **366**(4): 1087-98.

Zhuang, X., H. Kim, et al. (2002). "Correlating structural dynamics and function in single ribozyme molecules." Science **296**(5572): 1473-6.